THE UNIVERSITY OF MANITOBA
ELECTRICAL ENGINEERING DEPARTMENT

SIMULATION OF CYLINDRICAL REFLECTOR ANTENNAS

A Dissertation
Presented to the Faculty of Graduate Studies
University of Manitoba

In Partial Fulfillment
of the Requirements for the Degree
Doctor of Philosophy

by

HASSAN ALY RAGHEB

B.Sc., Elec. Eng., 1977, Cairo Univ., Egypt.
B.Sc., Appl. Phys., 1980, Cairo Univ., Egypt.
M.Sc., Elec. Eng., 1984, Manitoba Univ., Canada

May 1987

ISBN 0-315-37361-X

SIMULATION OF CYLINDRICAL REFLECTOR ANTENNAS

BY

HASSAN ALY RAGHEB

A thesis submitted to the Faculty of Graduate Studies of
the University of Manitoba in partial fulfillment of the requirements
of the degree of

DOCTOR OF PHILOSOPHY

ABSTRACT

This thesis aims at simulating a single cylindrical reflecting surface by a collection of cylinders or strips to produce approximately the same radiation pattern through single and multiple scattering and diffraction as from the re-radiation of the induced surface current on the solid reflector surface due to a line source or a long dipole excitation. Useful expressions for designing simulated reflectors are derived by solving the problem of multiple scattering of a plane or cylindrical wave by N conducting strips or circular cylinders (which are special cases of elliptic cylinders). Two methods are employed for solving this problem, the first is based on a rigorous boundary value approach while the second is asymptotic and essentially based on the Karp-Russek technique. The validity of equivalent line source solution of the Karp-Russek technique is found to be surprising for cases of large strip width or cylinder radius provided that the spacing between any two strips or cylinders is large relative to the wavelength. It is found that increasing the number of slits, which separate the strips or cylinders, is more effective for simulation, as long as the slit sizes are kept small, rather than increasing the strip width or cylinder radius. It is also shown that for specific case about 50% of the cylindrical surface is sufficient for simulation, using equally spaced strips of 0.1 λ width each, while the simulation by cylinders of different radii and spacing indicates an improvement in the far field pattern.

The long dipole antenna is also investigated for use as a feed of the simulated cylindrical reflector. The radiation from a long dipole in isolation is presented by first extending Hurd's Wiener-Hopf formulation for the input admittance of a center fed long dipole. The extension includes accurate expressions for the far-zone field, current distribution and input admittance of the arbitrarily fed dipole. The multiply fed dipole is also considered as a superposition of arbitrarily fed dipoles.

The scattering of a long dipole antenna field by N conducting circular cylinders is also examined for simulation purposes. The dipole field is considered as incident

on the cylinders resulting in multiply scattered fields among the cylinders as well as between each cylinder and the dipole. A self-consistent method is employed for calculating the multiply scattered fields among the cylinders while an iterative procedure is used for the multiple scattering between the cylinders and the dipole. The resulting radiation and scattered field expressions are found useful in optimizing the simulated cylindrical reflector antenna.

ACKNOWLEDGEMENT

The author is grateful to professor M. Hamid of the Electrical Engineering Department, University of Manitoba, for suggesting the topic and for his guidance, constant encouragement and constructive criticism throughout this project.

Special thanks to my wife Maysa for her help, patience and encouragement during my study and to my son Ahmed for his forbearance.

The financial assistance of the National Science and Engineering Research Council of Canada and the University of Manitoba Faculty of Graduate Studies in the form of a Fellowship is highly appreciated.

The use of the computer facilities at the University of Manitoba as well as the plotting and text writing facilities at the Electrical Engineering Department of the University of Manitoba are also acknowledged.

TABLE OF CONTENTS

ABSTRACT ii

ACKNOWLEDGEMENTS iv

TABLE OF CONTENTS v

LIST OF TABLES viii

LIST OF FIGURES ix

LIST OF PRINCIPAL SYMBOLS xii

CHAPTER 1– INTRODUCTION 1

CHAPTER 2– SIMULATION OF CYLINDRICAL SCATTERING SURFACE BY CONDUCTING STRIPS 12

2.1 *Introduction* 12

2.2 *Boundary value solution* 13

2.3 *Asymptotic solution* 21

2.4 *Plane wave excitation* 23

2.4.1 Boundary value solution 23

2.4.2 Asymptotic solution 25

2.5 *Scattering by a solid cylindrical surface using the method of moments* 26

2.6 *Numerical results and discussion* 27

2.6.1 Plane wave excitation 27

2.6.2 Line source excitation 36

CHAPTER 3– SIMULATION OF CYLINDRICAL SCATTERING SURFACE BY CONDUCTING CIRCULAR CYLINDERS 46

3.1 *Introduction* 46

3.2 *Boundary value solution* 47

3.3 *Asymptotic solution* 52

3.4 *Results and discussion* 56

3.4.1 Plane wave excitation 56

3.4.2 Line source excitation 59

3.5 *Engineering considerations* 73

CHAPTER 4– ANALYSIS OF A LONG DIPOLE ANTENNA WITH ARBITRARY FEED POSITION 83

4.1 *Introduction* 83

4.2 *Current distribution on a symmetrically driven dipole* 85

4.2.1 Formulation 85

4.2.2 Solution of the integral. equation using Wiener–Hopf technique 91

4.3 *Current distribution on anti–symmetrically driven dipole* 100

4.4 *Current distribution on the arbitrarily driven and asymmetrically driven dipole* 101

4.5 *Input admittance of arbitrarily driven dipole* 102

4.6 *Radiation pattern* 103

4.7 *Results and discussion* 105

CHAPTER 5– SIMULATION BY CIRCULAR CYLINDERS WITH A LONG DIPOLE EXCITATION 117

5.1 *Introduction* 117

5.2 *Radiation field of the dipole* 118

5.3 *first order fields scattered by cylinders* 122

5.4 *First order field scattered by the dipole* 126

5.5 *Higher order fields scattered by the dipole and cylinders* 129

5.6 *Radiation field* 132

5.7 *Simulation of cylindrical scattering surface by cylinders* 134

5.8 *Numerical results and discussion* 134

CHAPTER 6– GENERAL DISCUSSION AND CONCLUSIONS 147

6.1 *Future research* 152

REFERENCES 154

APPENDIX A– EVALUATION OF THE INTEGRAL $R_o(h)$ 164

APPENDIX B– EVALUATION OF THE CONSTANTS C_m 167

APPENDIX C– EXACT SOLUTION OF THE INTEGRAL $G(\beta,\alpha)$ 171

LIST OF TABLES

Table		page
3.1	Radiation characteristics of a cylindrical parabolic reflector simulated by circular cylinders.	79
3.2	Radiation characteristics of a cylindrical parabolic reflector simulated by circular cylinders.	80
3.3	Radiation characteristics of a cylindrical parabolic reflector simulated by conducting strips.	81
3.4	Radiation characteristics of a cylindrical parabolic reflector simulated by conductinf strips.	81
4.1	Input admittance of a multiply fed dipole.	115

LIST OF FIGURES

Figure		page
2.1	Geometry of the problem.	14
2.2	Echo width pattern of two parallel strips ($\phi_0 = 90^o, 2d = 0.5\lambda, \psi_1 = \psi_2 = 45^o$).	28
2.3	Echo width pattern of two parallel strips ($\phi_0 = 45^o, 2d = 1.5\lambda, \psi_1 = \psi_2 = -45^o$).	30
2.4	Echo width pattern of solid and simulated 1.0λ strip ($N = 8, 2d = 0.05\lambda, \phi_0 = 90^o$).	31
2.5	Echo width pattern of solid and simulated 1.0λ strip ($N = 3, 2d = 0.28\lambda, \phi_0 = 90^o$).	32
2.6	Echo width pattern of simulated and solid conducting cylinder ($N = 24, 2d = 0.1\lambda, \phi_0 = 90^o$).	34
2.7	Echo width pattern of five parallel strips ($N = 5, 2d = 0.5\lambda, \psi = -45^o, \phi_0 = 45^o$).	35
2.8	Simulated reflector antennas.	37
2.9	Far field pattern of solid and simulated 1.5λ strip excited by a line source ($N = 9, D = 1.5\lambda, S = 0.8\lambda, 2d = 0.1\lambda$).	38
2.10	Far field pattern of solid and simulated corner reflector antenna of 75^o corner angle ($N = 16, D = 1.38\lambda, S = 0.4\lambda, 2d = 0.1\lambda$).	39
2.11	Far field pattern of solid and simulated circular cylindrical reflector antenna ($N = 41, D = 6\lambda, R = 8\lambda, 2d = 0.1\lambda$).	40
2.12	Far field pattern of solid and simulated parabolic cylindrical reflector antenna ($N = 35, D = 5\lambda, F = 1.8\lambda, 2d = 0.1\lambda$)	42
2.13	Far field pattern of simulated parabolic cylindrical reflector antenna using different number of strips ($D = 5\lambda, F = 1.8\lambda, 2d = 0.1\lambda$).	43
2.14	Far field pattern of simulated parabolic cylindrical reflector antenna using different strip widths ($N = 29, D = 5\lambda, F = 1.8\lambda$).	44
3.1	Geometry of the problem.	48

3.2(a) Echo width pattern of two cylinders
($ka = 0.1, ks = 3.0, \phi_0 = 10^o$). 57

3.2(b) Echo width pattern of two cylinders
($ka = 1.0, ks = 3.0, \phi_0 = 10^o$). 58

3.3(a) Backscattering echo width of two cylinders
($ka = 0.1, \phi_0 = 60^o$). 60

3.3(b) Backscattering echo width of two cylinders
($ka = 1.0, \phi_0 = 60^o$). 61

3.4 Echo width pattern of three cylinders
($ka = 0.75, ks = 2\pi, \phi_0 = 90^o$). 62

3.5 Backscattering echo width of three cylinders
($ka = 0.75, \phi_0 = 90^o$). 63

3.6 Far field pattern of a strip in the vicinity of a line source
(simulated by equal radii and equally spaced circular cylinders). 64

3.7 Far field pattern of a strip in the vicinity of a line source
(simulated by unequal radii and unequally spaced circular cylinders). 66

3.8 Far field pattern of a parabolic reflector fed by a line source
(simulated by equal radii and equally spaced circular cylinders). 67

3.9 Far field pattern of a parabolic reflector fed by a line source
(simulated by unequal radii and unequally spaced circular cylinders). 68

3.10 Far field pattern of a circular reflector fed by a line source
(simulated by equal radii and equally spaced circular cylinders). 70

3.11 Far field pattern of a corner reflector fed by a line source
(simulated by equal radii and equally spaced circular cylinders). 71

3.12 Far field pattern of a corner reflector fed by a line source
(simulated by unequal radii and unequally spaced circular cylinders). 72

3.13 Axial field vs. the number of cylinders. 75

3.14 Simulated parabolic cylindrical reflector antenna. 77

3.15 Far field pattern of solid and simulated parabolic cylindrical

	reflector antenna.	82
4.1	Schematic diagram of different dipoles.	84
4.2	Geometry of the problem.	86
4.3	The integration contours in the complex plane.	93
4.4	Input admittance $Y = G + jB$ for a dipole antenna ($h/a = 74.2$).	106
4.5	Input impedance $Z = R + jX$ for a dipole antenna ($h/a = 74.2$).	107
4.6	Current distribution on a dipole antenna ($h/a = 74.2$, $h = 0.5\lambda$).	109
4.7	Current distribution on a dipole antenna ($h/a = 74.2$, $h = 0.75\lambda$).	110
4.8	Normalized power pattern of dipole antenna ($h/a = 74.2$, $h = 0.5\lambda$).	111
4.9	Normalized power pattern of dipole antenna ($h/a = 74.2$, $h = 0.75\lambda$).	112
4.10	Normalized power patterns of multiply fed dipole antenna.	114
4.11	(a) current distribution. (b) Normalized power pattern.	116
5.1	Schematic diagram of a long dipole in the presence of cylinders.	123
5.2	Far field pattern of a long dipole antenna in the presence of a cylinder.	136
5.3	Effect of the dipole-cylinder separation on the field pattern.	137
5.4	Far field pattern of a long dipole in the presence of two cylinders.	138
5.5	Far field pattern of a simulated strip nearby a long dipole.	140
5.6	Far field pattern of a cylindrical parabolic reflector antenna.	141
5.7	Far field pattern of a cylindrical circular reflector antenna.	142
5.8	Far field pattern of a corner reflector antenna.	143
5.9	Far field pattern of simulated parabolic reflector antenna.	144
5.10	Far field pattern of simulated parabolic reflector antenna.	146

LIST OF PRINCIPAL SYMBOLS

N	number of strips or cylinders
(x, y, z)	cartesian coordinate system
(ρ, ϕ, z)	circular cylindrical coordinates
$2d$	strip width
E_z^{inc}	z-component of the incident electric field
$H_0^{(1)}(x)$	Hankel function of the first kind of order zero and argument x
k	wave number
λ	wavelength
ω	angular frequency
j	$\sqrt{-1}$
(u, v, z)	elliptic cylindrical coordinates
$Re_m^{(1)}$	even radial Mathieu functions of first kind and order m
$Ro_m^{(1)}$	odd radial Mathieu functions of first kind and order m
Se_m	even angular Mathieu functions of order m
So_m	odd angular Mathieu functions of order m
$N_m^{(e)}$	normalized factor for even angular Mathieu functions
$N_m^{(o)}$	normalized factor for odd angular Mathieu functions
$Re_m^{(3)}$	even radial Mathieu functions of third kind and order m
$Ro_m^{(3)}$	odd radial Mathieu functions of third kind and order m
$A_m^{(i)}$	scattering amplitudes of the ith strip or cylinder
$H_n^{(1)}(x)$	Hankel function of the first kind of order n and argument x
ϵ_n	Neumann's number (1 for $n = 0$ and 2 for $n \geq 1$)
De_m^n	coefficients of the infinite series of the even angular Mathieu functions
Do_m^n	coefficients of the infinite series of the odd angular Mathieu functions
E_z^s	z-component of the scattered field
$\bar{A}$	vector contains the scattering amplitudes of N strips or cylinders
$\bar{L}$	vector whose elements represent the excitation to N strips or cylinders

B	a matrix whose elements depend on the geometry of the N strips or cylinders
E_z^{tot}	z-component of the total far field
$E_n(\phi)$	far field pattern
C_n	intensity of the nth fictitious line source
ϕ_0	plane wave incident angle
E_0	plane wave amplitude
$W(\phi)$	echo width pattern
$P(\phi)$	scattered field pattern
ΔS_n	nth surface element
Z_0	intrinsic impedance of free space
α_n	amplitudes of current density expansion
$J_n(x)$	Bessel function of the first kind of argument x and order n
$H_n^{(2)}(x)$	Hankel function of the second kind of argument x and order n
b	cylinder radius
$\delta(x)$	Dirac delta function
β	complex wave number
$A_i(\xi)$	complex amplitude functions
Π_z	z-component of the electric Hertz vector
$I_t(z)$	total current distribution along the dipole
$e_-(\xi)$	Fourier transform of the electric field in the lower half plane
$e_+(\xi)$	Fourier transform of the electric field in the upper half plane
$i(\xi)$	Fourier transform of the current distribution along the dipole antenna
ϵ_0	permittivity of free space
V^s	voltage applied across the delta function gap of symmetrically driven dipole
V^a	voltage applied across the delta function gap of anti-symmetrically driven dipole
h	half length of the dipole

a	radius of the dipole
E_θ	θ-component of the electric field
γ	Euler's number (0.57721...)
Y	input admittance of the dipole antenna ($G + jB$)
$E_z^{(d0)}$	radiation field of the dipole
$E_z(s)$	z-component radiated field of the symmetrically fed dipole
$E_z(a)$	z-component radiated field of the anti-symmetrically fed dipole
$i_s(\xi)$	Fourier transform of the current distribution along the symmetrically fed dipole
$i_a(\xi)$	Fourier transform of the current distribution along the anti-symmetrically fed dipole
ρ_Γ	reflection coefficient at the dipole open end
$E_{zl}^{(cn)}$	z-component of the nth order scattered field from the lth cylinder
$E_z^{(dn)}$	z-component of the nth order scattered field from the dipole
$E_z^{(tn)}$	z-component of the nth order total electric field
H_ϕ	ϕ-component of the magnetic field

CHAPTER 1

INTRODUCTION

A directional radiation pattern with small beam width can be produced using a reflector antenna. In general, a reflector antenna consists of two major parts denoted as the reflector surfaces and the feed. In most cases the reflector surfaces are made from a conducting material. The feed can be a horn antenna, open ended waveguide antenna, crossed dipole, line source or long dipole for example. Large solid reflectors may be costly due to excessive material, heavy weight, high wind load and difficulties in manufacturing. Thus a need often exists to modify these reflectors such that the resulting scattering characteristics are maintained or improved.

It is well known that the reflection coefficient of a strip grating due to a normally incident electromagnetic wave is very close to unity when the slit width between two successive strips in the grating is less than a quarter wavelength [1]. This is due to the multiply scattered fields among the strips which act as an electrical shield of the grating slits. Therefore a grating with slit widths less than quarter wave length acts electrically as a solid surface while physically it is partly an open surface. When applying this phenomenon, the reflecting surface can be partially removed without changing the antenna radiation characteristics. Hence the substitution or simulation of a conducting continuous surface reflector by mesh screen, rods or cylinders, wires, plates, strips or post tips may save material without loss of electrical characteristics, and strength. In fact the wind loading of simulated reflectors decreases and the rigidity, particularly with cylinders, increases. Also the susceptibility to damage by target practice (e. g. bolts, arrows, etc.) of a simulated reflector antenna is less than for a solid surface antenna. On the other hand the simulated reflector antenna may be employed for spacecrafts where wind loading, extreme temperatures, rotation and translation are important design factors.

The concept of simulated reflector antennas has been investigated and used in many applications. For instance, search radars in airport and ship navigation systems already employ a rod simulated reflector antenna fed by a sectoral horn and scanned in azimuth to detect in both planes. Post tips have been used in building a radio astronomy parabolic circular dish of several kilometers diameter outside Kingston, Ontario. Also mesh screens have been used for simulating parabolic reflector antennas for radio and radar astronomy applications. Not only reflector antennas are simulated but also scattering surfaces or ground planes can also be simulated. The wire grid concept was used by Richmond for simulating two and three dimensional scattering surfaces [2], while Otteni [3] and Hill and Wait [4] studied the properties of a wire grid screen acting as a conducting ground plane. While it may be a sound idea to use wire grid for simulating a three dimensional conducting surface, parallel wires may by the same reasoning be used for simulating two dimensional conducting surfaces [5]. This latter possibility was also investigated by Richmond [6] who found that the scattering pattern of an array of parallel wires placed on a cylindrical trajectory was very close to that of the solid cylinder when a sufficiently large number of wires was used. The design analysis of simulated scattering surface by mesh screen or parallel wires is restricted to small radius wires. Therefore the main objective of this thesis is to propose a general theoretical design analysis for simulating a cylindrical scattering surface by parallel circular cylinders or strips. The excitation of any simulated cylindrical surface is considered as a line source while plane wave excitation is also included because the reflector antenna may operate in a receiving mode. Also for practical use the long dipole antenna is investigated and used later to excite the simulated surface. The cylinder diameter or strip width as well as the number of cylinders (or strips), separation between adjacent cylinders (or strips), location of the axis of cylinder (or strip) relative to the trajectory of the solid surface and the location and type of feed of the dipole (center fed, multiple feed, arbitrary feed, etc.) are the main design parameters. There are other design parameters that can be

included such as the conductivity of cylinders and strips and permittivity of any dielectric coating of the conducting cylinders or strips.

The problem of multiple scattering of a plane wave, a line source or a long dipole field by a planar array of parallel conducting circular cylinders or strips needs to be solved. There are essentially three different analytical procedures which may be used to obtain a representation for the scattered field by multiple objects while taking into account the multiple scattering effects. These three methods were classified by Twersky as the boundary value problem for a compound body, the self-consistent method based on the known response of isolated objects and the iterative method corresponding to successive scattering of the primary field [7]. The class of many object scattering problems, for which one may obtain a solution for the compound body by solving a boundary value problem, is small. It has been applied by Rayleigh in treating the problem of the sinusoidal profile of a reflection grating [8].

In the self-consistent method, previous knowledge of the responses of the isolated objects in the multi-object scattering problem is used in considering the incident field on each object as sum of the source field and the scattered field from all other objects [9,10]. Application of the boundary conditions on each object surface gives a set of algebraic equations in terms of the unknowns. This method was applied exactly by Young and Bertrand for the scattering of a plane acoustic wave by two circular infinitely long conducting cylinders [11]. Also Millar solved the problem of scattering of a plane wave by N equi-spaced small cylinders in a row [12]. He used Green's theorem together with the appropriate boundary conditions to calculate a set of integral equations over the unknown function on the cylinders. A perturbation method was employed to reduce the integral equations to a set of linear algebraic equations which can be solved for the far-zone field and the scattering cross-section. An approximate treatment of the self-consistent method was used by Zitron and Karp [13,14] and Karp and Russek [15]; their approximations restrict the solution to the case where the spacing distances between the objects is much greater than the

maximum dimension of any object. The latter technique was recently extended to the case of scattering of plane waves by wide double wedges [16]. Hansen used the integral equation approach in order to calculate the diffracted field of a plane acoustic wave through two or more parallel slits in a plane screen [17]. The scattering of plane waves by two or N co-planer strips was the subject of articles by Saermark who formulated the general problem for different orientations of the strips but gave only a solution for the co-planar case [18,19]. Also he truncated the infinite series involved in the solution after one term assuming that the strip widths are small.

The iterative procedure has been widely used in multiple scattering problems [20-27]. The method initially calculates the scattered field from each object in isolation which is considered as the first order scattered field. The second order scattered field from any object can be generated by considering the first order field scattered from the other objects as incident field on this object. For the higher orders the same procedure has to be applied, in which the leading order of scattered field can be generated from the preceding one. In each iteration the boundary conditions have to be applied in order to calculate the scattering amplitudes for the new order of scattering. The method usually involves a recurrence relation for the higher order scattered fields in terms of lower orders. The advantage of this procedure lies in calculating the scattering amplitudes for each order of scattering which lead, for simple cases, to an explicit expression for the multiply scattered fields rather than a matrix equation as in the self-consistent method. Unfortunately these various analytic methods are applicable only to problems with simple geometry. For complicated geometries numerical methods along with the integral equation formulation of a compound body may have to be employed.

The rapid development of computer capabilities as well as numerical techniques have increased the interest in treating electromagnetic scattering problems involving arbitrarily shaped objects [28-31]. The moment method described by Harrington [32] has been employed by many authors for solving multi-object scattering problems [33].

For the two dimensional case the method is based on solving an integral equation for the current density on the object surface. Once the current density is evaluated, the electric field everywhere can be calculated. For large size cylindrical surfaces two different approaches have been employed for modifying the moment method. The first by Kinzel [34], who suggested dividing the scatterer cross-section contour into a number of small sections where each section might be of the order of one wavelength long. Each section is then further divided into subsections. Evaluation of the surface current is then essentially based on the assumption that the current on one section is significantly affected by currents in adjoining sections. The second approach by Azarbar and Shafai [35] considers the induced surface current as a sum of the physical optics and an unknown difference current. This difference current is then found by applying the moment method. Such approaches are employed for reducing computation time and storage memory and increasing the computation accuracy.

It should be pointed out that many techniques have been developed to handle edge singularities in the current distribution [36,37]. Wilton and Govind [38] incorporated an edge correction term in the moment method solution in order to avoid the edge singularities. Tsai et al. [39] sampled the current function at progressively smaller intervals near the edges. The idea of incorporating an edge correction was modified by Richmond [40] who solved the problem of scattering of a plane wave by a strip or strip grating. He included the edge mode in the basis functions of the current distribution which improved the convergence of the moment method solution. His results were compared favourably with other workers.

For the three dimensional case, integral equations are obtained and can be solved by a variety of methods and are widely used in the investigation of scattering and radiation by metallic objects. The most popular technique is the wire-grid model [2] which has been remarkably successful in many problems, particularly in those requiring the prediction of far-field quantities such as radiation patterns and radar

cross-section. Surface patch models are also used in which the object is described by non-planar quadrilateral patches for the magnetic field integral equation [41], planar quadrilateral patches for the electric field integral equation [42], or by plane triangular patches [43].

In practice, the feed of a simulated reflector antenna has to be of a finite nature rather than an infinite line source. The long dipole antenna is one of the suitable feeds for cylindrical reflectors. Therefore it is chosen to be the feed of the simulated cylindrical reflector in this thesis. The long dipole antenna has been extensively investigated by many authors. For instance, integral expressions for the outgoing current waves on a long antenna have been represented in the form of series expansions by Hallen [44]. Later, Hallen [45] used the Wiener-Hopf technique to find the reflection coefficient of a current wave at the open end of a dipole antenna. King [46] obtained a solution for the current distribution and input impedance of asymmetrically driven as well as sleeve dipoles. He considered two different currents along the antenna which are smoothly joined at the feed point. He derived two integral equations for the current distribution and solved them by the method of successive approximations. Using the Wiener-Hopf technique, Hallen [47] gave an exact solution of the integral equation for the current on a tube-shaped cylindrical antenna including all successively reflected current waves. He showed that his earlier approximate series solution [44] can be obtained by iterations of this solution. Wu [48] used the Wiener-Hopf technique to calculate the radiation pattern and input admittance of the dipole antenna with the assumption that the vector potential equals zero on the extension of the antenna. Chen and Keller [49] assumed that the current waves consist of three terms, one emanating from the gap and the other two arising from reflections at the open ends. They calculated the reflection coefficient at the open ends and used the current on the infinitely long antenna as the source current. They included the gap thickness in their solution and derived two expressions for the current waves, one near the gap and the other far from the gap. King

and Wu [50] obtained an approximate solution which they presented in a trigonometric form for the current distribution and input admittance for the off-center driven cylindrical antenna. They solved the sleeve dipole when the driving voltages are in phase and out of phase by 180^o. A superposition of these two cases yielded the solution for the asymmetrically driven dipole antenna. Shen [51] gave a formula for the current distribution on a long dipole antenna based on Wu's work [48] which he then modified in order to increase the accuracy of the current formula near the driving point and the ends. In another article, Shen et al. [52] attempted to simplify the current formula for the arbitrarily fed dipole antenna, by using a three current formula. His solution was based on the current distribution on the infinitely long antenna and considered the current on the finite one as the current outgoing from the source plus two currents reflected from the ends.

The infinitely long dipole antenna has also been studied by Duncan [53], Kunz [54], Fante [55] and Miller [56]. Miller's treatment for the input admittance is the simplest and most accurate , particularly since it includes the gap thickness which is important in the susceptance calculation. Hurd [57] gave a variational solution for input admittance of a long cylindrical antenna which he repeated for a long center-fed dipole antenna using the Wiener-Hopf technique [58].

The presence of a cylindrical scatterer in a long dipole antenna field will add difficulty in evaluating the multiple scattering terms which have not been investigated before. Moreover the addition of more cylindrical scatterers in the dipole field will further complicate the problem of multiple scattering. In earlier investigations the interaction effects between the dipole and a cylindrical scatterer were not considered [59]. Also the scattering of the long dipole field by more than one cylindrical scatterer has received less attention. Carter [60] reported the effects of an infinitely long circular cylinder on the radiation patterns of vertical and horizontal infinitesimal dipoles. His method is based on obtaining the far field directly by means of reciprocity between the radiating element and a passive receiving dipole

situated in the far field of the radiator. A theoretical examination was also made by Luck [61] for the electromagnetic fields of infinitesimal electric dipoles in the presence of infinitely long, perfectly conducting elliptic and circular cylinders. He applied the Green's function approach to that problem and obtained expressions for the fields in terms of an integration in the complex plane. He also gave a simplified expression for the far-zone field. A dipole in the presence of a ground plane, which is finite in one dimension and infinite in the other, was included in Luck's work as a special case of the elliptic cylinder when the minor axis vanishes.

For a finite cylinder in the presence of an infinitesimal electric dipole, Kuehl [62] derived approximate expressions for the two components of the far-zone electric field. He considered the case of a radial dipole and used the current distribution on the infinite cylinder as an approximate estimation of the current on the finite one. His solution is valid when the length of the cylinder is much larger than the wavelength. A comparison of his theoretical results with experimental data showed reasonable agreement. Goldhirsh et al. [63] used a numerical method for solving the same problem. They used the integral equation formulation to calculate the surface current density on the cylinder surface. By dividing the cylinder surface into a set of N grids and using the boundary conditions at each grid center they obtained $2N$ simultaneous equations for the two components of the surface current. Once the surface current density is calculated, the secondary far-zone electric fields can be deduced by a straightforward integration procedure. Another numerical approach based on the plane-wave spectrum was introduced by Mao and Cheng [64] who considered the problem of a conducting tubular cylinder of finite length situated in the neighbourhood of a 2-by-4 dipole array. They represented the array field in terms of plane waves of different amplitudes, and by calculating the axial and circumferential current distributions induced on the cylinder due to a unit-magnitude incident plane wave, the scattered field due to the spectrum of plane waves was calculated.

The dielectric cylinder in the presence of an infinitesimal electric dipole has also been investigated by Tsandoulas [65]. He used the differential equation approach in order to calculate the formal exact solution for the fields due to an axial electric dipole in the presence of a homogeneous isotropic infinite circular cylinder. The scattered field was obtained in an integral form in which an asymptotic expansion of the integrals yielded the far field. He pointed out that more directive patterns could be obtained using a dielectric rather than a conducting cylinder.

In Chapter 2 an infinitely long strip is used as the basic simulating block for cylindrical reflectors. The problem of scattering of a line source field by N conducting strips is considered. Also plane wave excitation is considered as a special case when the line source goes to infinity. Two different self consistent methods are employed for solving this problem. The first is an exact solution in which the scattered field from each strip is written in terms of a Fourier infinite series involving Mathieu functions with unknown scattering coefficients. A simultaneous application of the boundary conditions on each strip surface leads to a set of algebraic equations in the unknown scattering coefficients which can be solved easily. This method is throughout denoted as the boundary value solution. The second method is an asymptotic solution based on the Karp and Russek technique [15]. In this method an artificial line source of unknown intensity is assumed at the center of each strip in order to account for the multiple interactions. The total scattered field from each strip is considered as the direct scattered field due to the incident wave plus the scattered fields due to all artificial line sources at the centers of the other strips. By matching the partial scattered fields at specific directions, the line source intensities are calculated. It is worthwhile to mention that the time dependence $e^{-j\omega t}$ assumed in Chapter 2, for comparing some basic analytical expressions of scattering by a single strip with those given in [77], is changed to $e^{j\omega t}$ in the rest of the thesis, for comparing with other references. However, suitable special functions (i.e. Mathieu and Hankel functions) are employed depending on the time dependence in each case.

Results showing the echo width patterns due to a plane wave incident on two, four and eight strips are calculated. Also the echo width pattern of a simulated circular cylinder excited by a plane wave is obtained. Far field patterns of a simulated wide strip, corner reflector, circular cylindrical reflector and a parabolic cylindrical reflector fed by a line source are obtained and compared favourably with the corresponding solid reflector cases.

In Chapter 3 the methods used in Chapter 2 are employed again when the basic simulating object is a conducting circular cylinder. The solution in the case of plane wave excitation is presented in parallel with the line source excitation. The echo width patterns and the back-scattering echo width are calculated for different numbers of cylinders. Also, examples of simulated circular and parabolic cylindrical reflectors and corner reflector antennas fed by line sources are presented. It is also found that using cylinders with different radii and spacing along the reflector trajectory improves the radiation characteristics of the antenna.

In Chapter 4 the long dipole antenna in isolation is examined for use as feed for the simulated reflector. An extension to Hurd's work [58] on the input admittance of long center fed dipole is introduced. The analysis used closely parallels that given by Hurd with appropriate modifications. The arbitrarily fed dipole is considered as a superposition of symmetrically and anti-symmetrically fed dipoles while the multiply fed dipole is treated as a superposition of the arbitrarily fed dipole. Accurate expressions for the current distribution, radiation pattern and input admittance of the arbitrarily fed dipole are derived. Results for the input admittance, current distribution and radiation patterns are in very good agreement with published data.

In Chapter 5 the reflector simulated by circular cylinders with long dipole feed is examined. This requires consideration of the problem of a long dipole antenna in the vicinity of N infinitely long conducting circular cylinders. The dipole field is considered as incident on the cylinders. Multiply scattered fields are then introduced

among the cylinders as well as between each cylinder and the dipole. The method employed in solving this problem is a combination of the self consistent and iterative methods. The dipole radiation field is considered as the incident field on the cylinders, then the first order scattered field from the cylinders (including all multiple interactions among the cylinders) is found using method 1 in Chapter 3. The first order scattered field from the cylinders is then considered as the incident field on the dipole and by calculating the current density on the dipole surface, we obtain the first order far scattered field from the dipole. Again this first order scattered field is considered as incident on the cylinders and a second order scattered field from the cylinders is then calculated. By repeating this process the higher order scattered fields from the dipole and cylinders are obtained. Results for the far field patterns for one and two cylinders in the dipole vicinity are given. Also examples illustrating the radiation patterns of simulated parabolic and circular cylindrical and corner reflector antennas are presented. It is also shown that one can improve the simulated reflector pattern over the solid reflector by proper choice of the radii and positions of simulating cylinders along the reflector trajectory.

Finally Chapter 6 draws the general conclusions of this thesis and possible areas of future research arising from this project.

CHAPTER 2

SIMULATION OF CYLINDRICAL SCATTERING SURFACE BY CONDUCTING STRIPS

2.1 *Introduction*

In this chapter an infinitely long conducting strip is used as a basic block for simulation purposes. The exact solution of a plane wave scattered by a single conducting strip was given by Morse and Rubenstein in terms of Mathieu functions by solving the Helmholtz equation in elliptic cylindrical coordinates [66]. Also approximate solutions for low and high frequencies were studied by many other investigators [67-70]. The strip grating was also examined theoretically and experimentally by many authors while the multiple scattering of an electromagnetic wave by a finite number of strips has received less attention. The simulation of cylindrical scattering surface by conducting strips needs the solution of multiple scattering of a plane or cylindrical wave by N infinitely long conducting strips. Therefore the general solution for this problem is presented using two different methods. The solution is given for a line source excitation, while the plane wave excitation is considered later as a special case when the line source goes to infinity. The two methods are classified as self consistent methods in which the first is an exact treatment for the problem while the second is an approximate treatment using the Karp and Russek technique [15]. The latter technique is valid when the distance between any two strips is much greater than the width of either strip.

The echo width patterns for different configurations of strips due to plane wave incidence are evaluated in this chapter by both methods. The same methods are also used to calculate the far field patterns of different simulated cylindrical reflector antennas. A comparison between these field patterns and those corresponding to

solid cylindrical reflectors is illustrated. A brief description of the method of moments for solving solid cylindrical reflector antennas is also presented.

2.2 *Boundary value solution*

Figure 2.1 shows a cross section of N parallel infinitely long conducting strips with nonintersecting edges. The strips are situated such that their axes are parallel to the z-axis of the local coordinate system $(x\ ,y\ ,z)$. The center of the ith strip is located at $(x_i\ ,y_i)$ with respect to the global coordinates, while $2d_i$ is its width. The strips are randomly oriented such that the angle between the direction of orientation of the ith strip and the x-axis is ψ_i. For the sake of convenience N coordinate systems are defined, one at the center of each strip. The plane of the ith strip lies in the $x_i'-z_i'$ plane.

Consider a line source located at (x_0,y_0) as shown in Fig. 2.1. The incident field on the strips due to this line source is given by

$$E_z^{inc} = H_0^{(1)}(k|\bar{\rho} - \bar{\rho}_0|) \tag{2.1}$$

where (ρ,ϕ) and (ρ_0,ϕ_0) are the cylindrical coordinates of the observation point and the line source with respect to the global coordinate system, respectively, while $H_0^{(1)}(x)$ is the first kind Hankel function of order zero and argument x. k is the wave number $2\pi/\lambda$ where λ is the wave length. The time dependence is considered as $e^{-j\omega t}$ and omitted throughout. In this analysis the E-polarized field will be considered where the electric field has only a z-component. The H-polarized field when the magnetic field has only a z-component can be treated in the same way with appropriate boundary conditions.

The incident wave may be transformed to any of the coordinate systems defined at the strip centers and then expanded in terms of elliptic wave functions [71]. Upon transforming the incident field to the ith coordinates, one obtains

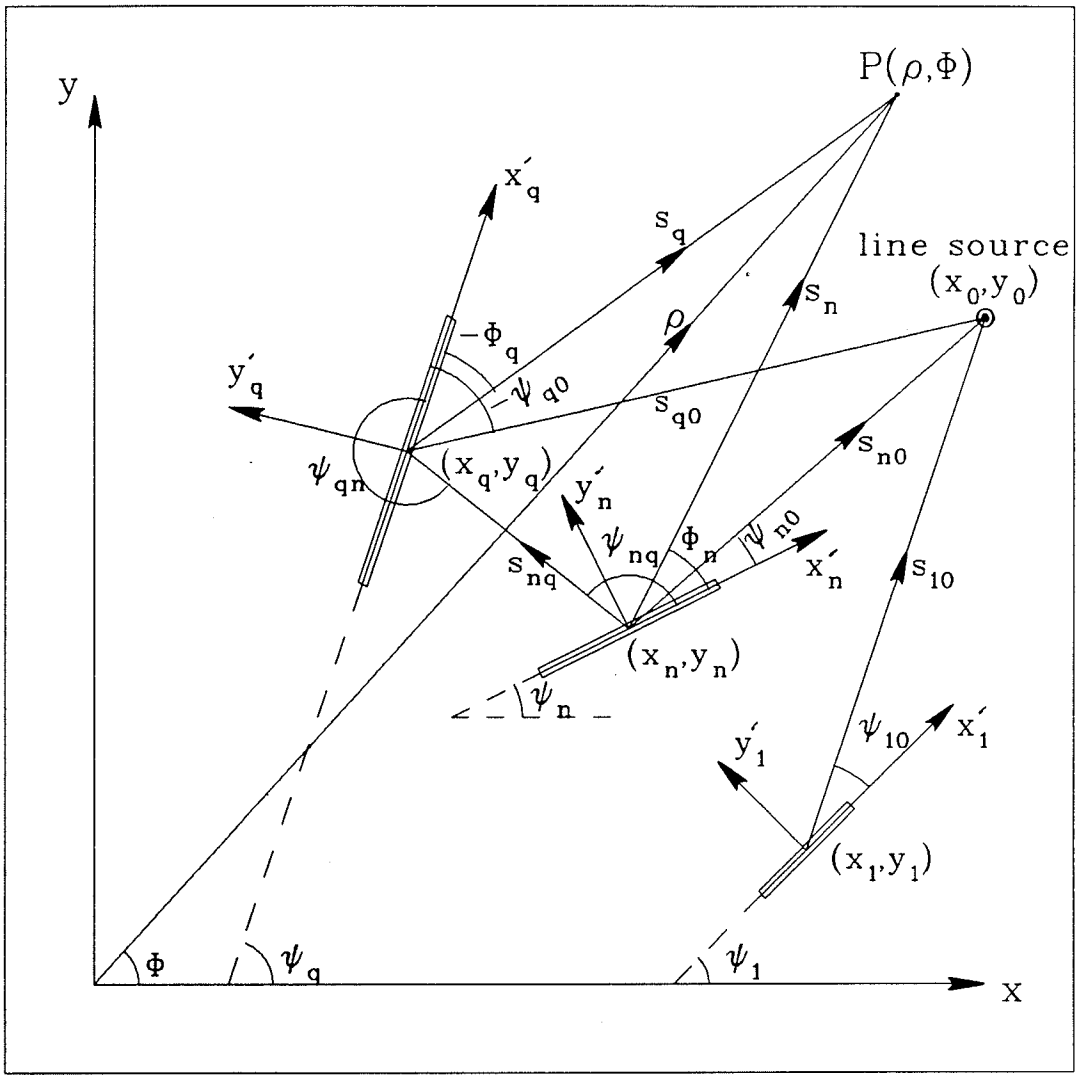

Fig. 2.1 : Geometry of the problem.

$$E_z^{inc} = 4\left[\sum_{m=0}^{\infty} \frac{Se_m(a_i,\eta_{i0})}{N_m^{(e)}(a_i)} Se_m(a_i,\eta_i) \begin{cases} Re_m^{(1)}(a_i,\zeta_{i0})\ Re_m^{(3)}(a_i,\zeta_i) & , \quad u_i > u_{i0} \\ Re_m^{(1)}(a_i,\zeta_i)\ Re_m^{(3)}(a_i,\zeta_{i0}) & , \quad u_i < u_{i0} \end{cases}\right.$$

$$\left. + \sum_{m=1}^{\infty} \frac{So_m(a_i,\eta_{i0})}{N_m^{(o)}(a_i)} So_m(a_i,\eta_i) \begin{cases} Ro_m^{(1)}(a_i,\zeta_{i0})\ Ro_m^{(3)}(a_i,\zeta_i) & , \quad u_i > u_{i0} \\ Ro_m^{(1)}(a_i,\zeta_i)\ Ro_m^{(3)}(a_i,\zeta_{i0}) & , \quad u_i < u_{i0} \end{cases}\right] \tag{2.2}$$

where i takes the values 1 to N, $Re_m^{(1)}$ and $Ro_m^{(1)}$ are even and odd modified radial Mathieu functions of first kind and order m, while Se_m and So_m are even and odd angular Mathieu functions of order m, respectively. $N_m^{(e)}$ and $N_m^{(o)}$ are normalized factors defined in [70]. $Re_m^{(3)}$ and $Ro_m^{(3)}$ are the even and odd modified radial Mathieu functions defined as

$$Re_m^{(3)}(x,y) = Re_m^{(1)}(x,y) + j\ Re_m^{(2)}(x,y) \tag{2.3}$$

Here $Re_m^{(2)}$ is the even modified radial Mathieu function of second kind and order m. A similar definition for the odd function $Ro_m^{(3)}$ can also be made. The arguments a_i, ζ_i, η_i, ζ_{i0} and η_{i0} are defined as follows

$$a_i = kd_i \tag{2.4}$$

$$\zeta_i = \cosh u_i \tag{2.5}$$

$$\eta_i = \cos v_i \tag{2.6}$$

$$\zeta_{i0} = \left[\frac{1}{2}\left(\frac{s_{i0}^2}{d_i^2} + 1\right) + \sqrt{\frac{1}{4}\left(\frac{s_{i0}^2}{d_i^2} + 1\right)^2 - \frac{x_{i0}^2}{d_i^2}}\right]^{1/2} \tag{2.7}$$

$$\eta_{i0} = \frac{x_{i0}}{\zeta_{i0}\, d_i} \tag{2.8}$$

where

$$s_{i0} = \sqrt{(y_i - y_0)^2 + (x_i - x_0)^2} \tag{2.9}$$

$$\psi_{i0} = \tan^{-1}\left[\frac{y_0 - y_i}{x_0 - x_i}\right] - \psi_i \tag{2.10}$$

$$x_{i0}' = s_{i0} \cos \psi_{i0} \tag{2.11}$$

$$y_{i0}' = s_{i0} \sin \psi_{i0} \tag{2.12}$$

while (u_i, v_i) and (u_{i0}, v_{i0}) are elliptic cylindrical coordinates of the observation point and the line source with respect to the coordinates of the i th strip, respectively.

The scattered field from the i th strip can be represented by a Fourier infinite series of Mathieu functions, i. e.

$$E_{z(i)}^s = \sum_{m=0}^{\infty} A_m^{(i)} \, Re_m^{(3)}(a_i, \zeta_i) \, Se_m(a_i, \eta_i) \tag{2.13}$$

where $A_m^{(i)}$ are the scattering coefficients of the i th strip to be calculated.

It is assumed that the scattered field (2.13) includes all interactions between the i th strip and all other strips. To apply the boundary conditions on the surface of each strip it is necessary to transform the scattered field from one coordinate system to another (i.e. from the q th coordinates to the l th coordinates). This can be done using the addition theorem of Mathieu function [72-75], namely

$$Re_m^{(3)}(a_q, \zeta_q) \, Se_m(a_q, \eta_q) = \sum_{n=0}^{\infty} U_{n,m}(l, q) \, Re_n^{(1)}(a_l, \zeta_l) \, Se_n(a_l, \eta_l)$$

$$+ \sum_{n=1}^{\infty} E_{n,m}(l, q) \, Ro_n^{(1)}(a_l, \zeta_l) \, So_n(a_l, \eta_l) \tag{2.14}$$

where

$$U_{n,m}(l,q) = \frac{\pi\,(j)^{n-m}}{N_n^{(e)}(a_l)} \sum_{i=0}^{\infty} \sum_{p=0}^{\infty} (j)^{-i-p}\, De_p^n(a_l)\, De_i^m(a_q)$$

$$\left\{ H_{p-i}^{(1)}(ks_{lq}) \cos(p\psi_{lq} - i\psi_{ql}) + (-1)^i\, H_{i+p}^{(1)}(ks_{lq}) \cos(p\psi_{lq} + i\psi_{ql}) \right\} \qquad (2.15)$$

$$E_{n,m}(l,q) = \frac{\pi\,(j)^{n-m-1}}{2N_n^{(o)}(a_l)} \sum_{i=0}^{\infty} \sum_{p=0}^{\infty} \epsilon_i\, (j)^{-i-p}\, Do_p^n(a_l)\, De_i^m(a_q)$$

$$\left\{ H_{p-i}^{(1)}(ks_{lq}) \cos(p\psi_{lq} - i\psi_{ql}) + (-1)^i\, H_{i+p}^{(1)}(ks_{lq}) \cos(p\psi_{lq} + i\psi_{ql}) \right\} \qquad (2.16)$$

$$s_{lq} = \sqrt{(x_l - x_q)^2 + (y_l - y_q)^2} \qquad (2.17)$$

$$\psi_{lq} = \tan^{-1}\left[\frac{y_q - y_l}{x_q - x_l}\right] - \psi_l \qquad (2.18)$$

Here ϵ_i takes the value 1 for $i=0$ and 2 for $i>0$. Only the terms in which $(n-p)$ and $(i-m)$ are even under the summation signs in (2.15) and (2.16) are considered, while other terms are zeros. The constants De_m^n and Do_m^n are coefficients of the infinite series of the angular Mathieu functions in terms of trigonometric functions as defined in [76].

Now the total electric field (i.e. incident plus scattered) can be completely written in any of the coordinate systems given above using the addition theorem of Mathieu functions. The boundary condition on the surface of each strip is given by

$$E_z^{inc} + \sum_{n=1}^{N} E_{z(n)}^{s} = 0 \qquad , \quad \zeta_i = 1 \qquad , \quad i = 1, 2, \ldots, N \qquad (2.19)$$

Applying this boundary condition to the surface of the ith strip and using the addition theorem of Mathieu functions leads to

$$4 \sum_{m=0}^{\infty} \frac{Re_m^{(1)}(a_i,1)}{N_m^{(e)}(a_i)} Se_m(a_i,\eta_i)\, Re_m^{(3)}(a_i,\zeta_{i0})\, Se_m(a_i,\eta_{i0})$$

$$+ \sum_{\substack{n=1 \\ n\neq i}}^{N} \sum_{m=0}^{\infty} A_m^{(n)} \sum_{l=0}^{\infty} U_{l,m}(i,n)\, Re_l^{(1)}(a_i,1)\, Se_l(a_i,\eta_i)$$

$$+ \sum_{m=0}^{\infty} A_m^{(i)}\, Re_m^{(3)}(a_i,1)\, Se_m(a_i,\eta_i) = 0 \qquad (2.20)$$

Multiplying by $Se_n(a_i,\eta_i)$ and integrating over v_i from 0 to 2π, we obtain

$$A_m^{(i)} = \frac{-4}{N_m^{(e)}(a_i)} Se_m(a_i,\eta_{i0})\, Re_m^{(3)}(a_i,\zeta_{i0}) \frac{Re_m^{(1)}(a_i,1)}{Re_m^{(3)}(a_i,1)}$$

$$- \sum_{\substack{n=1 \\ n\neq i}}^{N} \frac{Re_m^{(1)}(a_i,1)}{Re_m^{(3)}(a_i,1)} \sum_{l=0}^{\infty} U_{m,l}(i,n)\, A_l^{(n)} \qquad (2.21)$$

The application of similar boundary conditions on the surfaces of the other strips leads to $(N-1)$ equations similar to (2.21) which are written in N matrix equations given by

$$A^{(l)} = L^{(l)} + \sum_{\substack{s=1 \\ s\neq l}}^{N} B^{(ls)} A^{(s)} \qquad , \quad l = 1, 2, 3, \ldots, N \qquad (2.22)$$

where $A^{(l)}$ and $A^{(s)}$ are infinite vectors containing the scattering coefficients corresponding to l th and s th strips, respectively, while $B^{(ls)}$ are infinite dimensional matrices with elements

$$B_{nm}^{(ls)} = \frac{-Re_n^{(1)}(a_l,1)}{Re_n^{(3)}(a_l,1)} U_{n,m}(l,s) \qquad (2.23)$$

$L^{(l)}$ are infinite vectors whose elements are given by

$$L_m^{(l)} = \frac{-4}{N_m^{(e)}(a_l)} \frac{Re_m^{(1)}(a_l,1)}{Re_m^{(3)}(a_l,1)} Re_m^{(3)}(a_l,\zeta_{l0})\, Se_m(a_l,\eta_{l0}) \tag{2.24}$$

Equations (2.22) have infinite dimensions and they should be truncated in order to generate a numerical solution. If a conducting strip is the basic block for simulation, a number of Mathieu function terms should be taken such that the convergence of the infinite series can be achieved. Since for wide strips a large number of terms must be considered, we only consider narrow strips which are suitable for simulation purposes and where few terms of Mathieu functions are sufficient to give accurate results. Moreover the convergence check is built into the computer program such that enough terms of the Mathieu function are taken. Assuming the number of terms necessary for the convergence is M, equations (2.22) are lumped together in a single matrix equation of the form

$$A = L + BA \tag{2.25}$$

where B is a square matrix of dimension (NM), A and L are vectors of the same dimension. Equation (2.25) is now written in the form

$$(I - B)A = L \tag{2.26}$$

which can be easily solved as a set of ordinary linear algebraic equations of the unknown vector A. The vector A of dimension (NM) contains all the scattering coefficients of the N strips.

Now, upon solving equation (2.26), the scattering coefficients of the N strips are available, and accordingly the scattered field from the N strips is completely defined. Hence

$$E_z^{tot} = H_o^{(1)}(k|\bar{\rho} - \bar{\rho}_o|) + \sum_{l=1}^{N} \sum_{m=0}^{M} A_m^{(l)}\, Re_m^{(3)}(a_l,\zeta_l)\, Se_m(a_l,\eta_l) \tag{2.27}$$

The far field can be evaluated using the asymptotic expansion of $Re_m^{(3)}$ and $H_0^{(1)}$. For $Re_m^{(3)}$ we have,

$$Re_m^{(3)}(a,\zeta) = \frac{1}{\sqrt{a\zeta}}\, e^{j(a\zeta - \frac{2m+1}{4}\pi)} \tag{2.28}$$

while the asymptotic value of $H_0^{(1)}(x)$ is given by

$$H_0^{(1)}(x) \approx \sqrt{\frac{2}{\pi x}}\, e^{j(x - \frac{\pi}{4})} \tag{2.29}$$

Also, for large product $a\zeta$ one can assume $a_i \zeta_i = k\rho_i$, where i takes the values 1 to N, while $\eta_i = \cos\phi_i$ in the far field calculation. In addition to the previous approximations we employ the approximation

$$\rho_l \approx \rho - (x_l \cos\phi + y_l \sin\phi) \tag{2.30}$$

Now, the total far electric field from the system of N strips and the line source is given by

$$E_z^{tot} = c'(k\rho)\, E_n(\phi) \tag{2.31}$$

where

$$E_n(\phi) = e^{-jk(x_0\cos\phi + y_0\sin\phi)}$$

$$+ \sqrt{\frac{\pi}{2}} \sum_{l=1}^{N} e^{-jk(x_l\cos\phi + y_l\sin\phi)} \sum_{m=0}^{M} (-j)^m\, A_m^{(l)}\, Se_m(a_l, \cos(\phi - \psi_l)) \tag{2.32}$$

$$c'(k\rho) = \sqrt{\frac{2}{\pi k\rho}}\, e^{jk\rho} e^{-j\frac{\pi}{4}} \tag{2.33}$$

It should be noted that multiple interactions among strips are included in the scattering coefficients.

2.3 *Asymptotic solution*

The asymptotic technique used for solving the problem at hand is based on considering the scattered field from each strip as a sum of the scattered field from that strip due to cylindrical wave incidence plus the scattered field due to fictitious line sources of unknown intensities located at the centers of the other strips. The line sources account for the multiple interaction. The technique is valid as long as the separation between any two strips is large compared to either strip width. In order to carry out this technique, one needs the far scattered field from a single strip due to line source excitation. Thus, consider a line source whose field (2.1) is incident on an infinitely long conducting strip of width $2d_p$. The strip center is located at (x_p, y_p), while the plane of the strip is inclined with respect to the x-axis by an angle ψ_p. Following the solution given in [77], the far scattered field is given by

$$E_z^s = c'(k\rho_p)\, g(a_p, \phi_p, \zeta_{p0}, \eta_{p0}) \tag{2.34}$$

where

$$g(a_p, \phi_p, \zeta_{p0}, \eta_{p0}) = -\sqrt{8\pi} \sum_{m=0}^{\infty} \frac{(-j)^m}{N_m^{(e)}(a_p)} \frac{Re_m^{(1)}(a_p, 1)}{Re_m^{(3)}(a_p, 1)} Re_m^{(3)}(a_p, \zeta_{p0})$$

$$Se_m(a_p, \eta_{p0})\, Se_m(a_p, \cos\phi_p) \tag{2.35}$$

while (x_p', y_p', z_p') is a cartesian coordinate system defined at the strip center such that the strip plane lies in the $x_p'-z_p'$ plane and the line source is located at (x_0, y_0). ζ_{p0} and η_{p0} are given by (2.7) and (2.8), respectively.

Now, consider the problem of N strips shown in Fig. 2.1. Assume a fictitious line source at the center of each strip. In this case the total far scattered field from the l th strip due to a line source excitation is given by

$$E_{z(l)}^s = c'(k\rho_l) \left\{ g(a_l, \phi_l, \zeta_{l0}, \eta_{l0}) + \sum_{\substack{p=1 \\ p \neq l}}^{N} C_p\, g(a_l, \phi_l, \zeta_{lp}, \eta_{lp}) \right\} \tag{2.36}$$

where ζ_{lp} and η_{lp} are given by expressions similar to (2.7) and (2.8), respectively, while C_p is the unknown intensity of the p th line source.

To obtain the unknown intensities of the line sources, the partial scattered field from the s th strip due to the scattered field from the l th strip can be evaluated in two ways. First, at $\phi_l = \psi_{ls}$ the value of $E^s_{z(l)}[c'(k\rho)]^{-1}$ can be considered as the intensity of a line source. Thus

$$E^s_{z(sl)} = \left\{ g(a_l, \psi_{ls}, \zeta_{l0}, \eta_{l0}) + \sum_{\substack{p=1 \\ p \neq l}}^{N} C_p \; g(a_l, \psi_{ls}, \zeta_{lp}, \eta_{lp}) \right\}$$

$$c'(k\rho_s)\, g(a_s, \phi_s, \zeta_{sl}, \eta_{sl}) \quad , \quad s = 1, 2, 3, \ldots, N \tag{2.37}$$

Second, this partial scattered field is given by

$$E^s_{z(sl)} = C_l \; c'(k\rho_s)\, g(a_s, \phi_s, \zeta_{sl}, \eta_{sl}) \quad , \quad s = 1, 2, 3, \ldots, N \quad , \quad s \neq l \tag{2.38}$$

By equating (2.37) and (2.38), taking into account the partial scattered field from all strips due to the scattered field from the l th strip, the line source intensities can be evaluated from the following expressions :

$$\sum_{\substack{s=1 \\ s \neq l}}^{N} g(a_l, \psi_{ls}, \zeta_{l0}, \eta_{l0}) + \sum_{\substack{s=1 \\ s \neq l}}^{N} \sum_{p=1 \; p \neq l}^{N} C_p \; g(a_l, \psi_{ls}, \zeta_{lp}, \eta_{lp}) = (N - 1)\, C_l \tag{2.39}$$

The last equation can be presented in the following matrix form

$$B \; C = L \tag{2.40}$$

where

$$L_l = - \sum_{\substack{s=1 \\ s \neq l}}^{N} g(a_l, \psi_{ls}, \zeta_{l0}, \eta_{l0}) \tag{2.41}$$

$$B_{lp} = \begin{cases} \sum_{\substack{s=1 \\ s \neq l}}^{N} g(a_l, \psi_{ls}, \zeta_{lp}, \eta_{lp}) & , \quad p \neq l \\ (1 - N) & , \quad p = l \end{cases} \tag{2.42}$$

Equation (2.40) can be easily solved as a set of N linear algebraic equations of unknown vector C which contains the intensities of the line sources. Once they are calculated, the total far field is given by

$$E_z^{tot} = c'(k\rho)\, E_n(\phi) \tag{2.43}$$

where

$$E_n(\phi) = e^{-jk(x_0 \cos\phi + y_0 \sin\phi)} + \sum_{l=1}^{\infty} e^{-jk(x_l \cos\phi + y_l \sin\phi)} \cdot$$

$$\left\{ g(a_l, \phi - \psi_l, \zeta_{l0}, \eta_{l0}) + \sum_{\substack{s=1 \\ s \neq l}}^{N} C_s\, g(a_l, \phi - \psi_l, \zeta_{ls}, \eta_{ls}) \right\} \tag{2.44}$$

2.4 *Plane wave excitation*

2.4.1 **Boundary value solution**

Consider the special case when the radial position of the line source in the above formulation goes to infinity. In this case one uses the asymptotic expansion of the Hankel function and calculates the incident field as

$$E_z^{inc} = E_0\, e^{-jk(x \cos\phi_0 + y \sin\phi_0)} \tag{2.45}$$

which is a plane wave impinging at an angle ϕ_0 with respect to the x-axis. The incidence angles of this plane wave with respect to the other coordinate systems are given by

$$\phi_{i0} = \phi_0 - \psi_i \qquad , \qquad i = 1, 2, \ldots, N \tag{2.46}$$

The plane wave in (2.45) can be transformed and expanded in terms of the ith coordinate system as

$$E_z^{inc} = E_0 \sqrt{8\pi}\, e^{-jk(x_i \cos\phi_0 + y_i \sin\phi_0)} \sum_{m=0}^{\infty} j^{-m} \left[\frac{1}{N_m^{(e)}(a_i)} Re_m^{(1)}(a_i, \zeta_i)\, Se_m(a_i, \eta_i) \right.$$

$$\left. Se_m(a_i, \cos\phi_{i0}) + \frac{1}{N_m^{(o)}(a_i)} Ro_m^{(1)}(a_i, \zeta_i)\, So_m(a_i, \eta_i)\, So_m(a_i, \cos\phi_{i0}) \right] \tag{2.47}$$

Again consider the scattered field from the lth strip given by

$$E_{z(l)}^s = E_0 \sqrt{8\pi} \sum_{m=0}^{\infty} A_m^{(l)}\, Re_m^{(3)}(a_l, \zeta_l)\, Se_m(a_l, \eta_l) \tag{2.48}$$

By applying the boundary conditions and using the addition theorem of the Mathieu functions, as described for the line source case, one can obtain matrix equations similar to (2.22), where $B_{nm}^{(ls)}$ are given by (2.23), while the elements of the vector $L^{(l)}$ are given by

$$L_m^{(l)} = \frac{-(-j)^m}{N_m^{(e)}(a_l)} \frac{Re_m^{(1)}(a_l, 1)}{Re_m^{(3)}(a_l, 1)} Se_m(a_l, \cos\phi_{l0})\, e^{-jk(x_l \cos\phi_0 + y_l \sin\phi_0)} \tag{2.49}$$

Similarly the far scattered field can be calculated using the asymptotic expression for Mathieu functions which is given by

$$E_z^s = E_0\, c'(k\rho)\, P(\phi) \tag{2.50}$$

where

$$P(\phi) = 2\pi \sum_{l=1}^{N} e^{-jk(x_l \cos\phi + y_l \sin\phi)} \sum_{m=0}^{M} (-j)^m A_m^{(l)} Se_m(a_l, \cos(\phi - \psi_l)) \qquad (2.51)$$

2.4.2 **Asymptotic solution**

Following the same steps described in section (2.3) and using (2.45) as excitation instead of (2.1) one can calculate the far scattered field using the asymptotic technique. i. e.

$$E_z^s = E_0 \; c'(k\rho) \, P(\phi) \qquad (2.52)$$

where

$$P(\phi) = \sum_{l=1}^{N} e^{-jk(x_l \cos\phi + y_l \sin\phi)} \left\{ f(a_l, \phi - \psi_l, \phi_{l0}) + \sum_{\substack{s=1 \\ s \neq l}}^{N} C_s \; g(a_l, \phi - \psi_l, \zeta_{ls}, \eta_{ls}) \right\} \qquad (2.53)$$

$$f(a_p, \phi_p, \phi_{p0}) = -2\pi \; e^{-jk(x_p \cos\phi_0 + y_p \sin\phi_0)} \sum_{m=0}^{\infty} \frac{(-1)^m}{N_m^{(e)}(a_p)} \frac{Re_m^{(1)}(a_p, 1)}{Re_m^{(3)}(a_p, 1)} Se_m(a_p, \cos\phi_p) \, Se_m(a_p, \phi_{p0}) \qquad (2.54)$$

The intensities of the line sources can be calculated from a matrix equation similar to (2.40) with B_{lp} given by (2.42) while L_l are given by

$$L_l = -\sum_{\substack{s=1 \\ s \neq l}}^{N} f(a_l, \psi_{ls}, \phi_{l0}) \qquad (2.55)$$

The plane wave scattering properties of two dimensional bodies of infinite length are conveniently described in terms of the echo width which is defined as

$$W(\phi) = \lim_{\rho \to \infty} 2\pi\rho \left| \frac{E_z^s(\rho,\phi)}{E_z^{inc}} \right|^2 \tag{2.56}$$

substituting from (2.45) and (2.50) or (2.52) into (2.56), we obtain

$$W(\phi) = \frac{4}{k} \left| P(\phi) \right|^2 \tag{2.57}$$

2.5 *Scattering by a solid cylindrical surface using the method of moments*

In order to compare the performance of the simulated cylindrical surface with the solid one, the total scattered field of the solid cylindrical surface due to line source excitation will be evaluated using the moment method. The details of the analysis and method of solution for large and small cylindrical reflectors are given by Kinzel [34] for a parabolic cylindrical reflector, Azarbar and Shafai [35] for a circular cylindrical reflector and by Tsai et. al. [39] for a corner reflector. The analysis presented by these authors is based on solving an integral equation for the current density on the cylindrical surface. This is always done by dividing the surface into small segments, then expanding the current density in terms of pulse or triangular functions of unknown amplitudes (α_n) over each segment. By applying the boundary conditions on the surface, the amplitudes (α_n) of the current density expansion can be calculated. Once the current density is evaluated, the far electric field pattern is given by

$$E_z^{tot}(\rho,\phi) = c'(k\rho)\, E_n(\phi) \tag{2.58}$$

where

$$E_n(\phi) = \left[e^{-jk\rho_o \cos(\phi - \psi_o)} - \frac{Z_0 k}{4} \sum_{n=1}^{N} \alpha_n \; e^{-jk\rho_n \cos(\phi - \psi_n)} \; \Delta S_n \right] \quad (2.59)$$

where ΔS_n is the nth segment of the surface, Z_0 is the intrinsic impedance of free space, (ρ_o, ψ_o) are the cylindrical coordinates of the line source and (ρ_n, ψ_n) are the coordinates of the nth segment of the surface. Coefficients α_n can be calculated by solving the following N algebraic equations

$$H_o^{(1)}(k\rho_m) = \frac{Z_0 k}{4} \sum_{n=1}^{N} \alpha_n \; H_o^{(1)}(k|\rho_m - \rho_n|) \; \Delta S_n \quad m = 1,2,\cdots,N \quad (2.60)$$

For $n = m$ the small argument approximation of the Hankel function may be used to simplify the solution.

2.6 *Numerical results and discussion*

2.6.1 Plane wave excitation

Throughout the following results the boundary value solution is denoted as method 1 while the asymptotic solution is denoted as method 2. The accuracy and limitations of both methods are examined in this section using examples of plane wave exciting different numbers of strips. Consider the simple case of two strips excited by a plane wave, where two examples are presented. In the first example, the two parallel strips are inclined relative to the x-axis of the local coordinate system by angles ψ_1 and ψ_2 which equal 45^o. The centers of these strips are located at $(1\lambda,0,0)$ and $(-1\lambda,0,0)$ with respect to the local coordinate system. The width of each strip is equal to $0.5\,\lambda$ while the angle of incidence is 90^o. The echo width pattern corresponding to this example is shown in Fig. 2.2 in which the results based on both methods are in excellent agreement. A main lobe appears at 180^o due to the reflection of the plane wave from the strips. The asymptotic technique gives very accurate results since the separation is very large with respect to the strip width. In

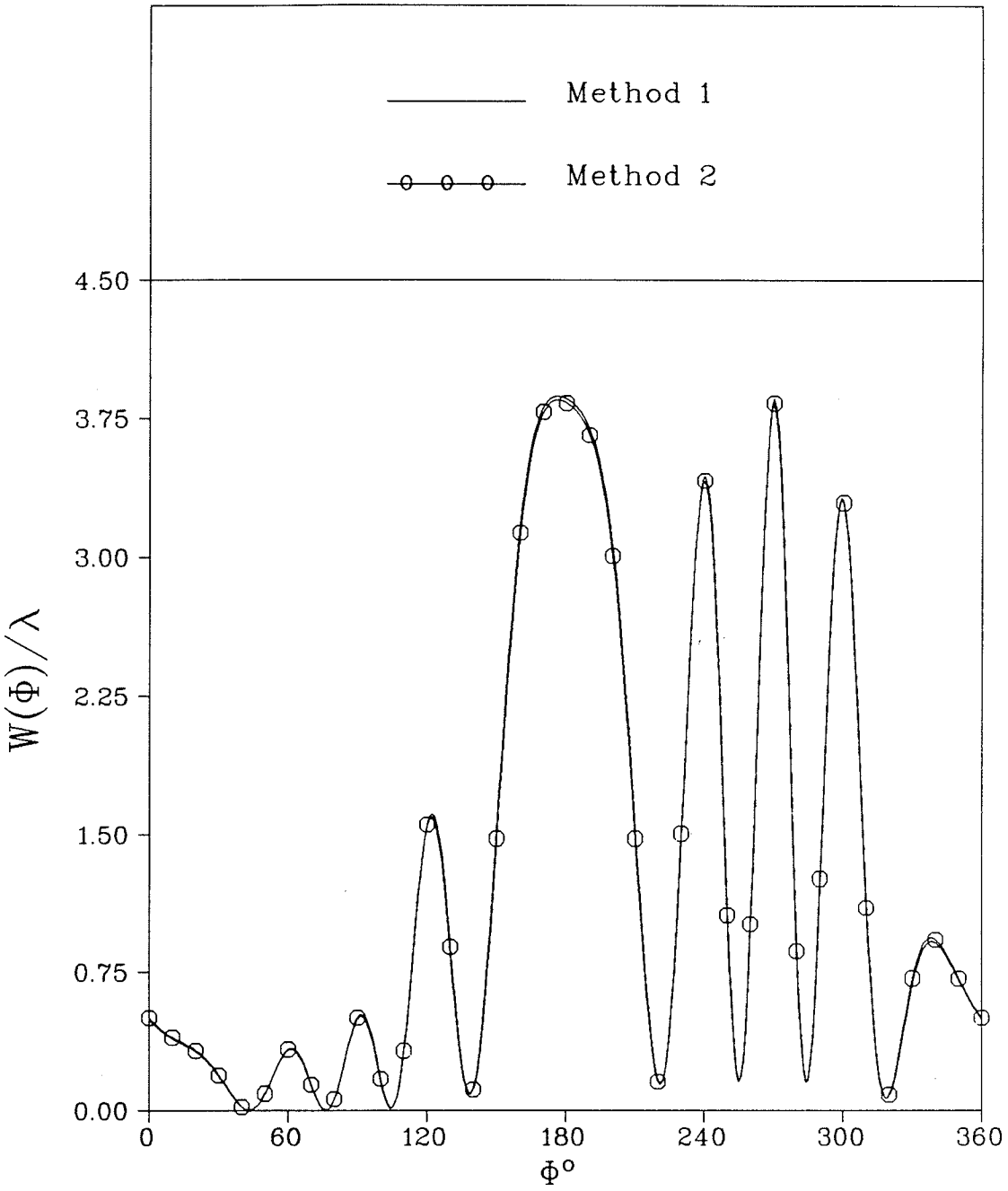

Fig. 2.2 : Echo width pattern of two parallel strips
(Φ_0= 90°, 2d = 0.5λ, ψ_1 = ψ_2= 45°)

the second example the effect on the echo width pattern of decreasing the separation between the two strips is examined. The two strips have the same width (1.5 λ) and their centers are at the same distance from the origin of the local coordinate system (0.75λ). These strips are inclined by ψ_1 and ψ_2 which equal -45^o relative to the x-axis of the local coordinate system while the angle of incidence is 45^o. As can be seen from Fig. 2.3, the echo width pattern based on method 2 is far from that based on method 1. This indicates that the asymptotic solution is only useful when the separation between the two strips is very large with respect to the maximum strip width.

The main goal of this study is to simulate a scattering surface such that the scattering pattern is the same as or comparable to the solid surface. Thus, the simple case of simulating a strip of width 1 λ by N parallel equi-spaced strips of small widths is considered. The exact solution of the solid strip of 1 λ width due to plane wave excitation is used for comparison purpose. Eight strips, each of width 0.05λ, are used for simulating the 1λ strip which is excited by a normally incident plane wave. The echo width pattern of the simulated strip is calculated by methods 1 and 2 as shown in Fig. 2.4. The comparison between the echo width pattern corresponding to the solid and simulated strips shows an excellent agreement. The metallic part used for simulating this strip is 40% of the total surface. But since we use a relatively large number of strips the response is almost exactly the same as the solid strip. If one wants to use a small number of strips for simulating the 1 λ strip, the width of the strips has to be increased. Thus three strips, each of width 0.28 λ, are used for simulating the 1 λ strip. The echo width patterns corresponding to the solid and simulated strips are given in Fig. 2.5 using both methods. Excellent agreement between the patterns of the solid and simulated strip using method 1 is found while the pattern of the simulated strip using method 2 deviates from the exact one. This is because method 2 is only useful when the separation between any two successive strips is much greater than the maximum strip width. With this small number of

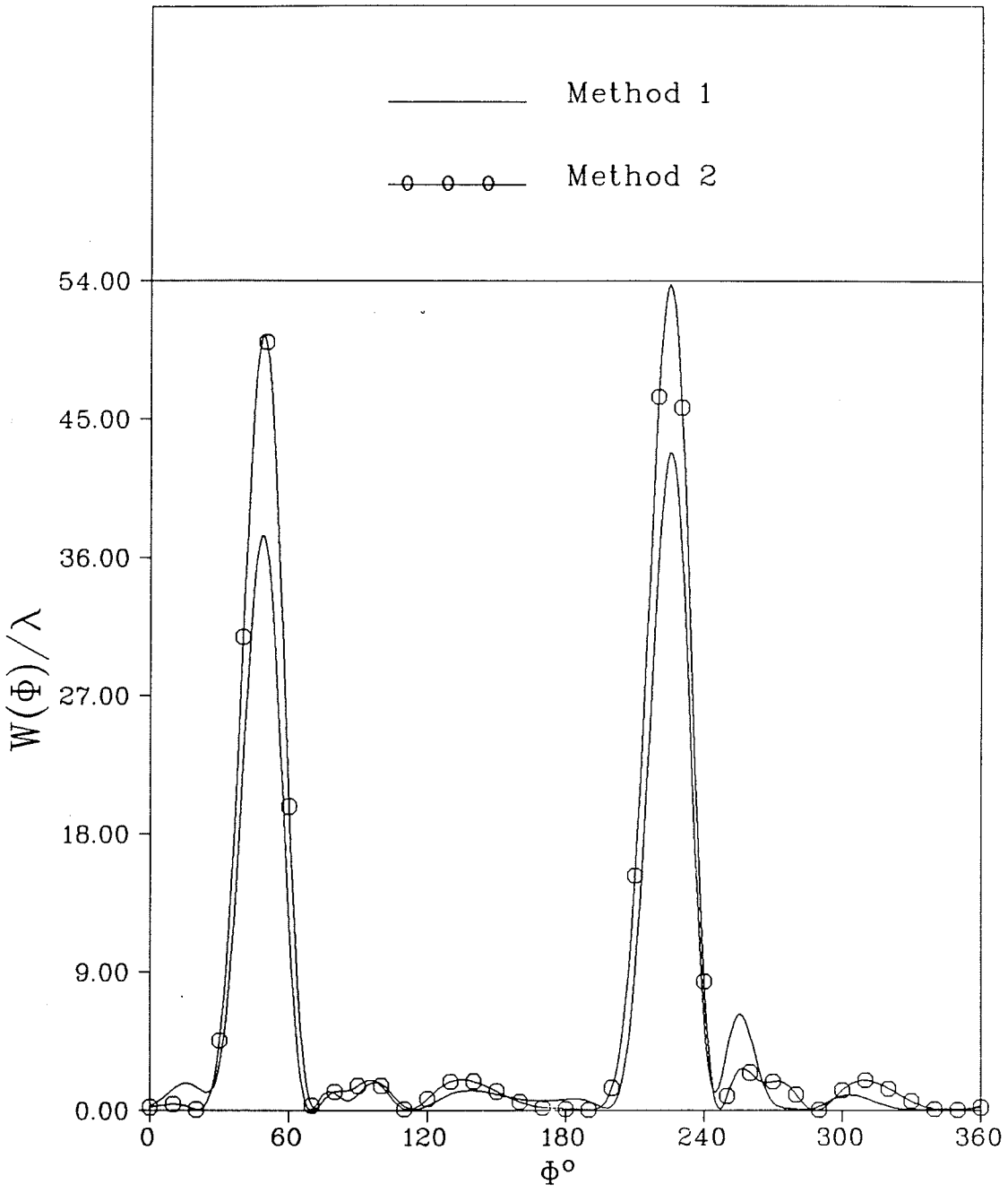

Fig. 2.3 : Echo width pattern of two parallel strips
(Φ_0= 45°, 2d = 1.5λ, ψ_1 = ψ_2= −45°)

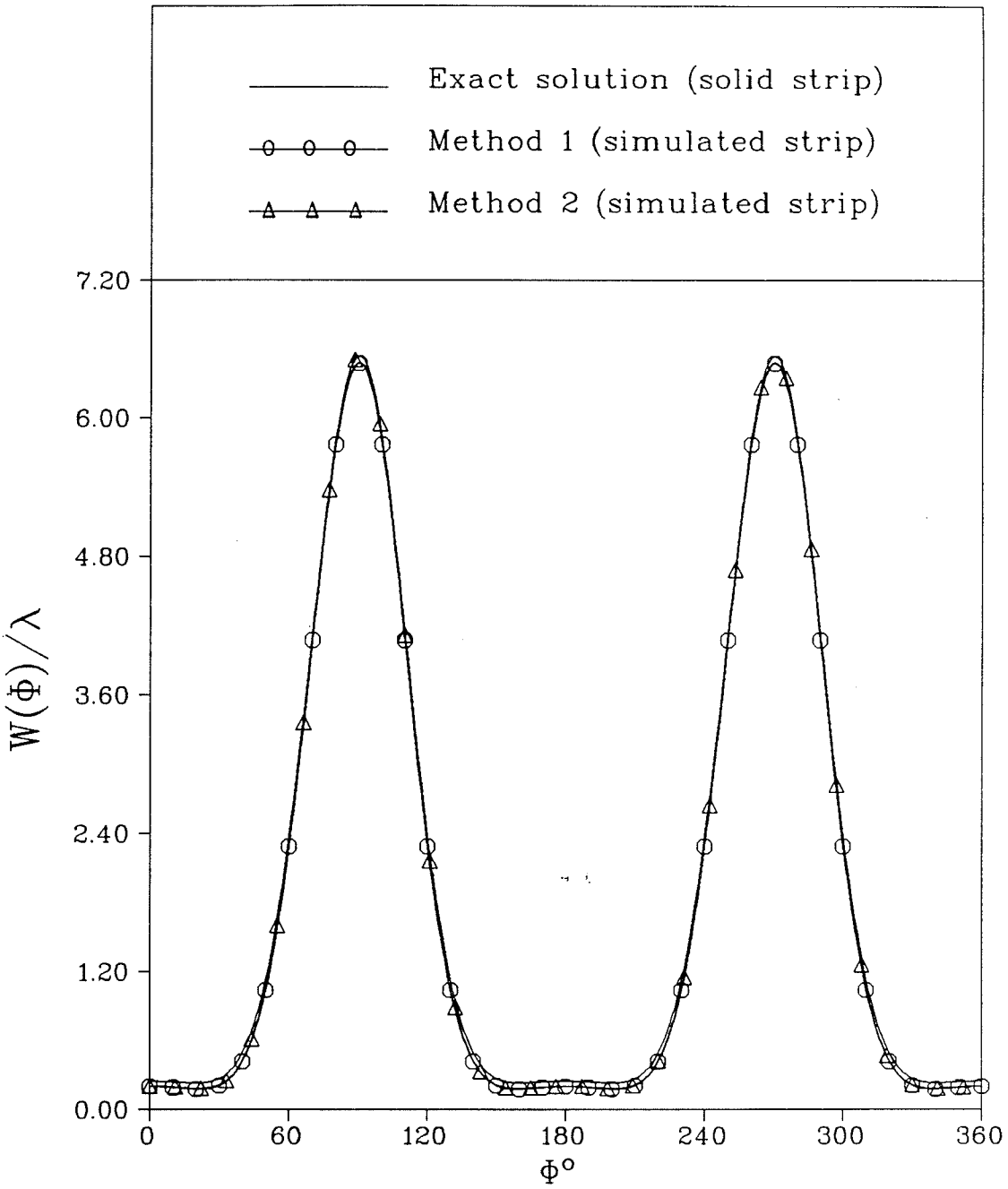

Fig. 2.4 : Echo width pattern of solid and simulated 1.0 λ strip (N = 8, 2d = 0.05λ, $\Phi_0 = 90^0$)

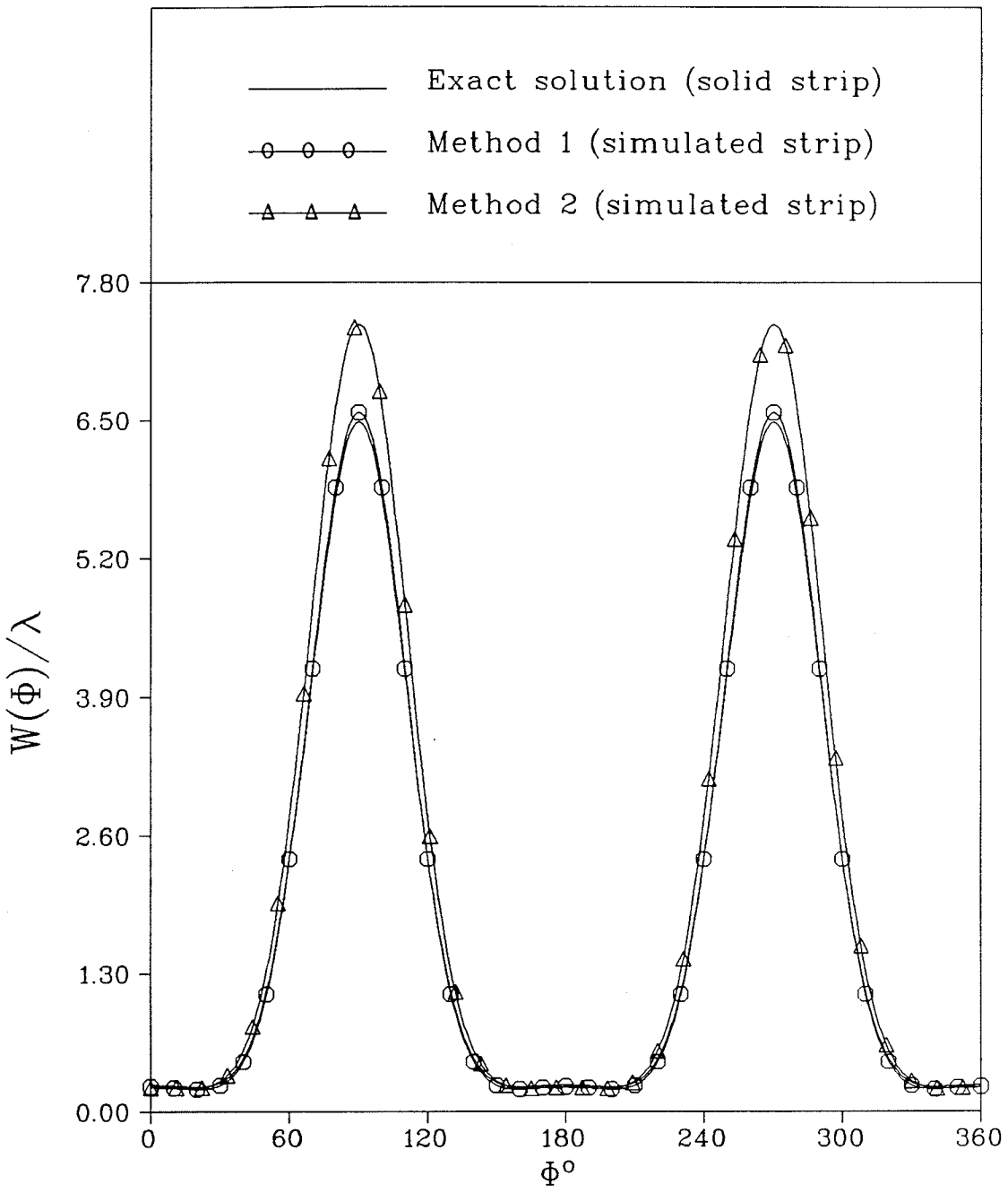

Fig. 2.5 : Echo width pattern of solid and simulated 1.0 λ strip (N = 3, 2d = 0.28λ, Φ_0= 90^0)

strips used for simulating the 1 λ strip the metallic part is 84% of the total surface which is more than twice the previous case. Thus, in simulating any surface, a large number of thin strips can produce closer results to the exact solution than a small number of wider strips.

Another example of simulating an infinitely long circular cylinder of radius 0.7958 λ is presented. Since the exact solution for the scattering of a plane wave by a circular conducting cylinder is well known, we compare the scattered field of the simulated cylinder with the original one. In simulating this cylinder, 24 strips each of width 0.1 λ are used. The strips are distributed equally on the circumference of a circle of radius 0.7958 λ in the cross section plane. The plane wave is incident at angle $\phi_o = 90^0$. As can be seen in Fig. 2.6 the echo width patterns of the solid and simulated cylinders using method 1 are in excellent agreement while method 2 leads to greater deviation from the exact value although still reasonably close. In this example the metallic part of the simulated cylinder is 48% of the total surface. Again the asymptotic solution leads to satisfactory results because the separation between successive strips is larger than the maximum strips width. The advantage of the asymptotic solution is obvious when dealing with problems requiring large numbers of strips where method 1 needs very large size matrices.

Finally, an example of a plane wave incident at 45^o on five parallel strips is presented. All strips have equal width of 0.5 λ and are placed such that their centers lie on the x-axis of the local coordinate system and each is inclined relative to the x-axis by an angle of -45^o. The distance between each two adjacent strips is 1.25 λ. As can be seen from Fig. 2.7 the echo width patterns of this example using both methods are in good agreement.

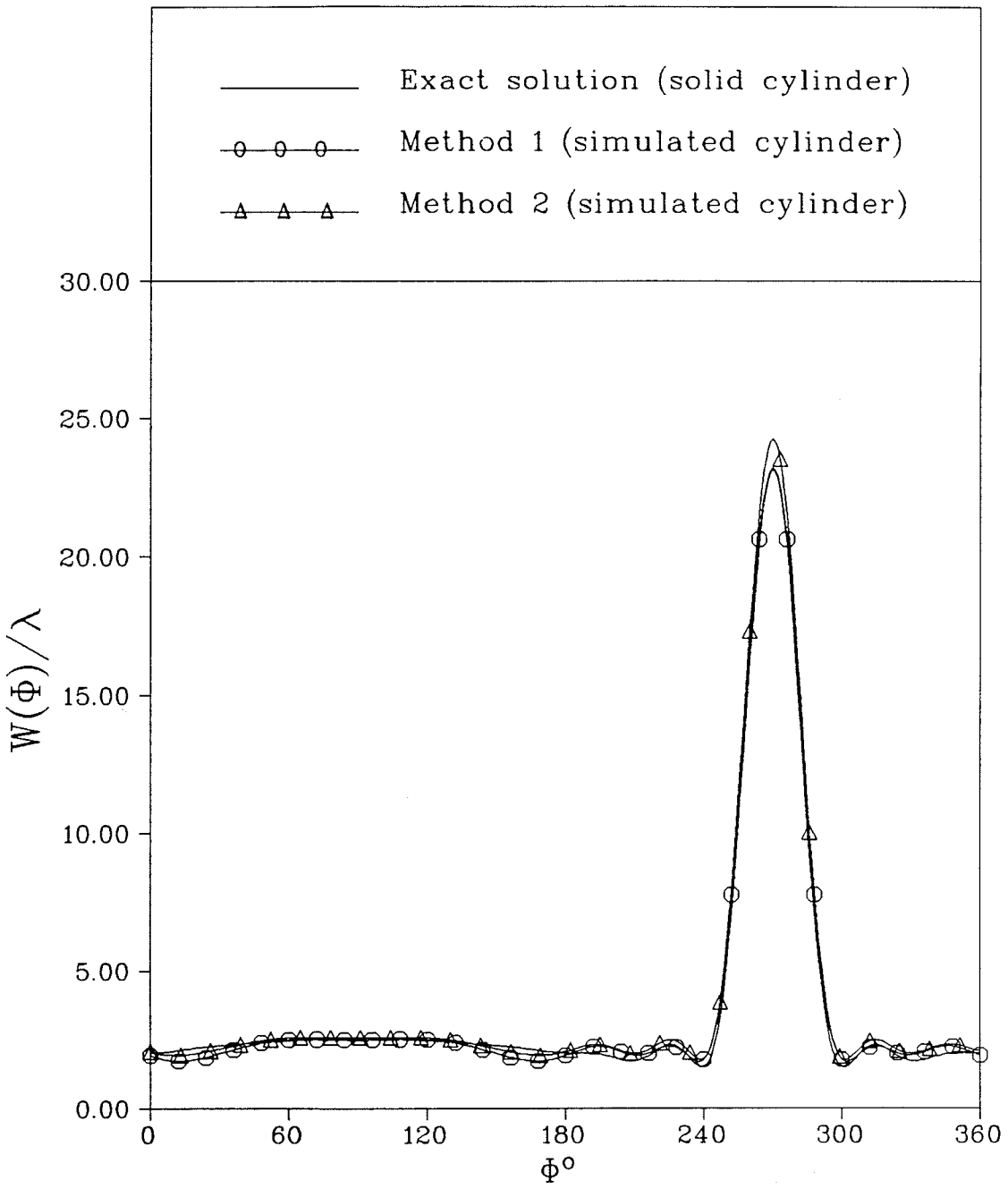

Fig. 2.6 : Echo width pattern of simulated and solid conducting cylinder (N = 24, 2d = 0.1λ, Φ_0= 90°)

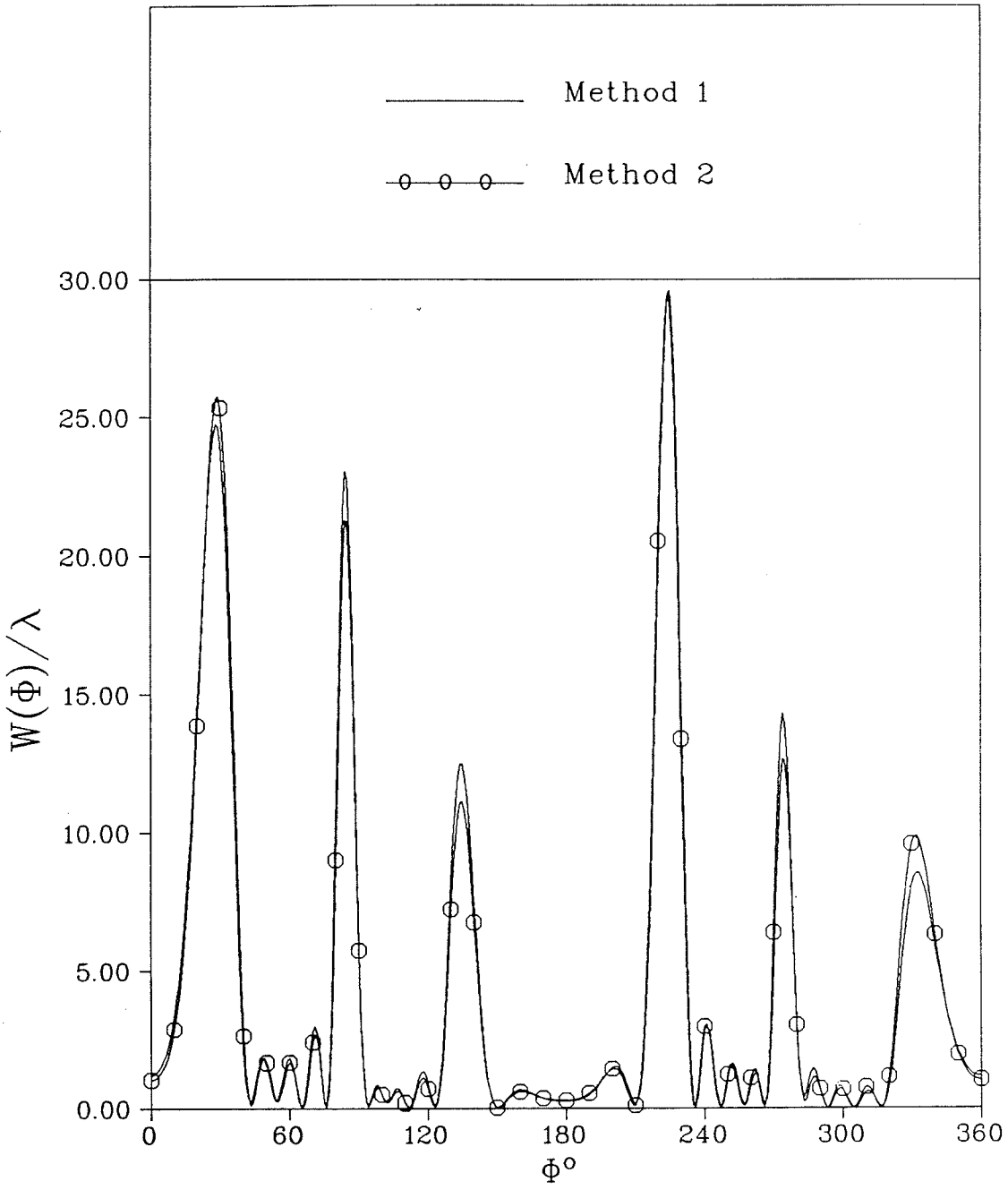

Fig. 2.7 : Echo width pattern of five parallel strips
(N = 5, 2d = 0.5λ, ψ = −45°, Φ_0= 45°)

2.6.2 Line source excitation

Our main study in this chapter is aimed at simulating cylindrical reflectors using conducting strips in order to obtain the same or better radiation characteristics compared to the solid reflectors. In this section four reflector geometries are simulated by equally-spaced equal-width conducting strips as shown in Fig. 2.8. For the purpose of comparison, the far field patterns corresponding to the solid reflector surface are evaluated in each case using the moment method along with the integral equation formulation (IEF). In the following four cases, strips of 0.1λ width each are used for simulating reflectors.

Consider for the first case a solid strip of 1.5λ width simulated by 9 strips and excited by a line source placed at 0.8λ from the strip center. The far field patterns of simulated and solid strips are shown in Fig. 2.9 using the IEF for the solid strip and methods 1 and 2 for the simulated one. The far field patterns of the solid and simulated strips show excellent agreement. In this case only 60% of the simulated strip is metal.

In the second case a corner reflector is considered, the corner angle being 75^o while the reflector length is 1.2 λ and the line source is placed at $S = 0.4\ \lambda$ from the apex. The reflector is simulated by 16 strips in which only 66.6% of the total surface is metal. As can be seen from Fig. 2.10 the far field pattern corresponding to the solid reflector using the IEF method is in reasonable agreement with that of the simulated reflector using methods 1 and 2.

The simulation of a circular cylindrical reflector is considered next. The aperture width D is 6 λ while the line source is placed at $R = 8.0\lambda$. The reflector is simulated by 41 strips which constitute 66.6% of the metal in the total reflector surface. The far field patterns of the solid and simulated reflectors are shown in Fig. 2.11 in which excellent agreement is found.

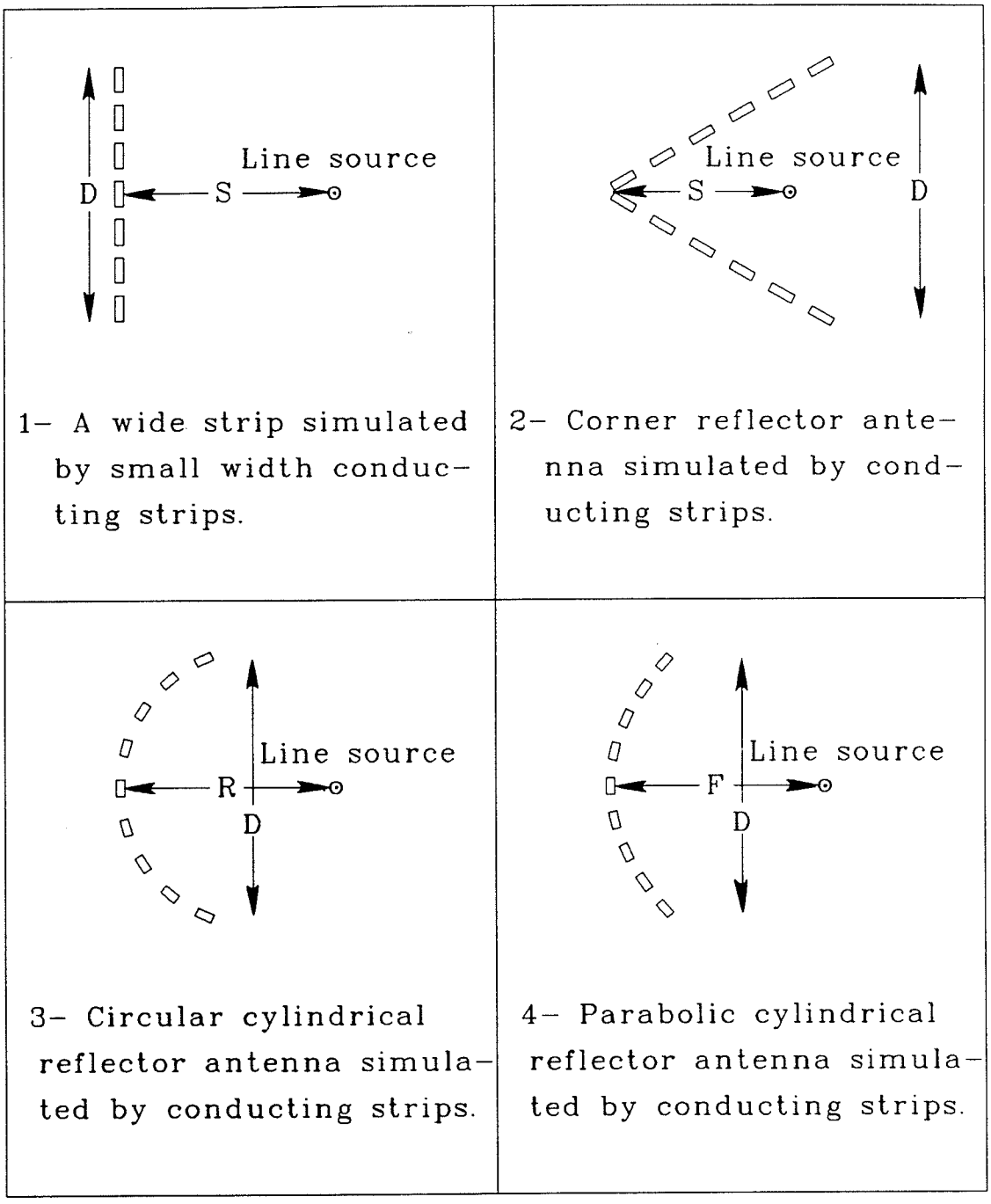

1- A wide strip simulated by small width conducting strips.

2- Corner reflector antenna simulated by conducting strips.

3- Circular cylindrical reflector antenna simulated by conducting strips.

4- Parabolic cylindrical reflector antenna simulated by conducting strips.

Fig. 2.8 : Simulated reflector antennas

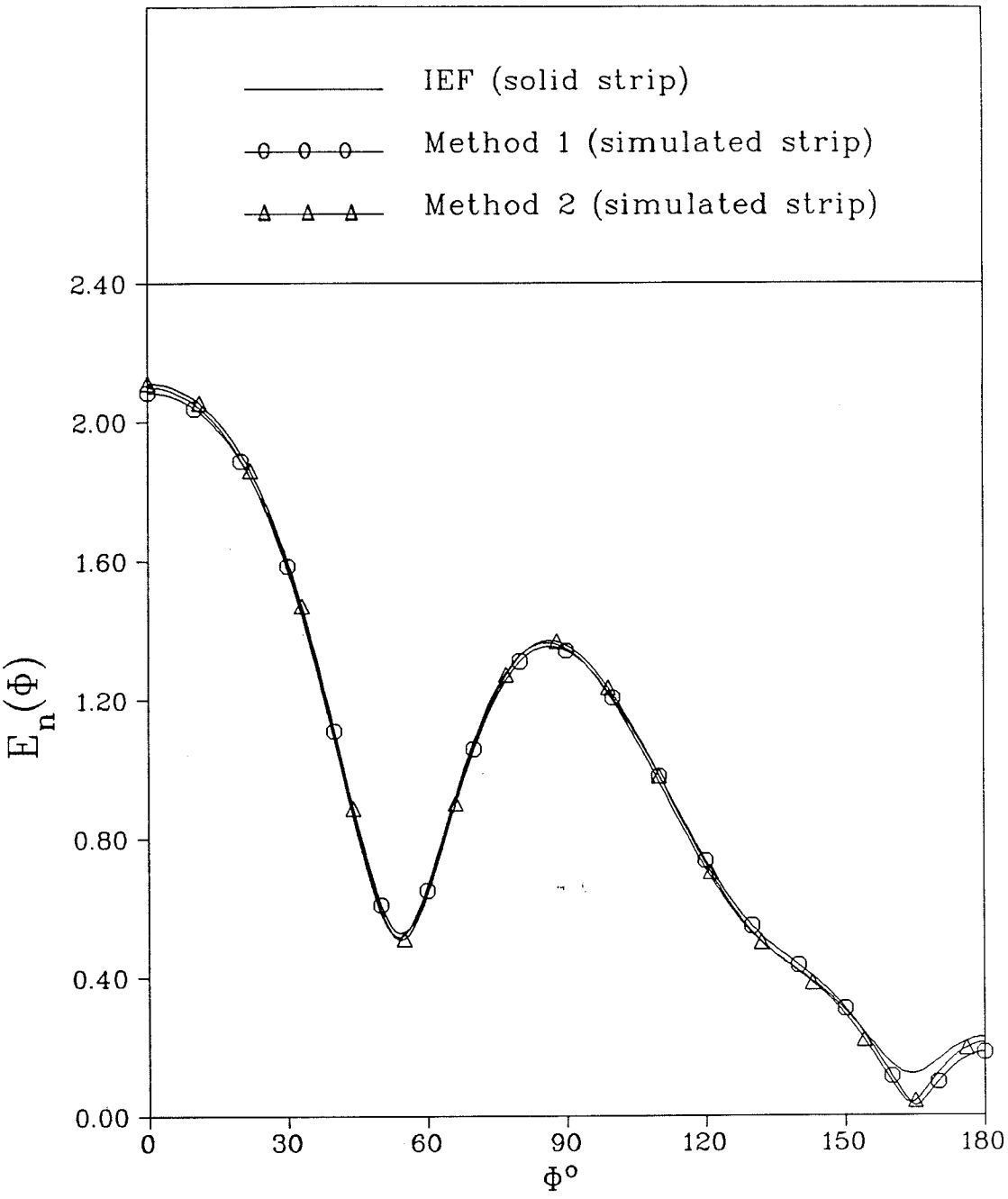

Fig. 2.9 : Far field pattern of solid and simulated 1.5 λ strip excited by a line source.
(N = 9, D = 1.5λ, S = 0.8λ, 2d = 0.1λ)

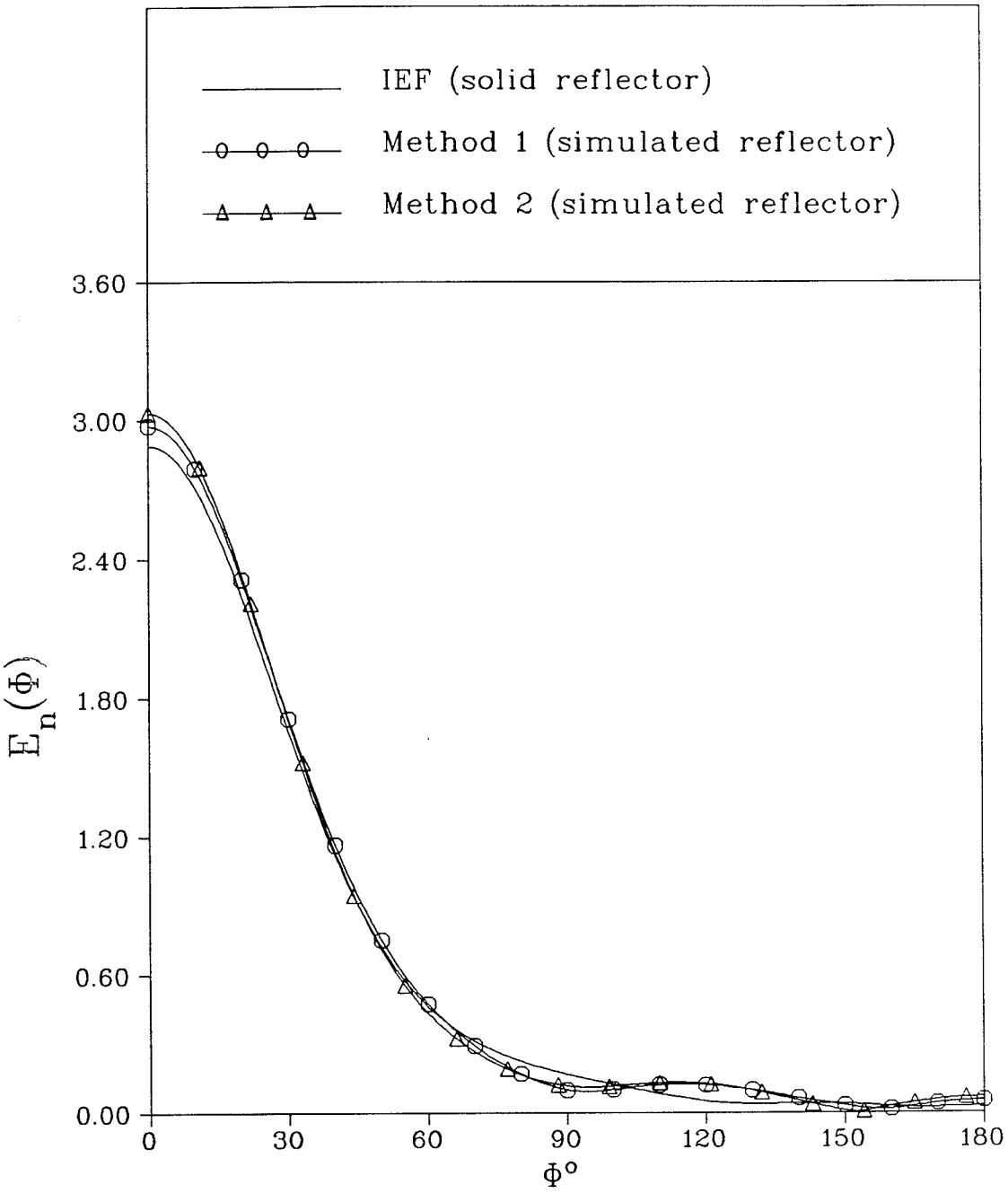

Fig. 2.10 : Far field pattern of solid and simulated corner reflector antenna of 75° corner angle (N = 16, D = 1.38λ, S = 0.4λ, 2d = 0.1λ)

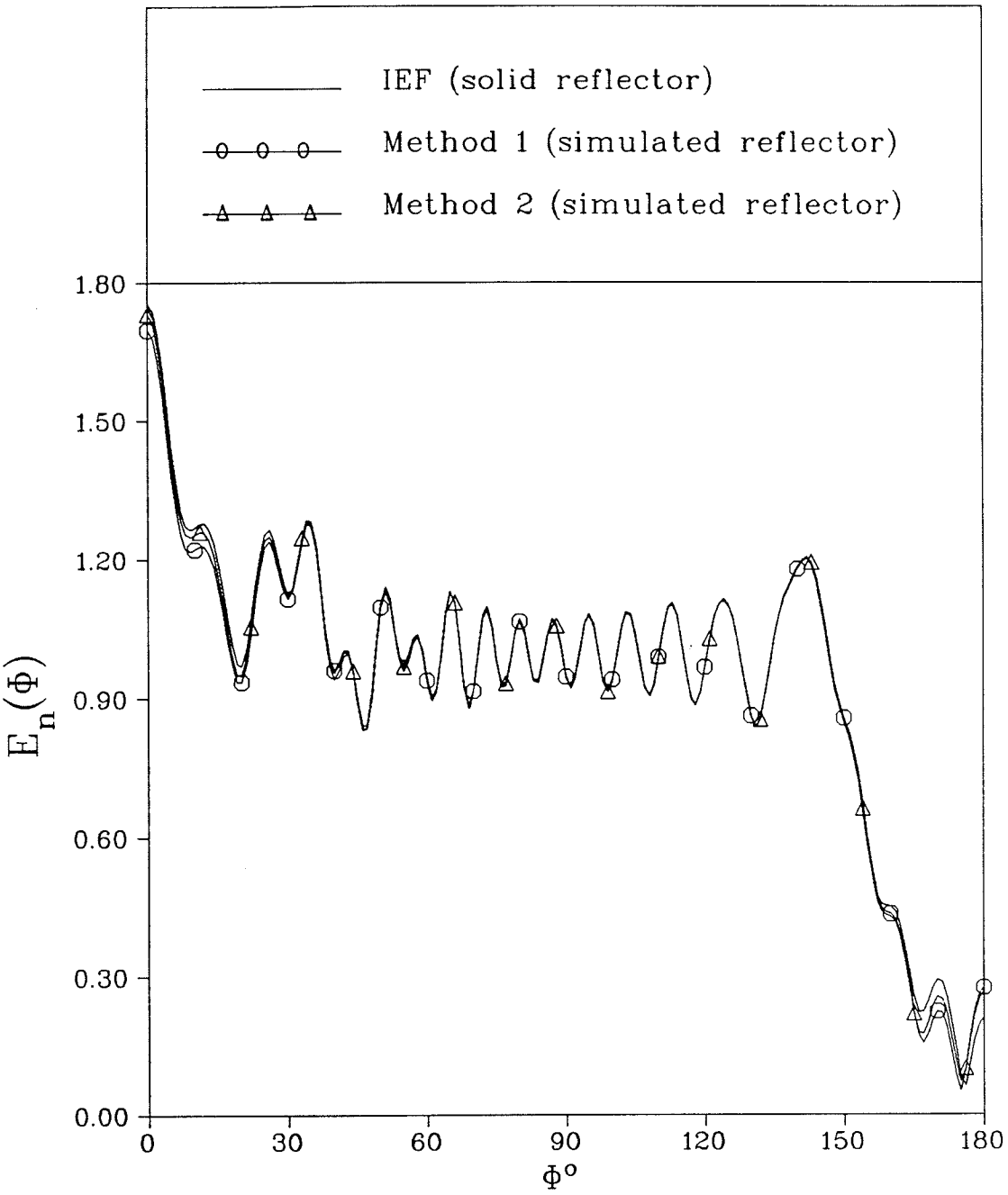

Fig. 2.11 : Far field pattern of solid and simulated circular cylindrical reflector antenna.
(N = 41, D = 6λ, R = 8λ, 2d = 0.1λ)

Finally a parabolic cylindrical reflector of width $D = 5.0\ \lambda$ is simulated by 35 strips. The focal distance F of the parabola is equal to 1.8λ where the line source is placed. Far field patterns corresponding to solid and simulated reflectors are obtained using the IEF method for the solid reflector and methods 1 and 2 for the simulated one. Satisfactory agreement between patterns corresponding to the solid and simulated reflectors is found as shown in Fig 2.12. Again the metallic part in the simulated reflector constitutes about 62% of the total surface.

It should be noticed that in the previous cases the number of strips used in each case is not the optimum. Accordingly the percentage metallic part of the simulated antenna is selected for achieving the same radiation characteristics as the solid reflector case. Hence two more examples are introduced, the first shows the effect of the number of strips on the radiation pattern while the second shows the effect of the strip width on the pattern. The parabolic reflector antenna given in the previous example is simulated using different numbers of strips. Four far field patterns are obtained corresponding to $N = 29, 21, 19$ and 15 strips each of width $0.1\ \lambda$. The corresponding metal percentages due to the four cases are 52%, 38%, 34% and 27%, respectively. The radiation patterns corresponding to these cases are calculated using method 1. As can be seen from Fig. 2.13 the pattern using 29 strips is in excellent agreement with that of the solid reflector presented in Fig. 2.12. In the other three cases we found that, by decreasing the number of strips, the value of the peak field is decreased while the back lobe is increased. Thus, the best simulation can be obtained using more than 50% metal.

The other example is also a simulation of the same parabolic cylindrical reflector antenna where 29 strips are used. The strips have equal width and are equally spaced on the reflector trajectory. Four cases are examined corresponding to strip widths of $0.01\ \lambda$, 0.05λ, 0.1λ and 0.15λ. As can be seen from Fig. 2.14 the peak level of the far field patterns decreases by decreasing the strip width while the back lobe increases. The percentages of the metallic portions are 5.2%, 26%, 52%

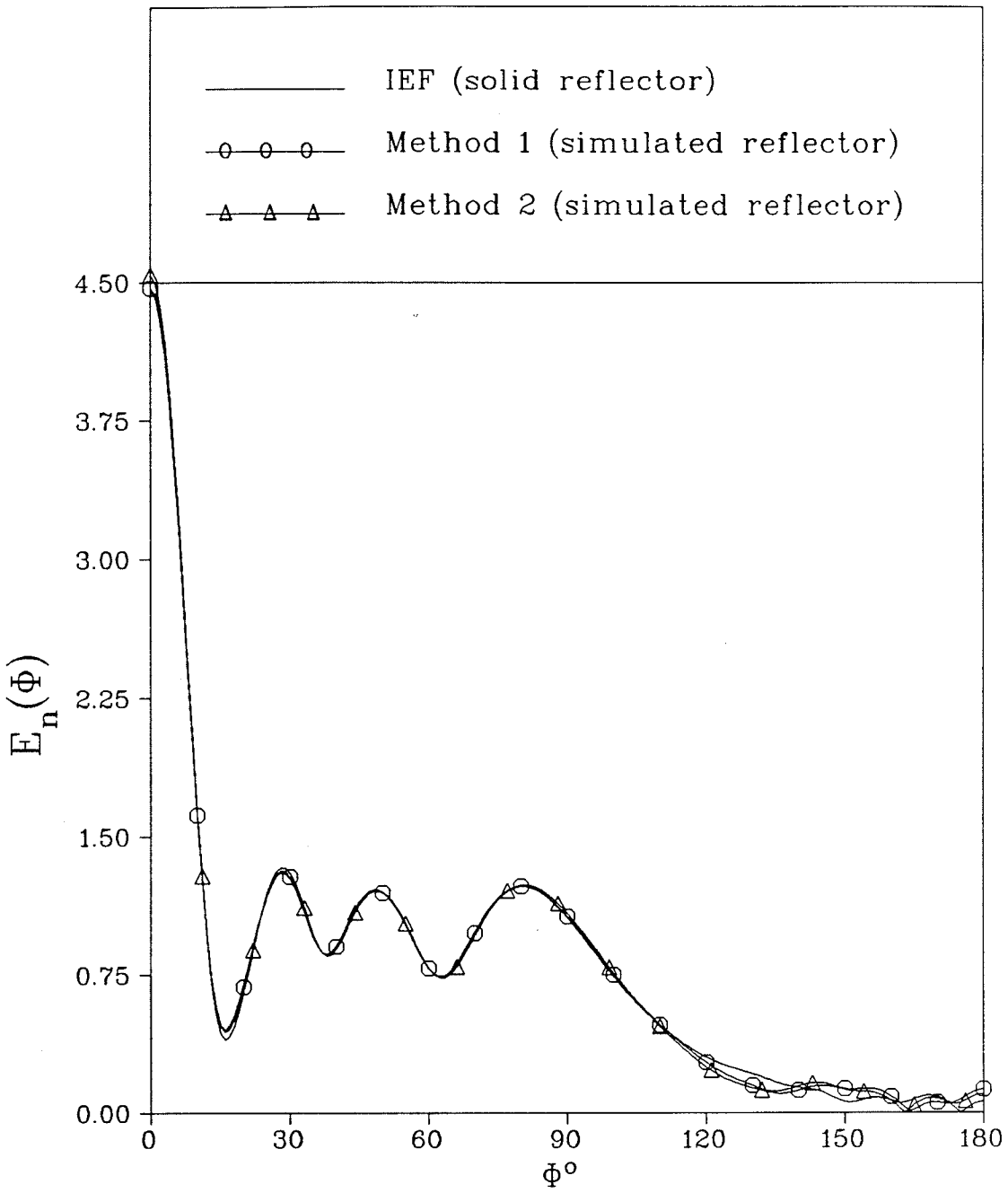

Fig. 2.12 : Far field pattern of solid and simulated parabolic cylindrical reflector antenna.
(N = 35, D = 5λ, F = 1.8λ, 2d = 0.1λ)

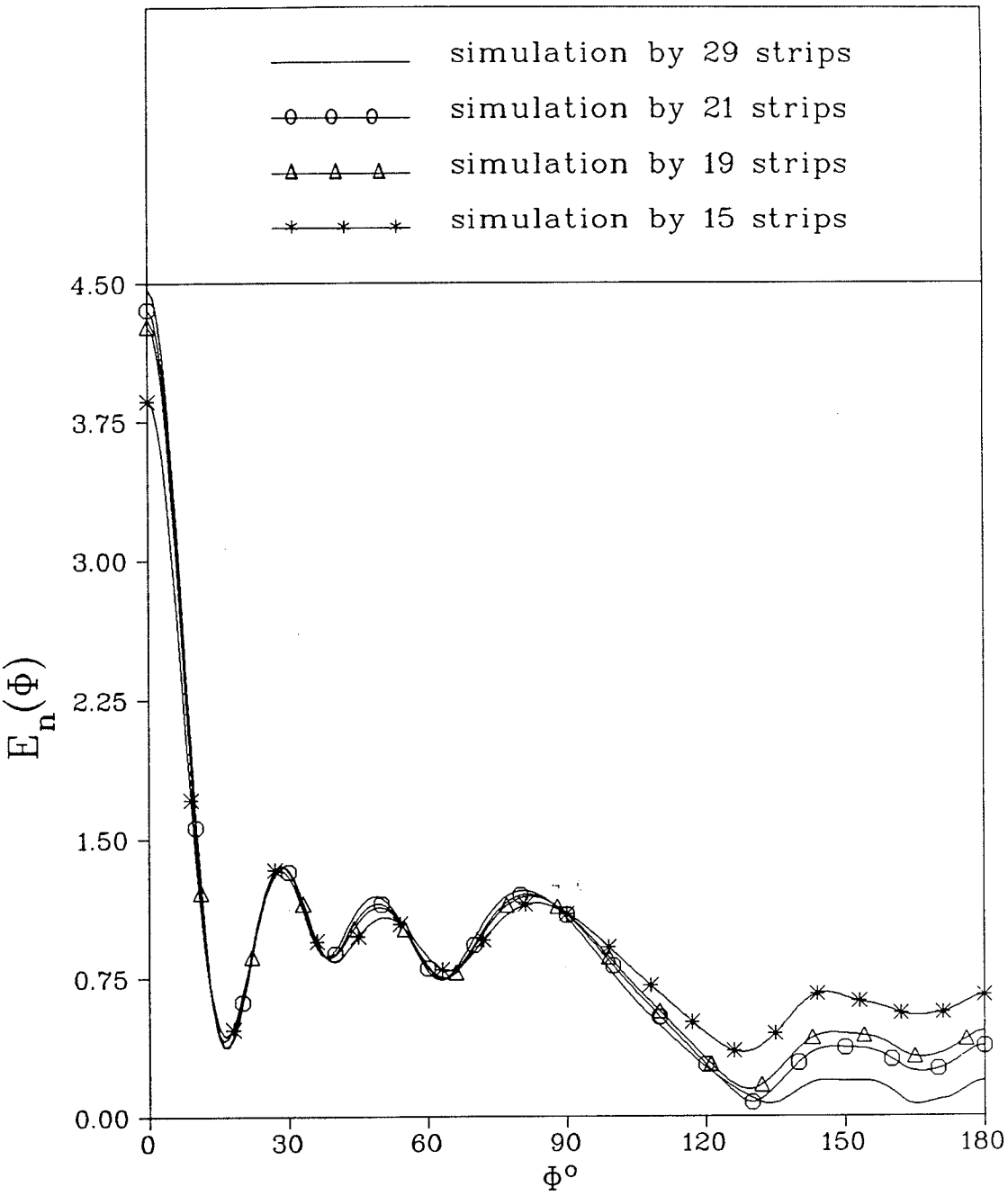

Fig. 2.13 : Far field pattern of simulated parabolic cylindrical reflector antenna using different number of strips (D = 5λ, F = 1.8λ, 2d = 0.1λ)

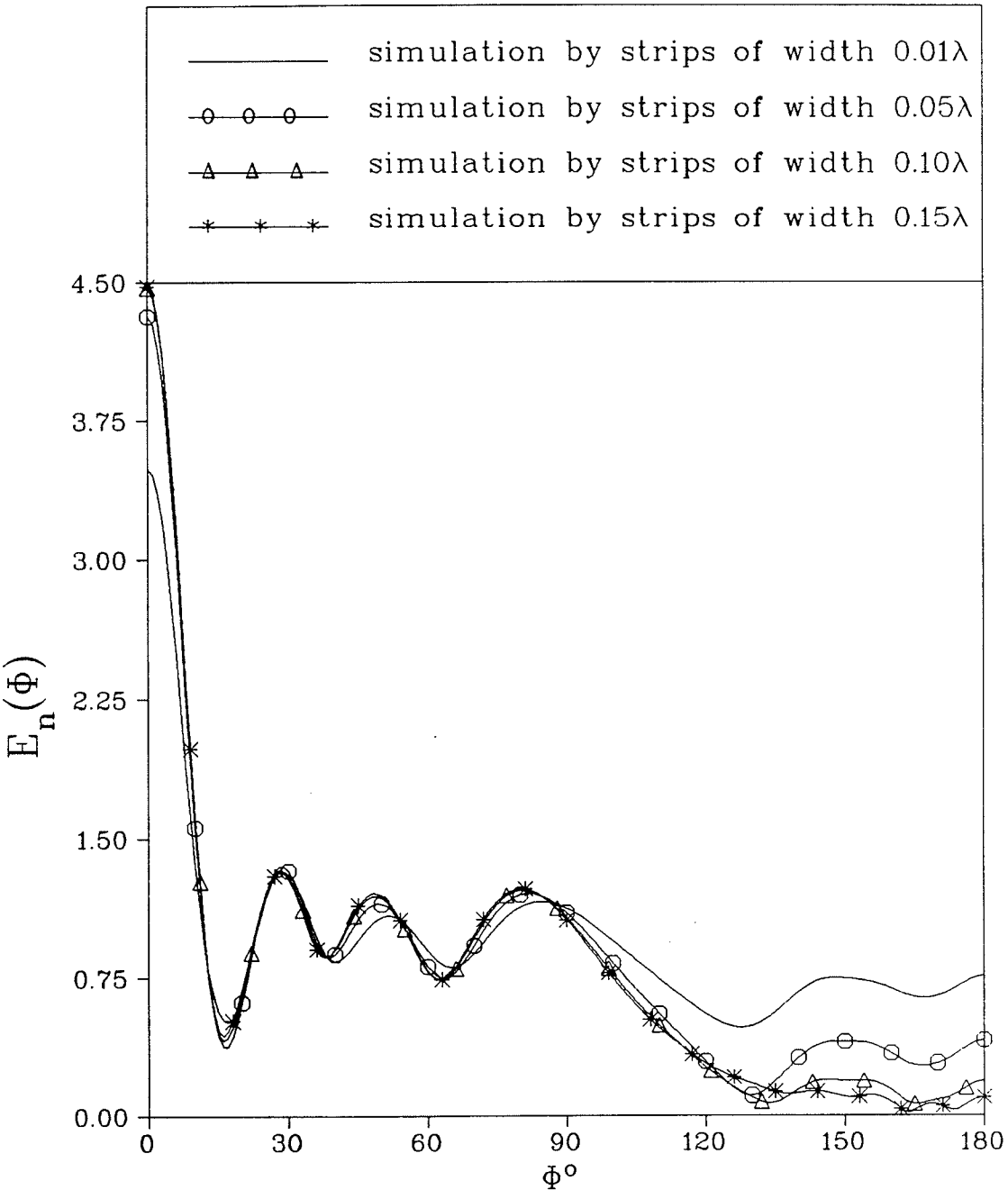

Fig. 2.14 : Far field pattern of simulated parabolic cylindrical reflector antenna using different strip widths (N = 29, D = 5λ, F = 1.8λ)

and 79%, respectively. Again the best simulation is obtained when the percentage metallic part of the simulated reflector occupies more than 50% of the total surface. It is also found that the radiation pattern of the simulated reflector cannot be improved over the solid reflector.

CHAPTER 3

SIMULATION OF CYLINDRICAL SCATTERING SURFACE BY CONDUCTING CIRCULAR CYLINDERS

3.1 *Introduction*

As stated in chapter 1, the conducting circular cylinder is one of the basic building blocks for simulating reflectors. The cylinders have to be parallel to each other and arranged on the cylindrical surface trajectory such that they act electrically in the same way as a solid surface. If each simulating cylinder is assumed to operate electrically in the same way as a current filament along its axis (which is more reasonable with small radii [6]) then the curve joining these filaments may or may not coincide with the actual surface trajectory. For either possibility the radii, spacing and number of cylinders are design variables requiring the solution of scattering by N parallel (nonintersecting) conducting circular cylinders. Such a solution can be rigorous (method 1) or asymptotic (method 2) and corresponding to line source or plane wave excitation. The solution of this problem for plane wave excitation will be presented in parallel with the line source excitation throughout this chapter.

Results for the backscattering echo width as well as the echo width patterns due to a plane wave incident on different configurations of cylinders are evaluated by both methods. The far field patterns of different simulated cylindrical reflector antennas are calculated by both methods and compared with those corresponding to the original solid cylindrical reflectors. It is also shown that by using cylinders with different radii and spacing along the reflector trajectory the far field pattern may be improved in some reflector configurations.

3.2 *Boundary value solution*

Consider N parallel nonintersecting infinitely long conducting circular cylinders as shown in Fig. 3.1. The cylinders are situated such that their axes are parallel to the z - axis of the circular cylindrical coordinate system used. The center of the i th cylinder is located at (s_i, ψ_i) with respect to the origin and b_i is the radius. For the sake of convenience N circular cylindrical coordinates are defined, one at the center of each cylinder. An incident plane wave of the form

$$E_z^{inc}(\rho,\phi) = e^{-jk\bar{\rho}} \tag{3.1}$$

impinges at an angle ϕ_0 with respect to the x-axis as shown in Fig.3.1. For the line source excitation the incident field is given by

$$E_z^{inc}(\rho,\phi) = H_0^{(2)}(k\,|\bar{\rho} - \bar{\rho}_0|) \tag{3.2}$$

where the line source is located at (ρ_0,ψ_0) as shown in Fig. 3.1. The time dependence $e^{j\omega t}$ is suppressed throughout. The incident wave may be expanded with respect to the coordinate system of the l th cylinder as follows:

- for the case of plane wave excitation, we have

$$E_z^{inc}(\rho_l,\phi_l) = e^{-jks_l\cos(\psi_l-\phi_0)} \sum_{n=-\infty}^{\infty} j^{-n}\, J_n(k\rho_l)\, e^{jn(\phi_l-\phi_0)} \tag{3.3}$$

- while for the case of line source excitation, we have instead

$$E_z^{inc}(\rho_l,\phi_l) = \begin{cases} \sum_{n=-\infty}^{\infty} H_n^{(2)}(k\rho_{l0})\; J_n(k\rho_l)\; e^{jn(\phi_l-\psi_{l0})}, & \rho_l < \rho_{l0} \\ \sum_{n=-\infty}^{\infty} H_n^{(2)}(k\rho_l)\; J_n(k\rho_{l0})\; e^{jn(\phi_l-\psi_{l0})}, & \rho_l > \rho_{l0} \end{cases} \tag{3.4}$$

where J_n is the Bessel function of the first kind, $H_n^{(2)}$ is the Hankel function of second kind, and l takes the integer values 1 to N, while ρ_{l0} and ψ_{l0} are given by

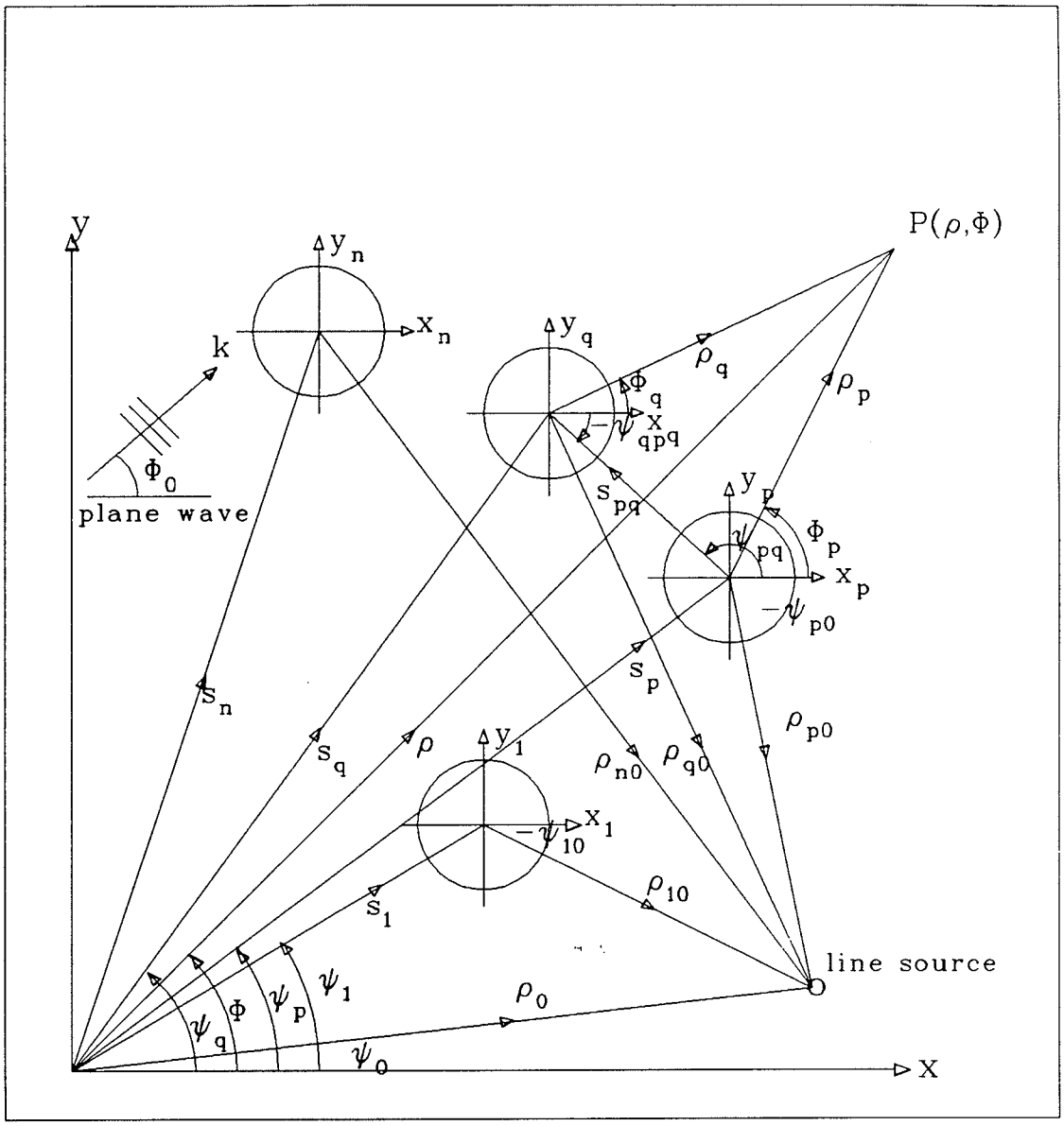

Fig. 3.1 : Geometry of the problem.

$$\rho_{l0} = \sqrt{s_l^2 + \rho_0^2 - 2\, s_l \rho_0 \cos(\psi_l - \psi_0)} \tag{3.5}$$

$$\psi_{l0} = \tan^{-1}\left[\frac{\rho_0 \sin\psi_0 - s_l \sin\psi_l}{\rho_0 \cos\psi_0 - s_l \cos\psi_l}\right] \tag{3.6}$$

The scattered field from the l th cylinder due to the plane wave or the line source is given by

$$E^s_{z(l)}(\rho_l, \phi_l) = \sum_{n=-\infty}^{\infty} A_n^{(l)} \; H_n^{(2)}(k\rho_l) \; e^{jn\phi_l} \tag{3.7}$$

where $A_n^{(l)}$ are the scattering coefficients of the l th cylinder. It is assumed that the scattered field (3.7) includes all the interactions between the l th cylinder and all other cylinders. Equation (3.7) gives the scattered field of the q th cylinder as well as the l th cylinder. On the other hand the expression for the scattered field from the q th cylinder can be expanded in terms of the l th coordinate system and vice versa. This can be done by using the addition theorem for the Hankel function, namely

$$H_n^{(2)}(k\rho_q)\, e^{jn\phi_q} = \sum_{m=-\infty}^{\infty} e^{-j(m-n)\psi_{lq}} \, J_m(k\rho_l) \; H^{(2)}_{m-n}(k s_{lq})\, e^{jm\phi_l} \tag{3.8}$$

where

$$s_{lq} = \sqrt{s_l^2 + s_q^2 - 2\, s_l s_q \cos(\psi_l - \psi_q)} \tag{3.9}$$

$$\psi_{lq} = \tan^{-1}\left[\frac{s_q \sin\psi_q - s_l \sin\psi_l}{s_q \cos\psi_q - s_l \cos\psi_l}\right] \tag{3.10}$$

provided that $s_{lq} = s_{ql}$ and $\psi_{lq} = \psi_{ql} + 180^o$.

Now the total electric field is given by

$$E_z^{tot}(\rho_p, \phi_p) = E_z^{inc}(\rho_p, \phi_p) + \sum_{n=1}^{N} E^s_{z(n)}(\rho_n, \phi_n) \tag{3.11}$$

where $E_z^{inc}(\rho_p,\phi_p)$ is the incident field in terms of the p th coordinate system of the plane wave or the line source. The total field $E_z^{tot}(\rho_p,\phi_p)$ can be written completely in any of the coordinate systems given by using the addition theorem of the Hankel function. The boundary condition on the conducting surface of the p th cylinder is

$$E_z^{tot}(\rho_p,\phi_p) = 0 \tag{3.12}$$

Applying this boundary condition N times, once on each cylinder surface, leads to the following N matrix equations

$$A^{(p)} = L^{(p)} + \sum_{q=1}^{N} B^{(pq)} A^{(q)} \qquad , \quad q \neq p \tag{3.13}$$

where p takes the values 1 to N, while $A^{(p)}$ and $A^{(q)}$ are infinite vectors containing the scattering coefficients corresponding to p th and the q th cylinders, respectively. $B^{(pq)}$ are infinite dimensional matrices with elements

$$B_{nm}^{(pq)} = -\frac{J_n(kb_p)}{H_n^{(2)}(kb_p)} \quad H_{n-m}^{(2)}(ks_{pq}) \quad e^{-j(n-m)\psi_{pq}} \qquad , \; p \neq q \tag{3.14}$$

while $L^{(p)}$ are infinite vectors, whose elements for the plane wave incidence are given by

$$L_n^{(p)} = -\frac{J_n(kb_p)}{H_n^{(2)}(kb_p)} \quad j^n \; e^{-jks_p cos(\psi_p - \phi_0)} \; e^{-jn\phi_0} \tag{3.15}$$

while for the line source excitation they are given by

$$L_n^p = -\frac{J_n(kb_p)}{H_n^{(2)}(kb_p)} \quad H_n^{(2)}(k\rho_{p0}) \quad e^{-jn\psi_{p0}} \tag{3.16}$$

Equations (3.13) include infinite dimensional matrices and some truncation must therefore be performed in order to generate a numerical solution. It is well known that for reasonably large values of kb, a number of Bessel function terms M, which

is approximately equal to $3kb$, should be computed to give a valid solution to the single cylinder scattering problem. We will assume that the same rule applies to the case of N cylinders because the factor $J_n(kb)/H_n^{(2)}(kb)$ which gives the rapid convergence is common in both single and N cylinders cases. According to this truncation the vectors and matrices in equations (3.13) will be of dimension $(2M+1)$. Moreover equations (3.13) can be written in a single matrix equation, i. e.

$$A = L + B\,A \tag{3.17}$$

where B is a square matrix of dimension $[N(2M+1)]$, A and L are vectors of the same dimension. Equation (3.17) can be written in the form

$$(I - B)\,A = L \tag{3.18}$$

which can be solved as a set of ordinary linear algebraic equations for the unknown vector A. The vector A contains N vectors each of length $(2M+1)$ corresponding to the scattering coefficients of each cylinder. Once the scattering coefficients are calculated, the total scattered field due to plane wave incidence is given by

$$E_z^s(\rho,\phi) = \sum_{l=1}^{N} \sum_{n=-M}^{M} A_n^{(l)}\, H_n^{(2)}(k\rho_l)\; e^{jn\phi_l} \tag{3.19}$$

and for the line source excitation the total electric field is

$$E_z^{tot}(\rho,\phi) = H_0^{(2)}(k|\rho - \rho_0|) + \sum_{l=1}^{N} \sum_{n=-M}^{M} A_n^{l}\, H_n^{(2)}(k\rho_l)\; e^{jn\phi_l} \tag{3.20}$$

In the far field, where $k\rho_l >> 1$, we employ the approximations

$$\rho_l = \rho - s_l\cos(\psi_l - \phi) \quad , \quad \phi = \phi_1 = \phi_2 = \cdots = \phi_l = \cdots = \phi_N \tag{3.21}$$

In addition, we use the asymptotic value of the Hankel function for large argument,

$$H_n^{(2)}(k\rho) = \sqrt{\frac{2}{\pi k \rho}}\ e^{-jk\rho}\ e^{j\pi/4}\ j^n \tag{3.22}$$

In this case the total scattered field due to plane wave incidence is given by

$$E_z^s(\rho,\phi) = c(k\rho)\, P(\phi) \tag{3.23}$$

$$P(\phi) = \sum_{l=1}^{N} \sum_{n=-M}^{M} j^n\ A_n^{(l)}\ e^{jks_l \cos(\psi_l - \phi)}\ e^{jn\phi} \tag{3.24}$$

where

$$c(k\rho) = \sqrt{\frac{2}{\pi k \rho}}\ e^{-jk\rho}\ e^{j\pi/4} \tag{3.25}$$

Also the total far electric field for the line source excitation is given by

$$E_z^{tot}(\rho,\phi) = c(k\rho)\, E_n(\phi) \tag{3.26}$$

$$E_n(\phi) = \left\{ e^{jk\rho_0 \cos(\phi - \psi_0)} + \sum_{l=1}^{N} \sum_{n=-M}^{M} j^n\ A_n^{(l)}\ e^{jks_l \cos(\psi_l - \phi)}\ e^{jn\phi} \right\} \tag{3.27}$$

In both expressions (3.23) and (3.26) the multiple interactions among cylinders are included in the coefficient calculations. In the special case of $N = 2$ our solution gives the same expressions given by Young and Bertrand [11].

3.3 *Asymptotic solution*

The Karp and Russek technique for diffraction of a plane wave by a wide slit [15] can be extended to the case of scattering by N circular cylinders due to plane or cylindrical incident waves. The technique is based on considering the scattered field from each cylinder due to plane or cylindrical wave incidence plus the scattered field due to line sources, of unknown intensity, located at the centers of the other cylinders. The line sources account in an approximate sense for the multiple

interaction between the cylinders. As stated before, the technique is based on the scattered field from a single cylinder due to plane wave or line source excitation. The far scattered field from a single cylinder, with center at (s_l,ψ_l) with respect to the origin, due to a plane wave incident at an angle ϕ_0 is given by

$$E_z^s(\rho,\phi) = c(k\rho)\ f(b,\phi,\phi_0) \tag{3.28}$$

where

$$f(b,\phi,\phi_0) = -e^{-jks_l\cos(\psi_l-\phi_0)} \sum_{n=0}^{\infty} \epsilon_n \frac{J_n(kb)}{H_n^{(2)}(kb)} \cos n(\phi-\phi_0) \tag{3.29}$$

while the far scattered field due to a line source located at (ρ_0,ψ_0), with respect to the center of the cylinder, is

$$E_z^s(\rho,\phi) = c(k\rho)\ g(b,\phi,\psi_0,\rho_0) \tag{3.30}$$

where

$$g(b,\phi,\psi_0,\rho_0) = -\sum_{n=0}^{\infty} \epsilon_n\ j^n\ \frac{J_n(kb)}{H_n^{(2)}(kb)}\ H_n^{(2)}(k\rho_0)\ \cos n(\phi-\psi_0) \tag{3.31}$$

Here b is radius of the cylinder. In order to calculate the scattered field due to the set of N cylinders shown in Fig. 3.1 we assume a line source of unknown intensity C at the center of each cylinder. The total scattered field from the qth cylinder due to an incident plane wave is

$$E_q^s(\rho_q,\phi_q)[c(k\rho_q)]^{-1} = f(b_q,\phi_q,\phi_0) + \sum_{\substack{l=1\\ l\neq q}}^{N} C_l\ g(b_q,\phi_q,\psi_{ql},s_{ql}) \tag{3.32}$$

while that due to line source excitation is

$$E_q^s(\rho_q,\phi_q)[c(k\rho_q)]^{-1} = g(b_q,\phi_q,\psi_{q0},\rho_{q0}) + \sum_{\substack{l=1\\ l\neq q}}^{N} C_l\ g(b_q,\phi_q,\psi_{ql},s_{ql}) \tag{3.33}$$

The first terms in equations (3.32) and (3.33) are the direct scattered fields from the q th cylinder due to plane wave and line source excitations, respectively. The second term in each of these equations is due to multiple interactions between the q th cylinder and all other cylinders. Now in order to calculate the unknowns C_l, the partial scattered field from the j th cylinder due to the scattered field from the q th cylinder (E^s_{jq}) can be determined by considering the scattered field from q th cylinder at ϕ_q equals ψ_{qj} as an intensity of a line source times the well known response (3.30). Thus, for plane wave incidence

$$E^s_{jq} = \left\{ f\,(b_q, \psi_{qj}, \phi_0) + \sum_{\substack{l=1 \\ l \neq q}}^{N} C_l \;\; g\,(b_q, \psi_{qj}, \psi_{ql}, s_{ql}) \right\}$$

$$c\,(k\rho_j)\; g\,(b_j, \phi_j, \psi_{jq}, s_{jq}) \quad , j = 1,2, \cdots, N \tag{3.34}$$

while for the line source excitation

$$E^s_{jq} = \left\{ g\,(b_q, \psi_{qj}, \psi_{q0}, \rho_{q0}) + \sum_{\substack{l=1 \\ l \neq q}}^{N} C_l \;\; g\,(b_q, \psi_{qj}, \psi_{ql}, s_{ql}) \right\}$$

$$c\,(k\rho_j)\; g\,(b_j, \phi_j, \psi_{jq}, s_{jq}) \quad , j = 1,2, \cdots, N \tag{3.35}$$

On the other hand this partial scattered field is given by

$$E^s_{jq} = C_q \; c\,(k\rho_j) \;\; g\,(b_j, \phi_j, \psi_{jq}, s_{jq}) \quad , j = 1,2, \cdots, N \quad , \; j \neq q \tag{3.36}$$

Using the equivalence between equations (3.36) and (3.34) or (3.35), and taking into account the partial scattered field from all cylinders due to the scattered field from the q th cylinder, the intensity of the line sources C can be determined from the following expressions:

- for the case of plane wave excitation

$$\sum_{\substack{j=1 \\ j \neq q}}^{N} f\,(b_q, \psi_{qj}, \phi_0) + \sum_{\substack{j=1 \\ j \neq q}}^{N} \sum_{\substack{l=1 \\ l \neq q}}^{N} C_l \; g\,(b_q, \psi_{qj}, \psi_{ql}, s_{ql}) = (N-1)\; C_q \tag{3.37}$$

- for the case of line source excitation

$$\sum_{\substack{j=1 \\ j \neq q}}^{N} g(b_q, \psi_{qj}, \psi_{q0}, \rho_{q0}) + \sum_{\substack{j=1 \\ j \neq q}}^{N} \sum_{\substack{l=1 \\ l \neq q}}^{N} C_l \, g(b_q, \psi_{qj}, \psi_{ql}, s_{ql}) = (N-1) \, C_q \tag{3.38}$$

Equations (3.37) and (3.38) can be written in the matrix form

$$B \, C = L \tag{3.39}$$

where

$$B_{ql} = \begin{cases} \sum_{j=1}^{N} g(b_q, \psi_{qj}, \psi_{ql}, s_{ql}) & j, l \neq q \\ 1 - N & q = l \end{cases} \tag{3.40}$$

$$L_q = \begin{cases} -\sum_{j=1}^{N} f(b_q, \psi_{qj}, \phi_0) \, e^{-jks_q \cos(\psi_q - \phi_0)}, & j \neq q \text{ for } \textit{plane wave} \\ -\sum_{j=1}^{N} g(b_q, \psi_{qj}, \psi_{q0}, \rho_{q0}), & j \neq q \text{ for } \textit{line source} \end{cases} \tag{3.41}$$

Once the intensities of the line sources are calculated, the total far scattered field due to plane wave incidence is given by

$$E_z^s(\rho, \phi) = c(k\rho) \, P(\phi) \tag{3.42}$$

where

$$P(\phi) = \sum_{q=1}^{N} \Big\{ f(b_q, \phi, \phi_0) \, e^{-jks_q \cos(\psi_q - \phi_0)} + \sum_{\substack{l=1 \\ l \neq q}}^{N} C_l \, g(b_q, \phi, \psi_{ql}, s_{ql}) \Big\} e^{jks_q \cos(\phi - \psi_q)} \tag{3.43}$$

For the case of a line source excitation the total far field is given by

$$E_z^{tot}(\rho,\phi) = E_z^{inc}(\rho,\phi) + E_z^{s}(\rho,\phi) = c\,(k\,\rho)\,E_n(\phi) \tag{3.44}$$

where

$$E_n(\phi) = e^{jk\,\rho_0 cos\,(\phi\,-\,\psi_0)} + \sum_{q\,=\,1}^{N} [\; g\,(b_q,\phi,\psi_{q0},\rho_{q0}) + \sum_{\substack{l\,=\,1 \\ l\,\neq\,q}}^{N} C_l\; g\,(b_q,\phi,\psi_{ql},s_{ql})]\;\; e^{jks_q\cos(\phi\,-\,\psi_q)} \tag{3.45}$$

Again the plane wave scattering properties of two dimensional bodies of infinite length are conveniently described in terms of the echo width which is given by

$$W\,(\phi) = \frac{4}{k}\;\; \left|P\,(\phi)\right|^2 \tag{3.46}$$

while the backscattering echo width W is given at $\phi = \phi_0 + \pi$.

3.4 *Results and discussion*

3.4.1 Plane wave excitation

The accuracy and restriction of the approximate solution will be examined with respect to the boundary value solution. Examples of a plane wave exciting different numbers of cylinders will be used. The two methods described earlier are employed, the boundary value solution is denoted by method 1 while the asymptotic solution is denoted by method 2. First consider the case of plane wave scattering by two cylinders. For simplicity the radii of the cylinders will be considered equal and denoted by kb in the following numerical calculations unless otherwise stated. Figs. 3.2(a) and 3.2(b) show the echo width patterns for $kb = 0.1$ and 1.0, respectively, while the separation between the centers of the two cylinders is $ks = 3$ and the

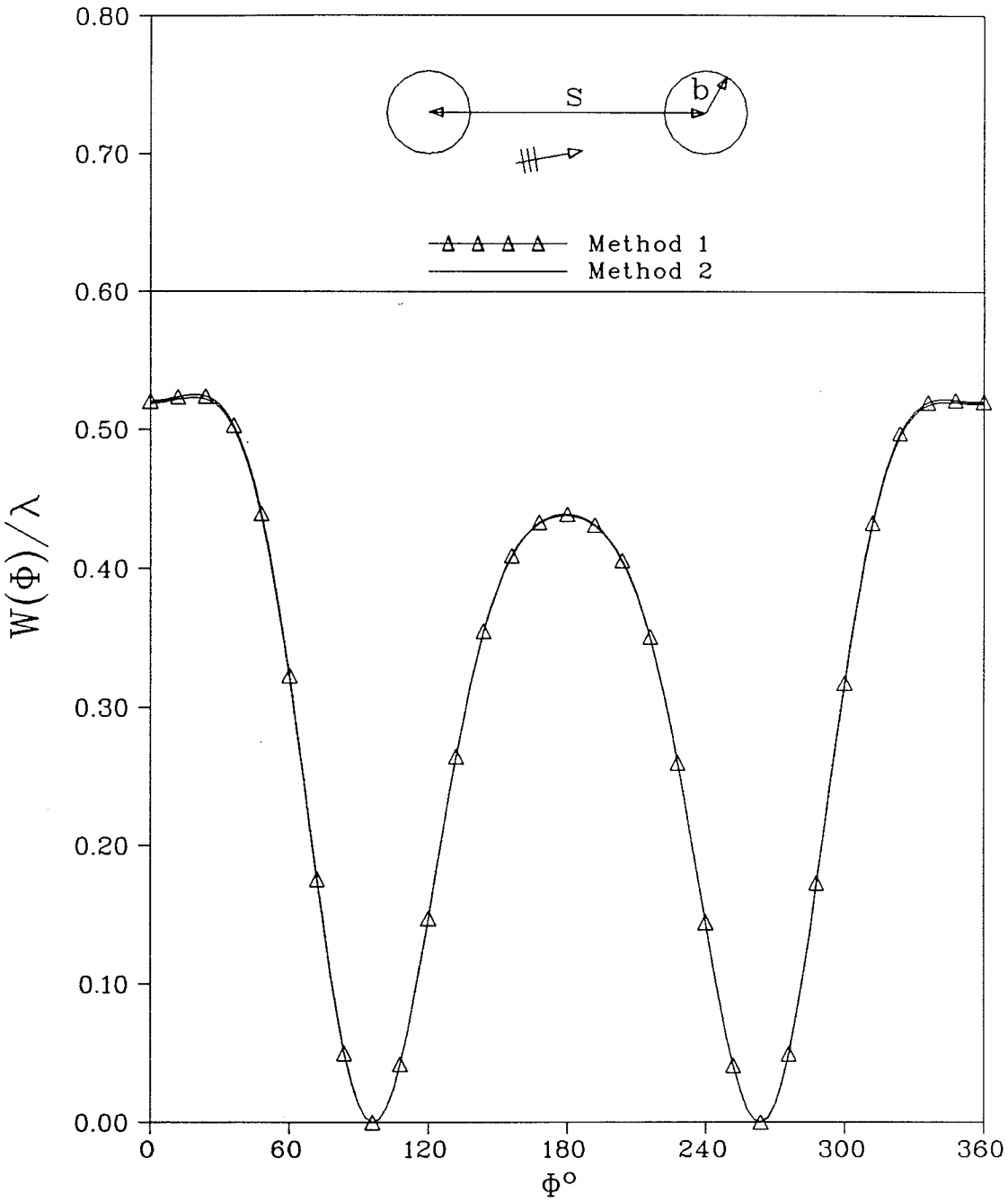

Fig. 3.2(a) : Echo width pattern of two cylinders (kb = 0.1, ks = 3.0, Φ_0 = 10°).

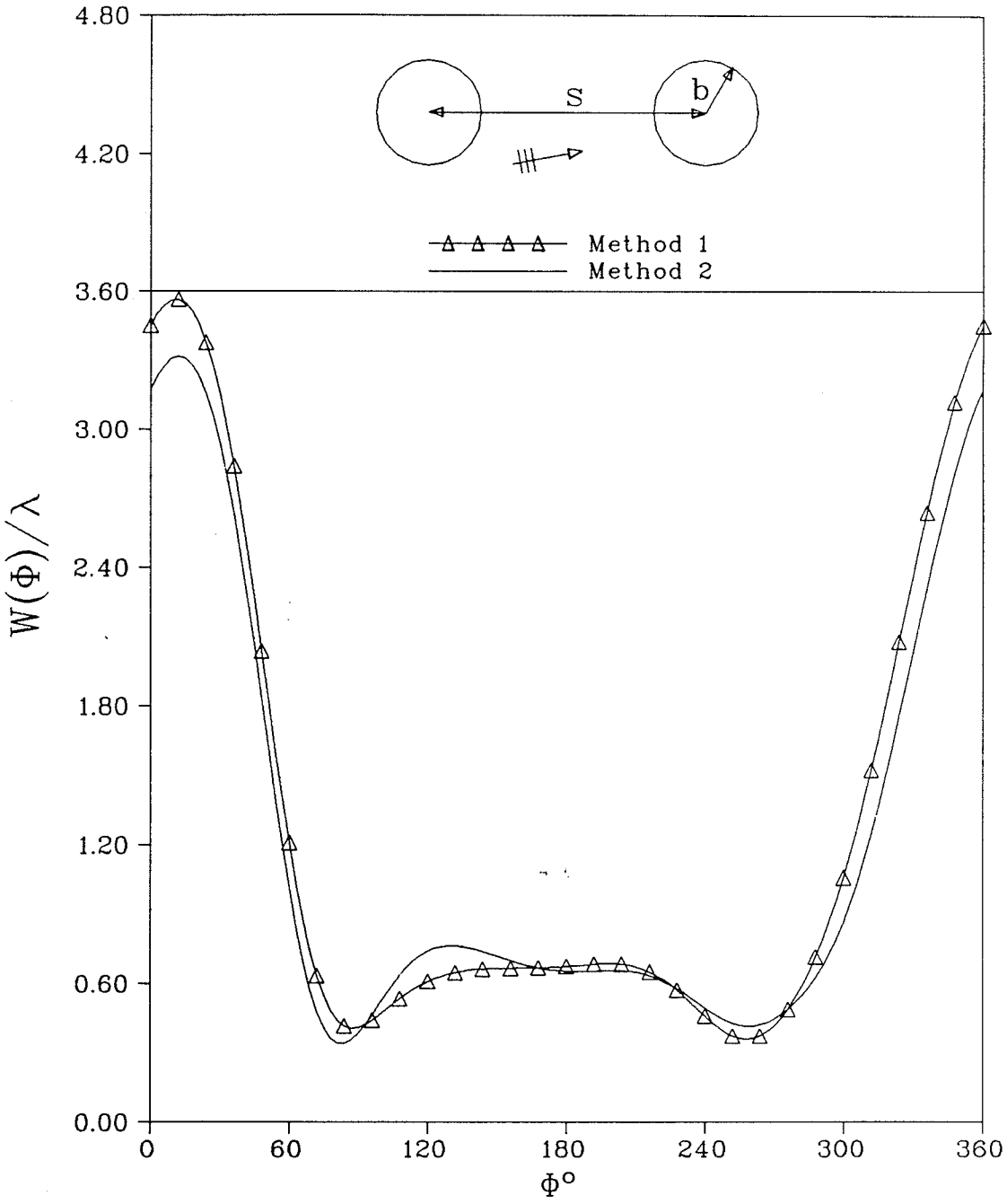

Fig. 3.2(b) : Echo width pattern of two cylinders (kb = 1.0, ks = 3.0, Φ_0 = 10°).

angle of incidence is $\phi_0 = 10^o$. The numerical results in Fig. 3.2 are based on methods 1 and 2. Agreement between the two methods is very good in Fig. 3.2(a) and somewhat better than in Fig. 3.2(b), since the approximations used in method 2 become restrictive when the separation between the two cylinders is very large relative to the radius. In Fig. 3.3 the backscattering echo width is calculated for different separations between the two cylinders in which ks' is equal to $(s - 2a)k$. Fig. 3.3(a) shows the backscattering echo width for $kb = 0.1$ and incidence angle of 60^o, while in Fig. 3.3(b) $kb = 1$ and the incident angle is 90^o. As can be seen from Fig. 3.3(a) the results based on methods 1 and 2 are identically the same, which confirms that method 2 is ideal for the case of thin cylinders. From Fig. 3.3(b) the backscattering echo width based on method 2 deviates at small separations from that of method 1, as expected, because the cylinders are thick in this case.

For the case of more than two cylinders, Fig. 3.4 presents the echo width patterns based on both methods for an equi-spaced linear array of three cylinders. The radius kb and the separation between the successive cylinders are 0.75 and 2π, respectively, while the incidence angle is 90^o. As can be seen, the results based on method 2 agree quite well with those based on the exact solution. Fig. 3.5 gives the backscattering echo width for an equi-spaced linear array of three cylinders at different separations ks'. The calculations based on method 2 deviate at small separations from those based on the exact method. But for larger separations the two methods give almost completely identical results.

3.4.2 Line source excitation

Our first example involves the simulation of a conducting strip where the results by methods 1 and 2 are compared with the integral equation formulation technique (IEF) solved by the method of moments. The strip width is 1 λ and is simulated by cylinders of equal radii (0.016 λ). Fig. 3.6 presents the far field patterns

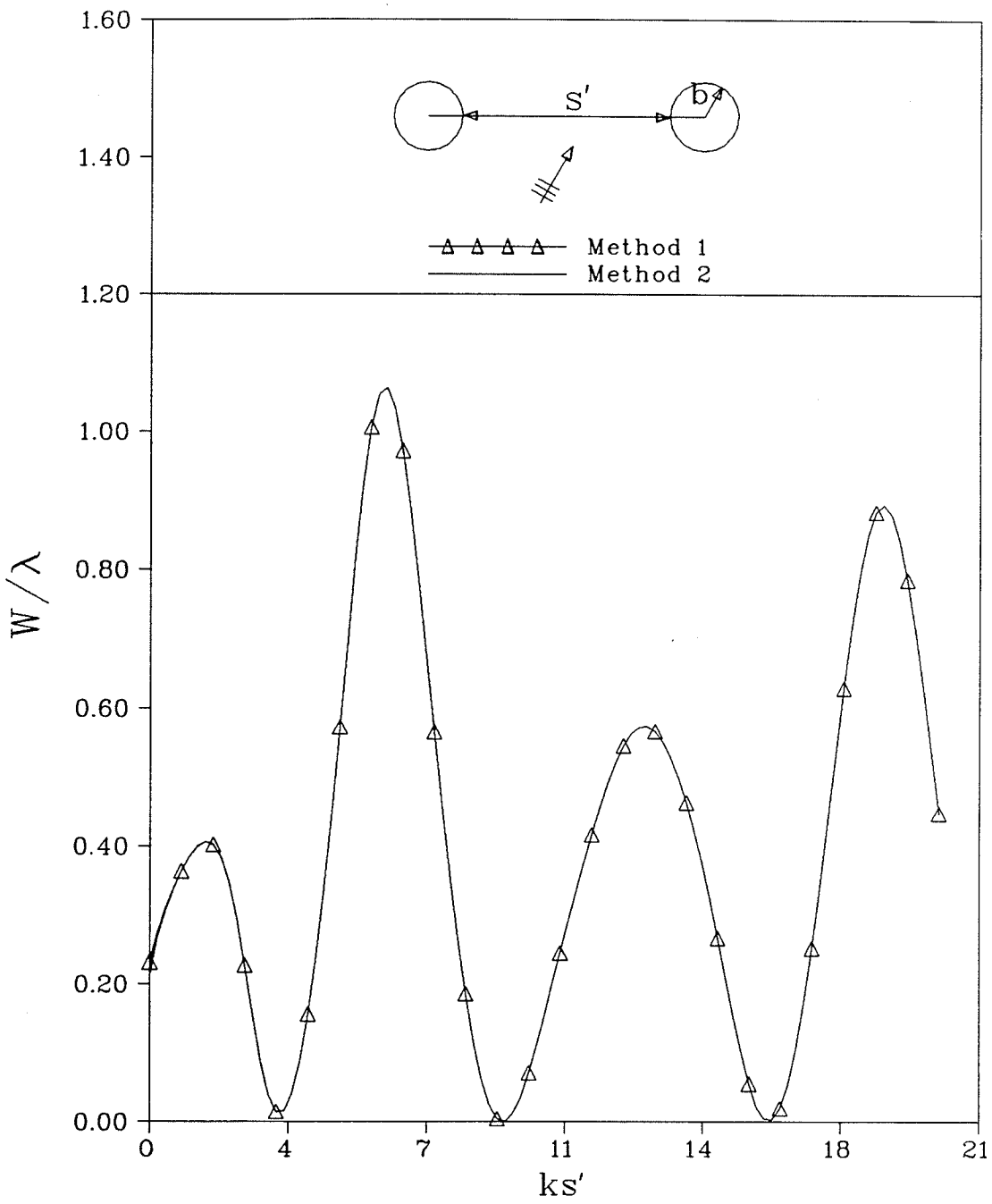

Fig. 3.3(a) : Backscattering echo width of two cylinders (kb = 0.1, Φ_0 = 60°).

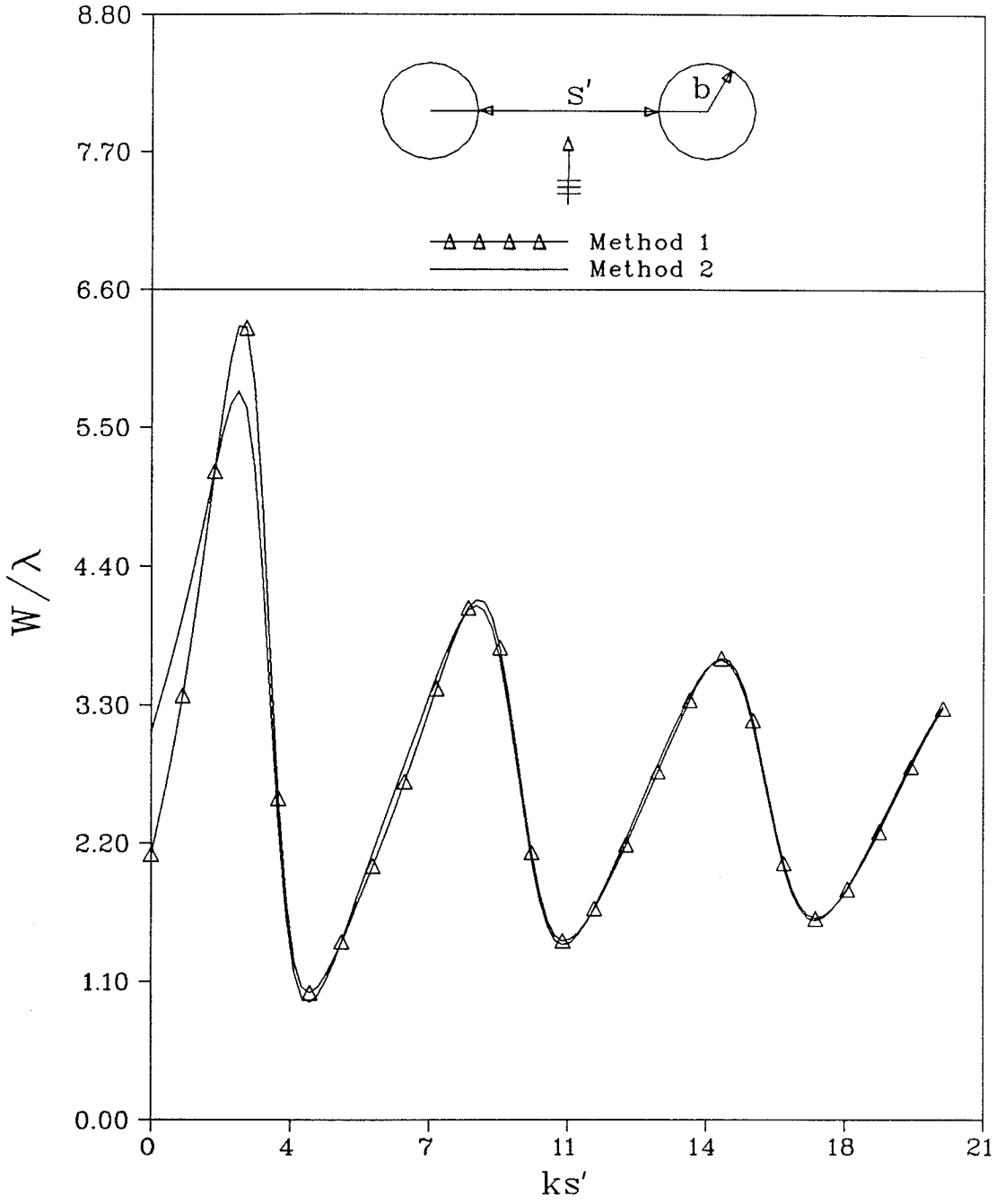

Fig. 3.3(b) : Backscattering echo width of two cylinders (kb = 1.0, Φ_0 = 90°)

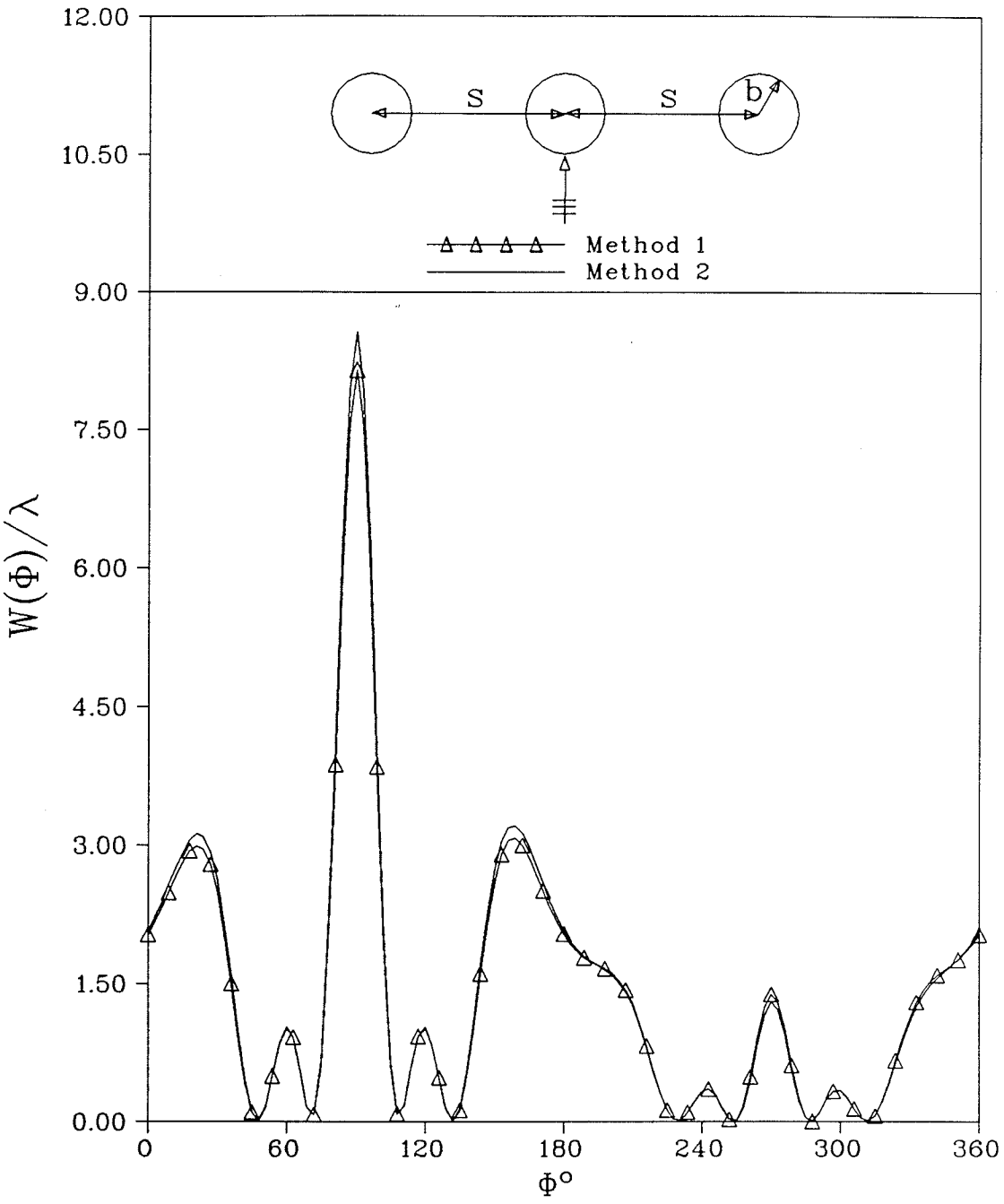

Fig. 3.4 : Echo width pattern of three cylinders (kb = 0.75, ks = 2π, Φ_0 = 90°).

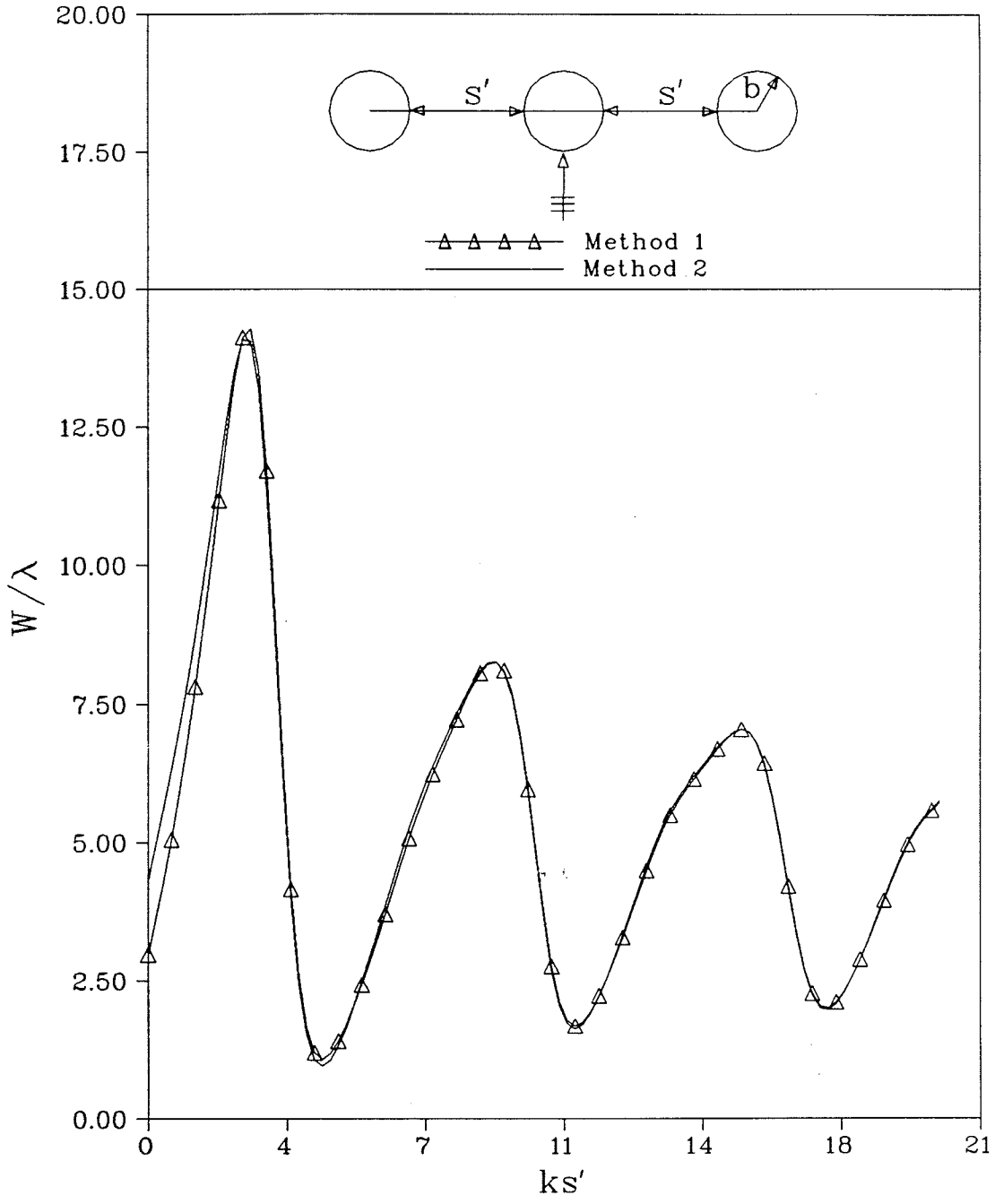

Fig. 3.5 : Backscattering echo width of three cylinders (kb = 0.75, Φ_0 = 90°).

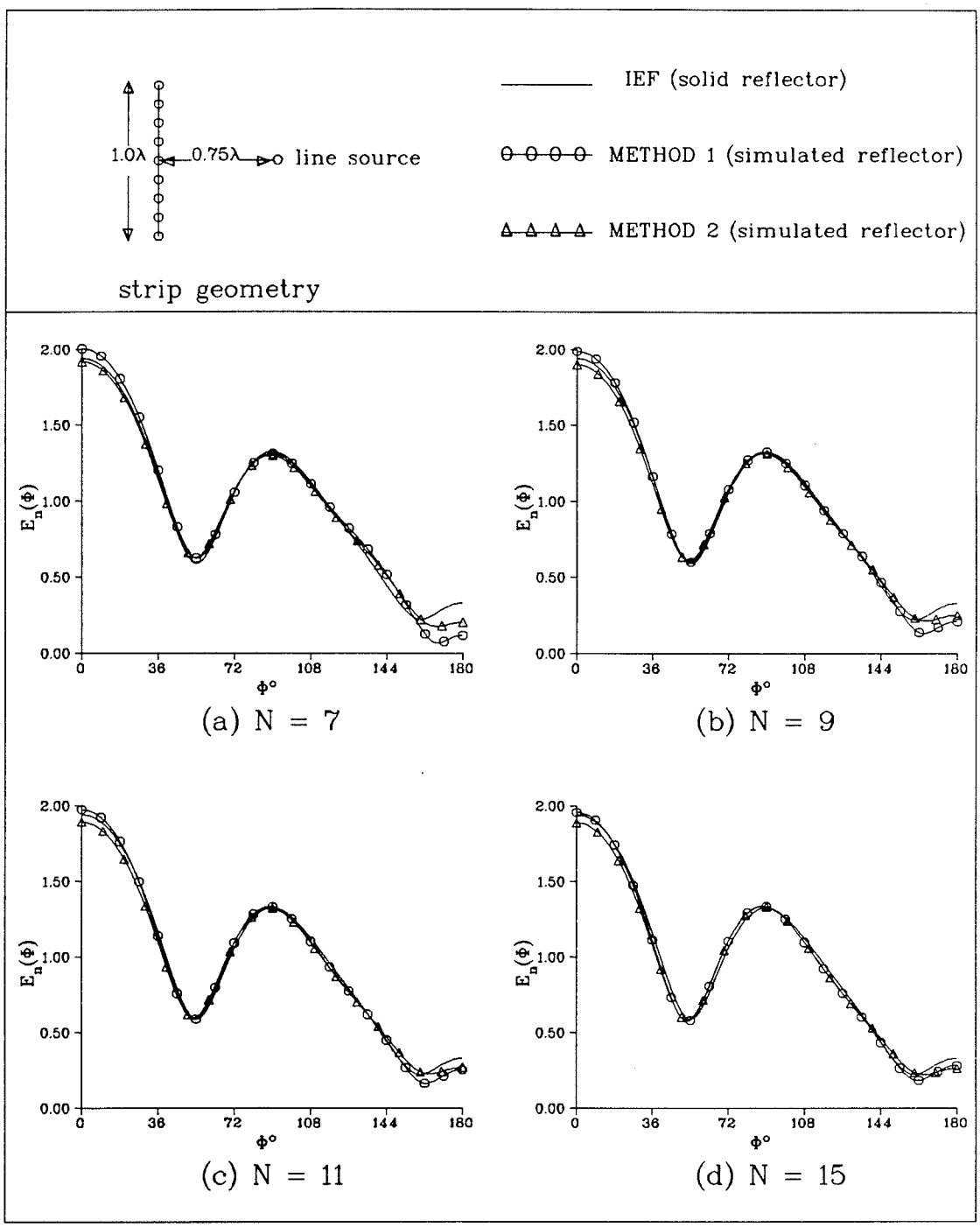

Fig. 3.6 : Far field pattern of a strip in the vicinity of a line source (simulation by equal radii and equally spaced circular cylinders).

corresponding to $N = 7, 9, 11$ and 15 cylinders simulating the strip. A comparison between the patterns of the simulated strip with that of the solid strip of the same total width indicates that the deviation in the back lobe level decreases by increasing the number of cylinders. Thus the case $N = 15$ gives a pattern very close to that of the solid strip. An attempt to improve the radiation pattern by simulating the strip using circular cylinders of unequal radii and spacing is shown in Fig. 3.7. Four cases are shown corresponding to $N = 7, 9, 11$, and 13. The cylinders are arranged so that the radius of the cylinder located at the strip center is equal to 0.01 λ , while the radii of the other cylinders increase by an increment of 0.004 λ towards the edges. The spacing between the centers of each two adjacent cylinders is increased by an increment of 0.008 λ in the edge direction. It is found that when $N = 13$ the beam width decreases by 4^o relative to that of the solid strip, while the first side lobe is very close to that of the solid strip.

Figure 3.8 presents the far field patterns due to a cylindrical parabolic reflector of 3 λ width and 1 λ focal length. Four cases are shown corresponding to $N = 21$, 31, 35 and 41. The cylinders have equal radii (0.016 λ) and spacing. It is noticed that for $N = 41$ the radiation pattern of the simulated reflector is very close to that of the solid reflector. Also by increasing the number of simulating cylinders the radiation pattern does not improve. To improve the radiation pattern of the simulated reflector, different radii and spacing of the simulating cylinders are used. Figure 3.9 indicates the far field patterns for four cases corresponding to $N = 17, 21, 25$, and 27. The radius of the cylinder at the center of the reflector is 0.01 λ and the radii of the other cylinders are increased by an increment of 0.004 λ while the spacing is increased by 0.008 λ towards the edge. The far field pattern of $N = 27$ shows an improvement in the first side lobe level by approximately 19% while the main beam field intensity is increased by 13% over that of the solid reflector. The deviation which appears in the pattern of the solution by method 2 is due to the larger radii of some cylinders used in simulating the reflector where a large spacing between each

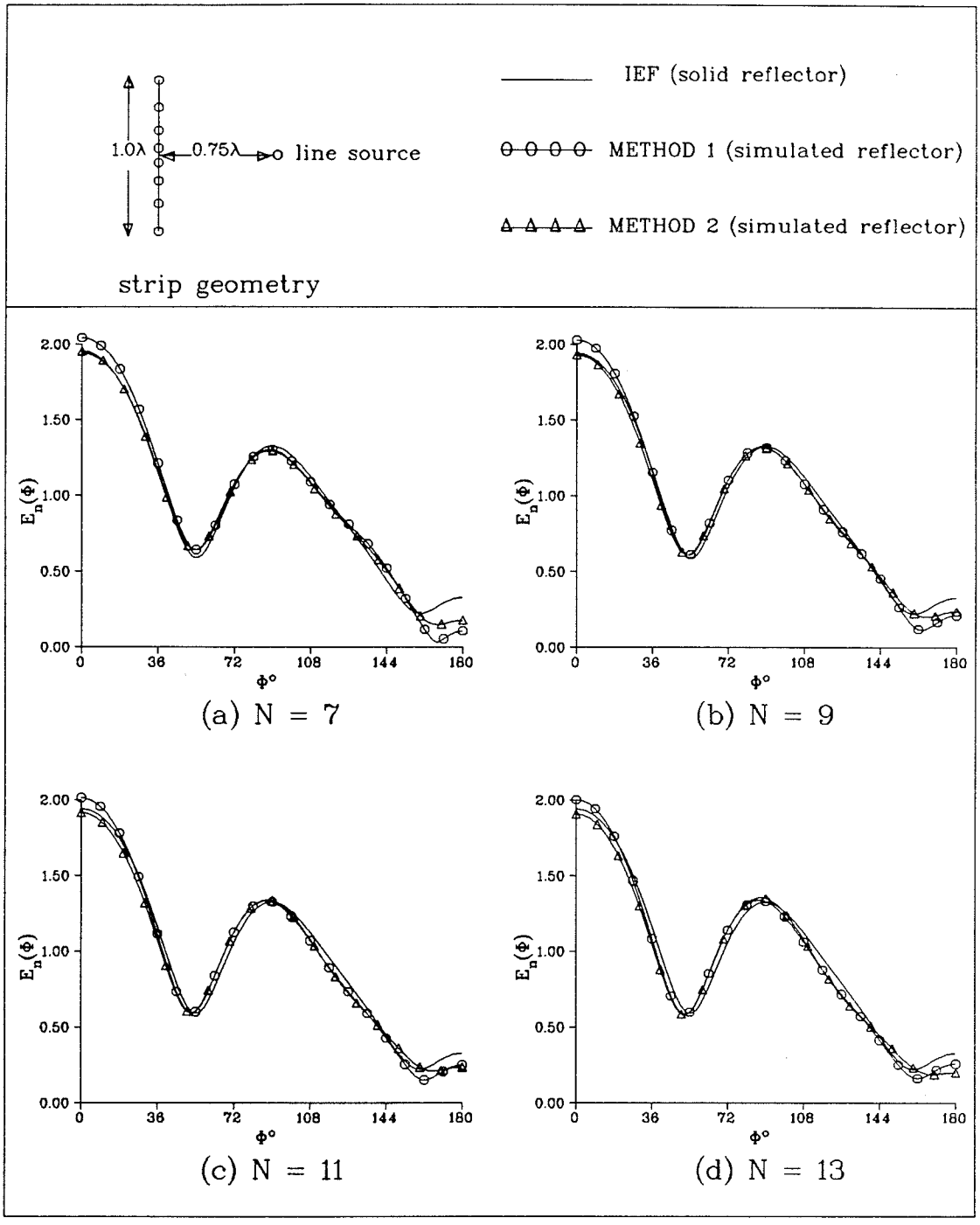

Fig. 3.7 : Far field pattern of a strip in the vicinity of a line source (simulation by unequal radii and unequally spaced circular cylinders).

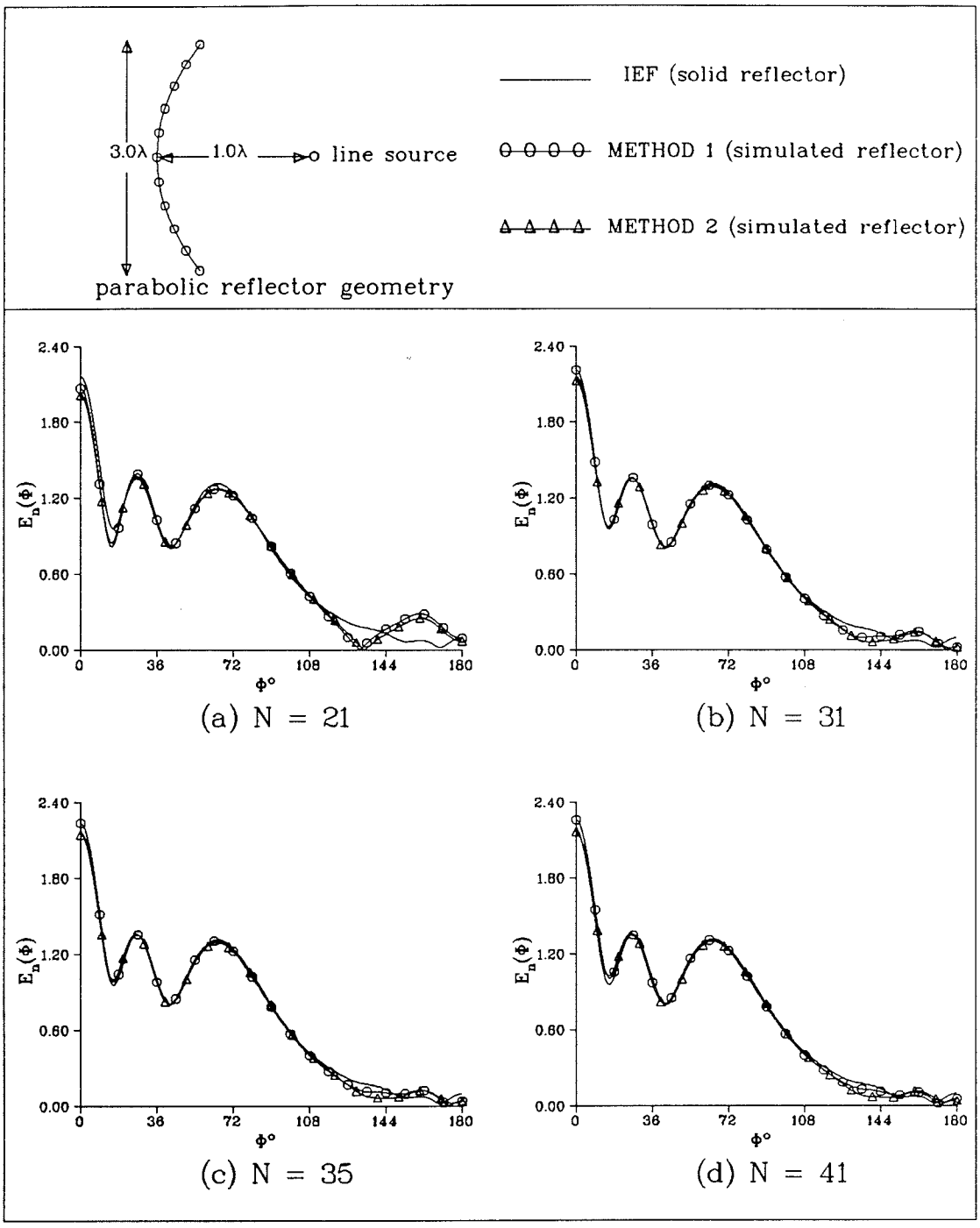

Fig. 3.8 : Far field pattern of a parabolic reflector fed by a line source (simulated by equal radii and equally spaced circular cylinders).

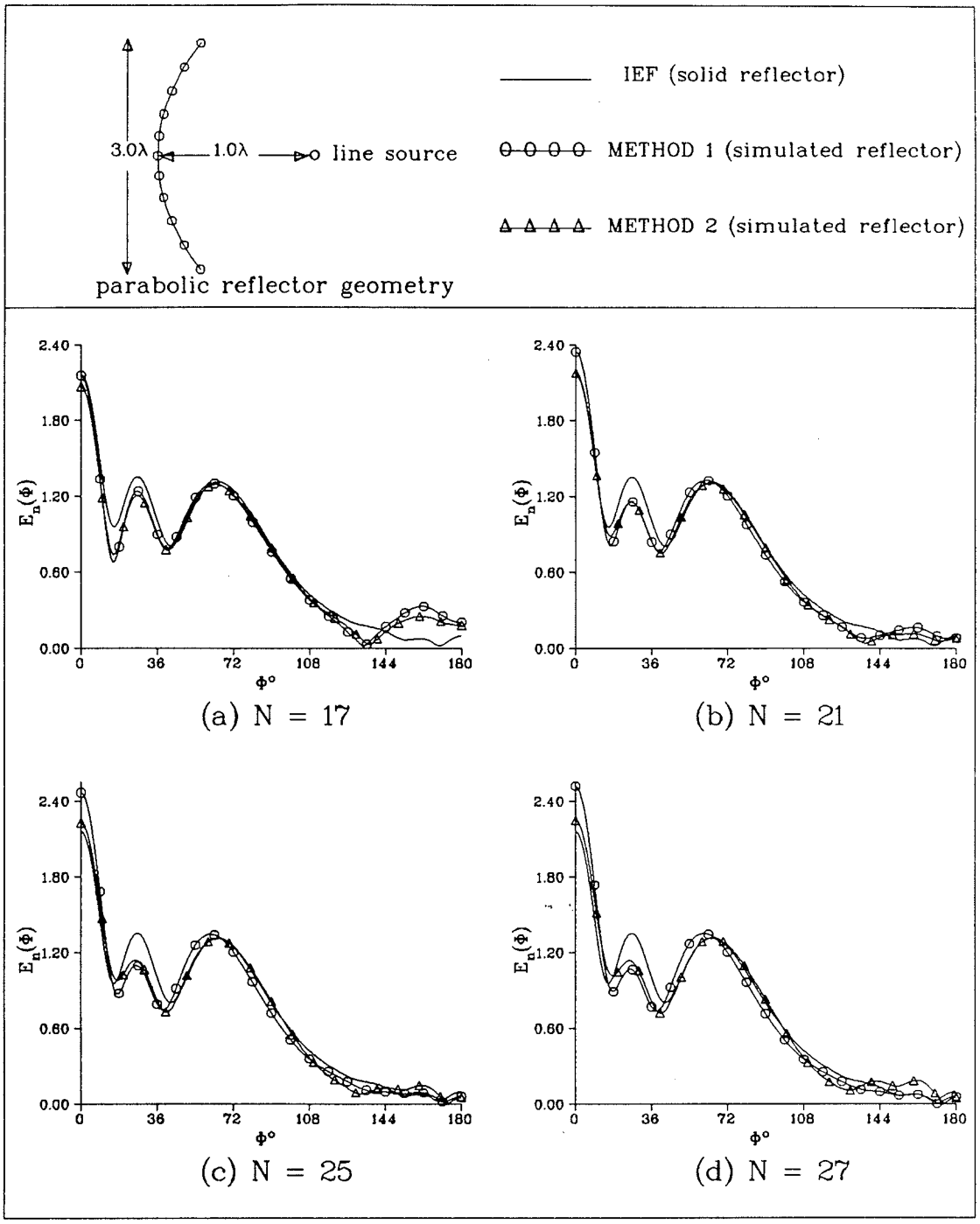

Fig. 3.9 : Far field pattern of a parabolic reflector fed by a line source (simulated by unequal radii and unequally spaced circular cylinders).

two adjacent cylinders with respect to their radii is required by the method. The solution by method 1 yields good results and shows that an improvement in the radiation pattern could be achieved using unequal radii and spacing.

Another example of simulating a cylindrical circular reflector is presented in Fig. 3.10. Four cases are shown corresponding to N = 41, 51, 55 and 57 cylinders. The cylinders have equal radii (0.016 λ) and spacing. The circular cylindrical reflector has a radius of 1.6 λ. The case of 55 cylinders yields a far field pattern close to that of the solid reflector with a higher main beam field intensity.

Finally the corner reflector is also simulated as shown in Fig. 3.11. The reflector has 1 λ length, 90^o corner angle and a source placed at 0.3 λ from the apex. Figure 3.11 presents the far field patterns corresponding to the cases N = 13, 17, 21 and 25. The simulating cylinders have equal radii (0.016 λ) and spacing. The patterns show good agreement with the solid reflector pattern in the case of N = 25. Figure 3.12 shows the results of a corner reflector simulation using unequal radii and spacing between the circular cylinders. The cylinder at the apex has a radius of 0.01 λ while the other radii are increased from the apex towards the edges by an increment of 0.003 λ with the spacing increased by an increment of 0.006 λ. Four cases are shown in Fig. 3.12 corresponding to N = 15,17,19 and 21. The case of N = 21 cylinders yields a very close pattern to that of the solid reflector pattern when using method 1 while method 2 gives a high back lobe. Also the beam width in this case is decreased while the main beam field intensity is decreased by 8% relative to that corresponding to the solid reflector.

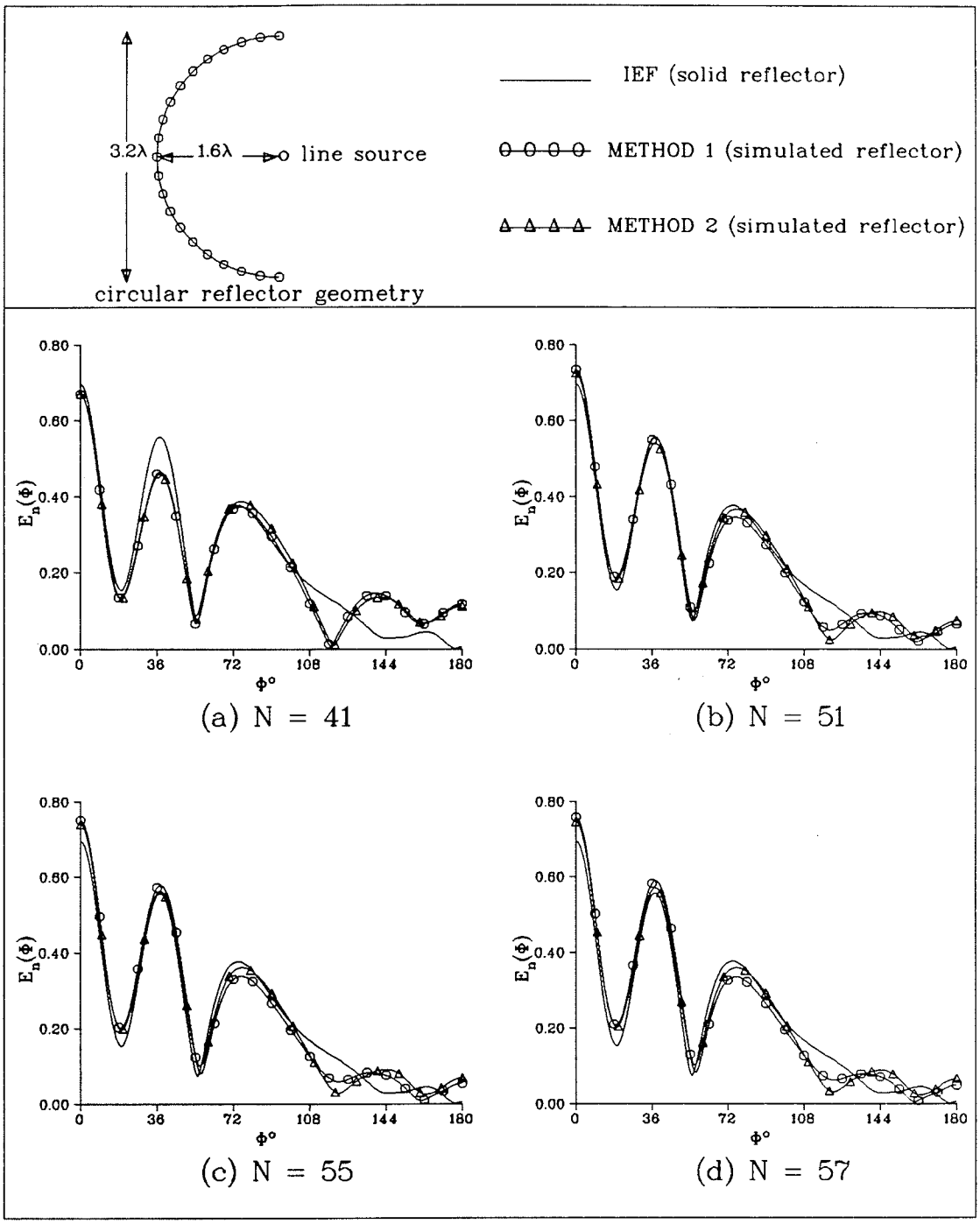

Fig. 3.10 : Far field pattern of a circular reflector fed by a line source (simulated by equal radii and equally spaced circular cylinders).

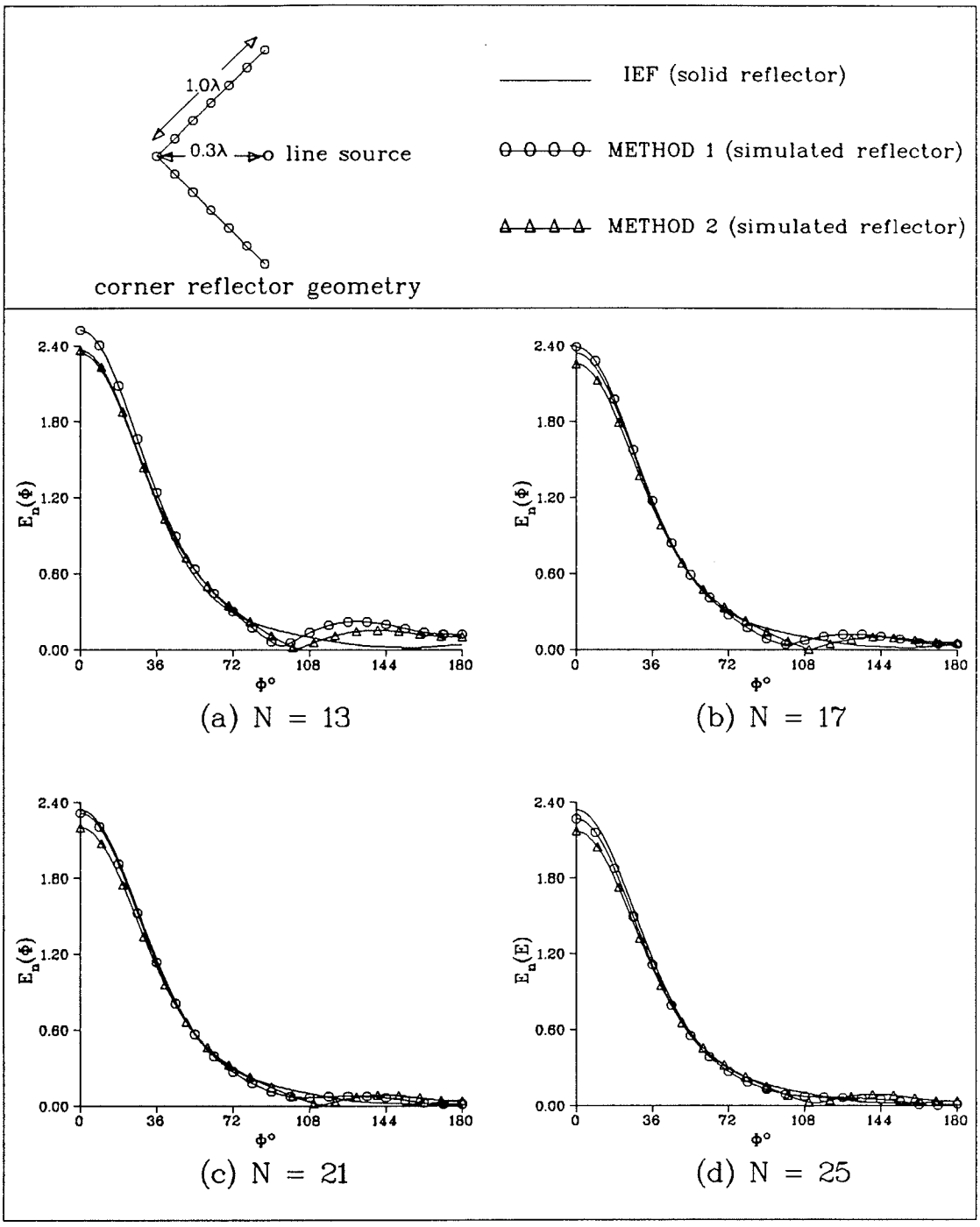

Fig. 3.11 : Far field pattern of a corner reflector fed by a line source (simulation by equal radii and equally spaced circular cylinders).

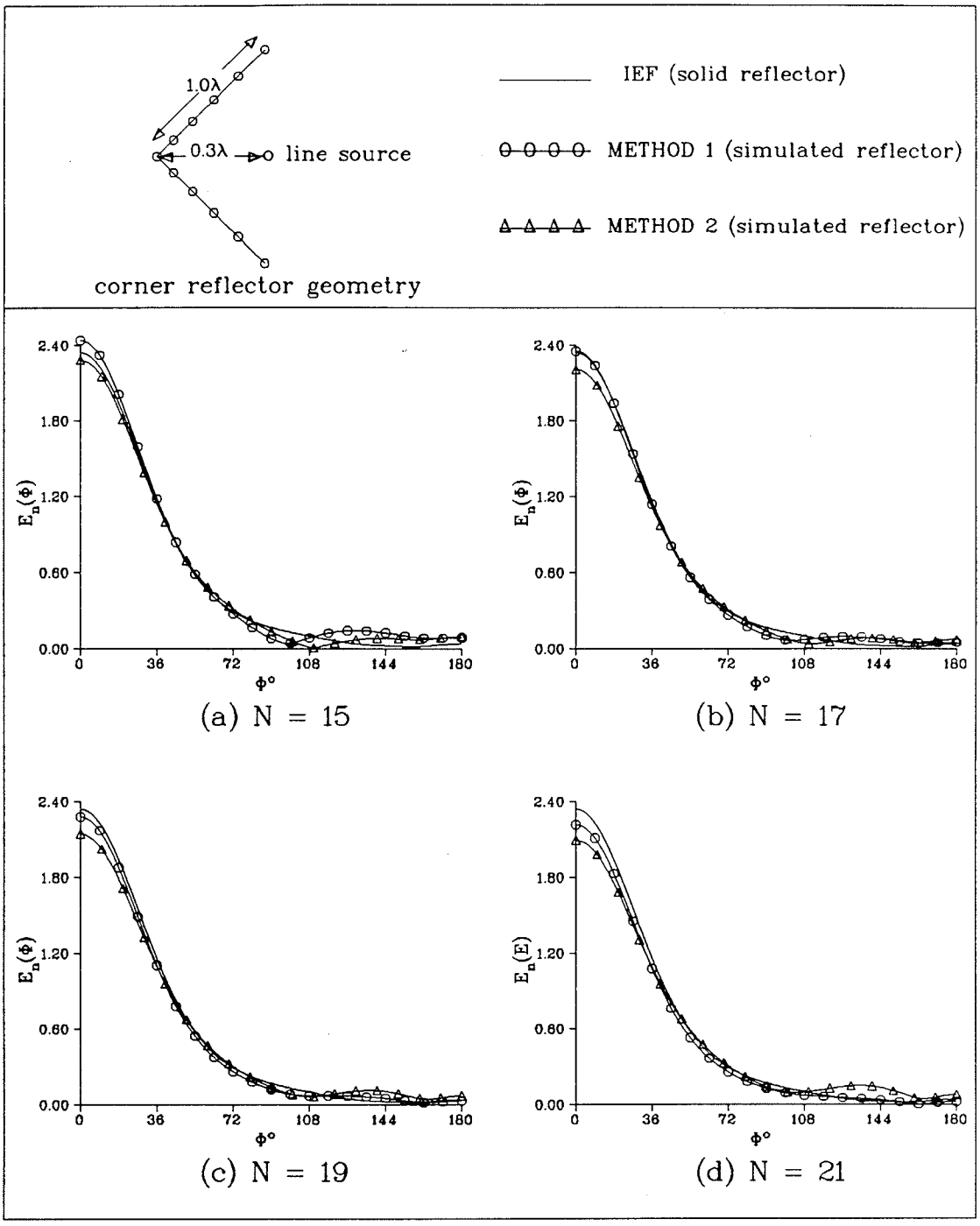

Fig. 3.12 : Far field pattern of a corner reflector fed by a line source (simulation by unequal radii and unequally spaced circular cylinders).

3.5 *Engineering considerations*

Primarily our study in Chapters 2 and 3 is aimed at presenting a design analysis to be used for a large variety of electromagnetic applications. The numerical results obtained throughout this project mainly recommend the simulation by both equally spaced equi-width strips and unequal radii and unequal spacing between circular cylinders for antenna applications. These distributions can improve or provide the same the electrical performance of simulated reflector antennas with respect to the corresponding continuous surface reflector antennas. However, an overall optimum design requires more information about other parameters such as surface stresses, weight, rigidity and thermal effects. For instance, if the weight is the main concern for a certain antenna application, hollow or half tubes facing the radiation zone may be used for simulation. In other applications when the stresses become a serious problem, as in the case of scanning radars, such stresses may destroy the reflector antenna surface and hollow rods may therefore be used for simulation for the outermost elements (i.e. near the outer edges) of that kind of reflector antenna. When wind loading and thermal effects are serious simulation by cylinders rather than strips is recommended. On the other hand, an advantage of using strips rather than cylinders is evident when the adjacent strips of a strip simulated reflector rotated sequentially to generate beam scanning in the horizontal plane for target detection. This avoids rotation of the whole reflector and can not be achieved with a cylinder simulated reflector.

It becomes therefore clear that in order to obtain an optimum design for a simulated antenna, other factors from the specified application has to be clearly recognized and incorporated in the design in a manner which is beyond the scope of this thesis. An example of simulating cylindrical parabolic reflector antenna of 4 λ width and 1.5 λ focal length is introduced here to illustrate the complexity of simulation by circular cylinders as opposed to strips. In case of the simulation

by circular cylinders a hypothetical assumption is made, due to mechanical considerations, that the radii of the cylinders lie between 0.01 λ and 0.06 λ, while for strip simulation widths lie between 0.06 λ and 0.15 λ.

Consider the simulation by circular cylinders, linear distributions for the radii and spacings can be expressed as

$$b_i = b_0 + i\ \Delta_1 \tag{3.47}$$

$$s_{ij}' = s_{01}' + i\ \Delta_2 \tag{3.48}$$

where Δ_1 and Δ_2 are the increments in the radius and spacing, respectively, i takes the values 0, 1,..., $(N-1)/2$ for the upper half of the simulated reflector while for the lower half similar distributions are assumed. b_0 is the radius of the cylinder at the middle of the reflector while s_{ij}' is the separation between the two successive cylinders i and j and $j = i + 1$. Using (3.47) and (3.48) the following distributions are produced :

(i) $\Delta_1 = \Delta_2 = 0$

(ii) $\Delta_1 = 0$, $\Delta_2 > 0$

(iii) $\Delta_1 = 0$, $\Delta_2 < 0$

(iv) $\Delta_2 = 2\,\Delta_1$, $\Delta_1 > 0$

(v) $\Delta_2 = 2\,\Delta_1$, $\Delta_1 < 0$

Now, let us examine the simulation by equal radii and spacing circular cylinders which corresponds to distribution (i). In this case we use $b_0 = 0.01$ in order to minimize the amount of material used for the simulation. Fig. 3.13 shows the axial field of the simulated reflector versus the number of cylinders used for simulation. From this figure one can predict what is the minimum number of cylinders necessary for simulation without a significant deterioration in the

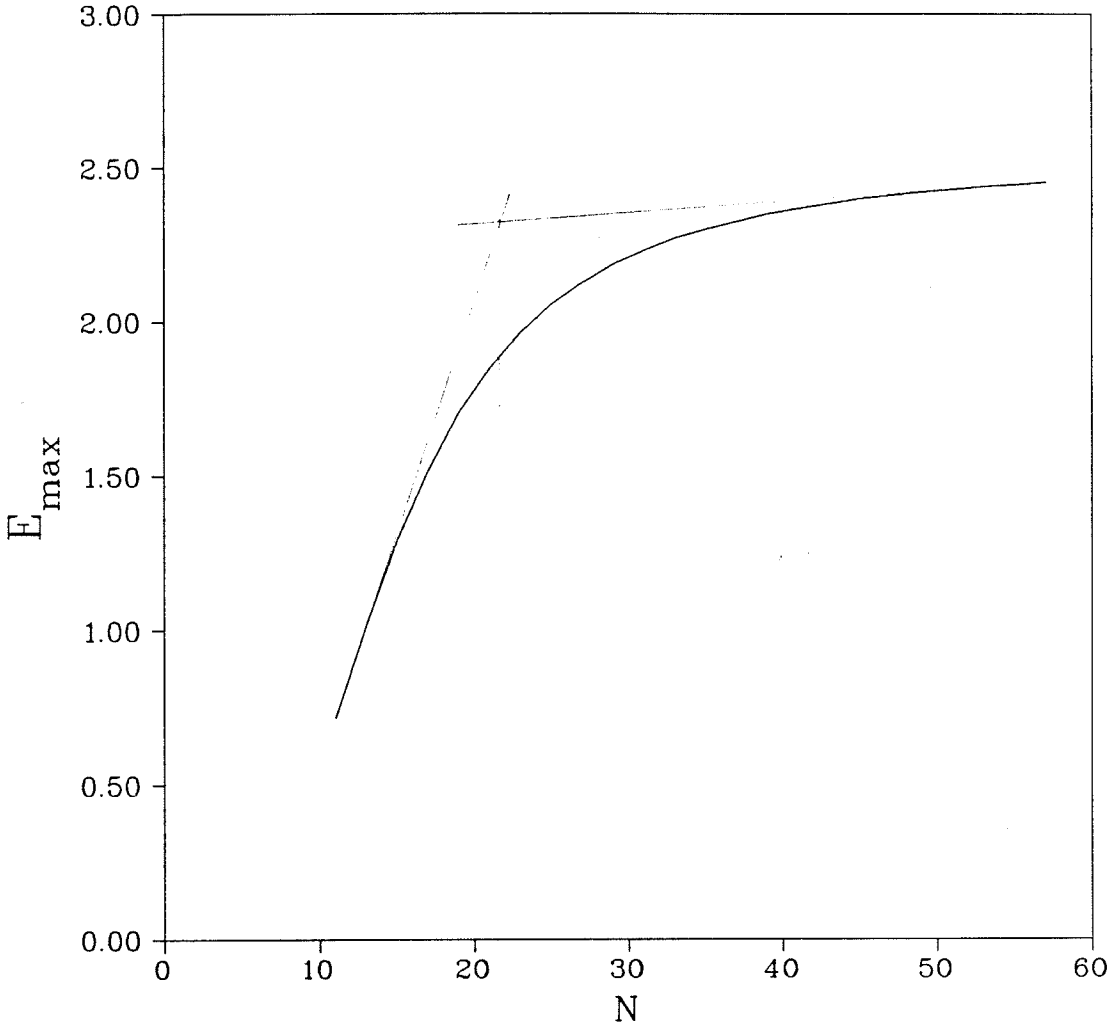

Fig. 3.13 : Axial field vs. the number of cylinders

antenna performance. This can be seen by first drawing a tangent to the lower part of the E_{max} versus N curve and another to the upper part and thus the number corresponding to the point of the intersection of the two tangents, which is 21 in this case, is the limit that one can reasonably use for simulation by cylinders of the specified size and separation. However if one uses 21 cylinders in this example and employ distribution (ii), which corresponds to equal radii and unequal spacing, one can still improve the radiation performance. But for any further improvement of the simulated antenna performance one needs to choose distribution (iv), shown in Fig. 3.14, which employs more material for simulation but offers the best electrical performance. Another scheme that might improve the performance of a simulated reflector using the minimum number of cylinders is to shift the locations of the axes of some simulating cylinders away from the original trajectory which requires an optimization procedure beyond the scope of this thesis. However, for all possible design cases, the electromagnetic analysis and tools given in the thesis should be sufficient to embark on an optimization path.

Since saving material is one of the simulation objectives, thus one should take $b_0 = 0.01\ \lambda$ which is the lowest permissible radius. The number of cylinders N and the increment Δ_1 are arbitrary and we can fix one parameter and study the effect of the other, and vice versa. In this case we consider $N = 35$ and Δ_1 is variable as shown in Table 3.1 while in Table 3.2 we fix Δ_1 at $0.003\ \lambda$ and vary N. The beamwidth (BW), maximum electric field intensity of the main lobe (E_{max}), electric field intensity of the back lobe (E_b) and the side lobe level (SLL) are evaluated in each case. The values of these quantities in case of the original reflector antenna (unsimulated) of the same dimension are 12.47^o, $7.76\ dB$, $-20.68\ dB$ and $2.79\ dB$, respectively. Comparing these values with the corresponding values in each case in Tables 3.1 and 3.2, one can make an intuitive decision based on how much deterioration in the electrical performance which

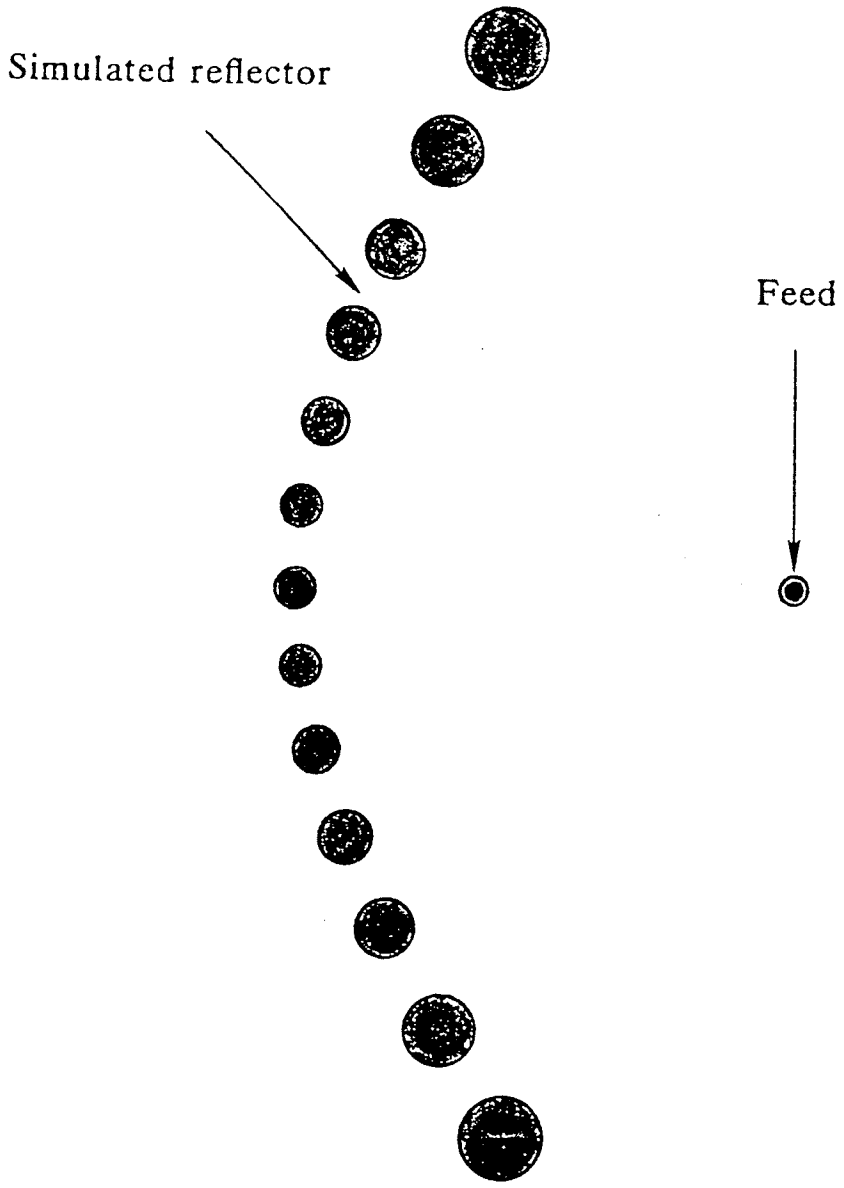

Fig 3.14 : Simulated parabolic cylindrical reflector antenna

can be tolerated for specific application. Of course one can produce a table similar to Table 3.1 for each value of N in Table 3.2 and also a table similar to Table 3.2 for each value of Δ_1 in Table 3.1 which lead to 28 Tables for making an intuitive decision. The best electrical performance from Tables 3.1 and 3.2 is found to be at $N = 35$ and $\Delta = 0.003\,\lambda$. The radiation pattern corresponding to this case is shown in Fig. 3.15.

It should be pointed out that, equal width equi-spaced strips, is the best distribution found so far. The strip width ($2d$) and the number of strips (N) are the only variables in this case. Again repeating the same procedure as in the case of simulation by cylinders, we obtain Tables 3.3 and 3.4. Our intuitive decision, based on the best electrical performance, leads to $2d = 0.14\lambda$ and $N = 25$. The radiation pattern corresponding to this case is shown in Fig. 3.15. Comparison between patterns corresponding to simulation by circular cylinders as opposed to simulation by strips with that of the solid surface reflector shows that the first excels the other two since it has higher main beam intensity and lower side lobe level.

$b_0 = 0.01$					
$BW\,(deg.)$	$E_{max}(dB)$	$E_b(dB)$	$SLL\,(dB)$	Δ_1/λ	N
11.73	7.43	-14.59	2.93	0.0002	35
11.82	7.58	-15.05	2.78	0.0004	35
11.91	7.72	-15.50	2.62	0.0006	35
11.99	7.84	-15.96	2.47	0.0008	35
12.06	7.96	-16.41	2.31	0.0010	35
12.13	8.06	-16.87	2.15	0.0012	35
12.19	8.16	-17.34	1.99	0.0014	35
12.25	8.26	-17.81	1.82	0.0016	35
12.32	8.35	-18.30	1.66	0.0018	35
12.38	8.45	-18.79	1.48	0.0020	35
12.44	8.54	-19.29	1.30	0.0022	35
12.50	8.63	-19.80	1.11	0.0024	35
12.56	8.72	-20.32	0.92	0.0026	35
12.62	8.81	-20.82	0.72	0.0028	35
12.68	8.89	-21.33	0.51	0.0030	35

Table 3.1 : Radiation characteristics of a cylindrcial parabolic reflector simuated by circular conducting cylinders.

$b_0 = 0.01$					
$BW\,(deg.)$	$E_{max}(dB)$	$E_b(dB)$	$SLL\,(dB)$	Δ_1/λ	N
8.09	0.04	-0.23	3.42	0.003	11
8.95	3.14	-1.62	3.63	0.003	13
9.79	5.02	-3.24	3.42	0.003	15
10.39	6.19	-5.03	3.03	0.003	17
10.87	6.95	-6.96	2.62	0.003	19
11.28	7.46	-8.96	2.24	0.003	21
11.62	7.82	-10.99	1.92	0.003	23
11.91	8.09	-13.00	1.65	0.003	25
12.12	8.31	-14.94	1.40	0.003	27
12.29	8.48	-16.79	1.17	0.003	29
12.43	8.63	-18.50	0.95	0.003	31
12.56	8.77	-20.02	0.73	0.003	33
12.68	8.89	-21.33	0.51	0.003	35

Table 3.2 : Radiation characteristics of a cylindrcial parapolic reflector simulated by circular conducting cylinders.

$BW\,(deg.)$	$E_{max}(dB)$	$E_b\,(dB)$	$SLL\,(dB)$	$2d/\lambda$	N
11.77	7.28	-16.65	3.05	0.080	25
11.84	7.34	-17.53	3.02	0.085	25
11.90	7.40	-18.36	3.00	0.090	25
11.96	7.45	-19.14	2.98	0.095	25
12.02	7.49	-19.83	2.96	0.100	25
12.06	7.53	-20.42	2.95	0.105	25
12.10	7.56	-20.90	2.93	0.110	25
12.13	7.59	-21.27	2.92	0.115	25
12.17	7.62	-21.53	2.91	0.120	25
12.25	7.68	-21.80	2.87	0.140	25
12.26	7.68	-21.71	2.87	0.160	25

Table 3.3 : Radiation characteristics of a cylindrical parabolic reflector simulated by conducting strips.

$BW\,(deg.)$	$E_{max}(dB)$	$E_b\,(dB)$	$SLL\,(dB)$	$2d/\lambda$	N
10.27	6.96	-6.85	3.53	0.14	14
10.77	7.50	-10.12	3.40	0.14	16
11.13	7.77	-13.28	3.20	0.14	18
11.40	7.90	-16.14	3.19	0.14	20
11.59	7.98	-18.47	3.11	0.14	22
11.72	8.00	-20.08	3.07	0.14	24
11.82	8.00	-20.98	3.00	0.14	26
11.88	8.00	-21.35	3.01	0.14	28
11.91	7.99	-21.38	3.00	0.14	30

Table 3.4 : Radiation characteristics of a cylindrical parabolic reflector simulated by conducting strips.

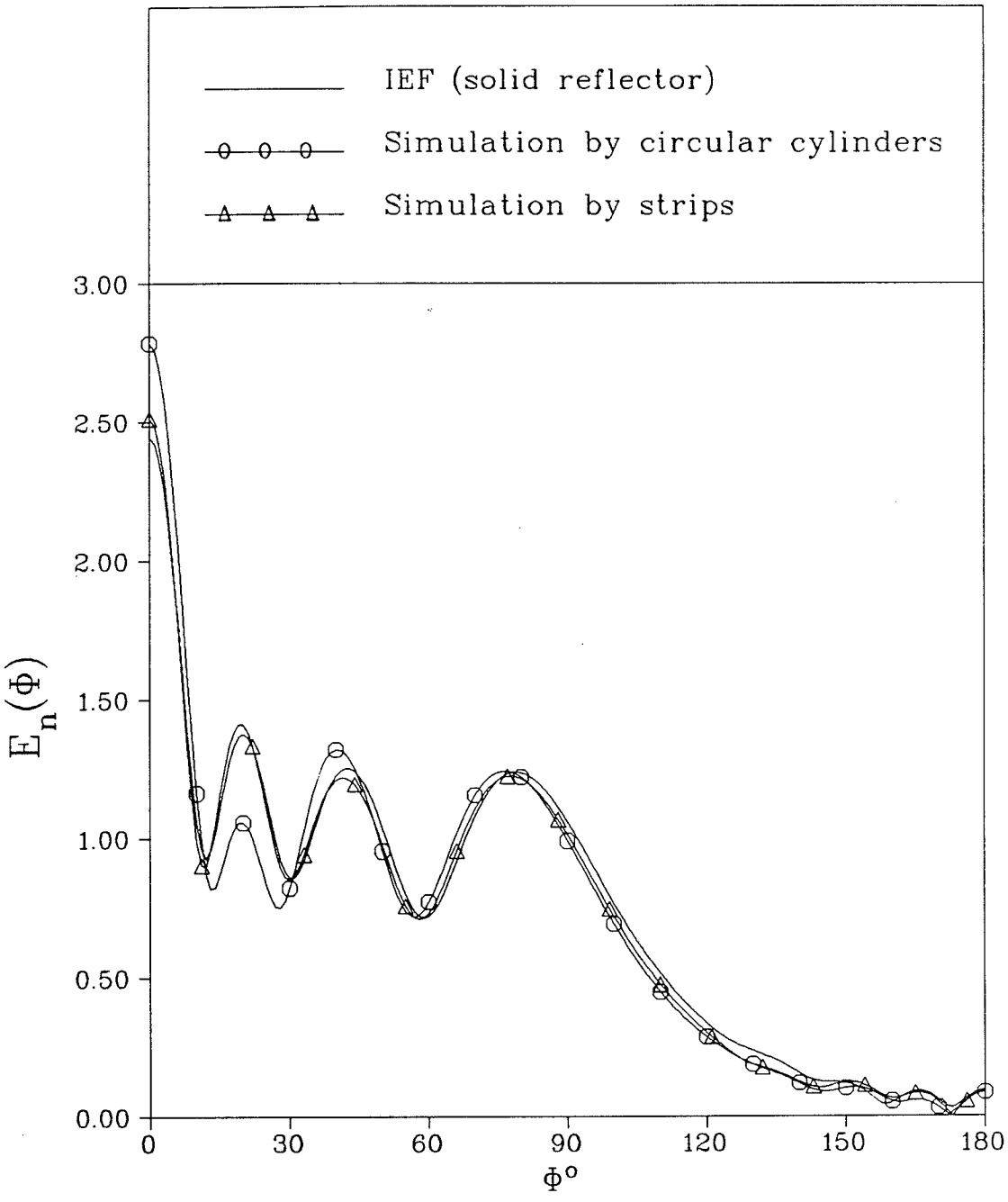

Fig. 3.15 : Far field pattern of solid and simulated parabolic cylindrical reflector antenna.

CHAPTER 4

ANALYSIS OF A LONG DIPOLE ANTENNA WITH ARBITRARY FEED POSITION

4.1 *Introduction*

In previous chapters an ideal line source has been used as a feed for the simulated reflector antenna. In practice, such a line source does not exist, therefore a thin long dipole antenna is chosen to be the feed for the simulated reflector. The long dipole antenna has been widely investigated as described earlier. Among those investigations is the work reported by Hurd [58] which is extended in this chapter since it is viewed as a special case of arbitrarily fed dipole. The extension includes expressions for the current distribution and radiation field of an arbitrarily fed dipole, which are not given in Hurd's work, as well as generalizing the input admittance formula of the center fed dipole to the case of an arbitrarily fed dipole. It is important to stress that the feed of the long dipole antenna used here is a delta function generator. It was pointed out by Chen and King [78] that for a thin dipole antenna it is essential to replace the Bessel and Hankel function involved in the current integral equation by their power series approximation in order to remedy the effect of the delta function generator. Since in our case only a thin dipole is considered and the Bessel and Hankel functions are approximated by leading terms in their power series, the solution is reasonable in practice.

The solution of the arbitrarily fed dipole is based on the solutions of two auxiliary problems as shown schematically in Fig 4.1. A symmetrically fed dipole (two identical sources located at the same distance l from the center as shown in Fig. 4.1-b) is treated first, then the antisymmetrically fed dipole (where one source is out of phase from the other by 180^o as shown in Fig. 4.1-c) is introduced. A superposition of the solutions of these two problems leads to the solution of the arbitrarily fed

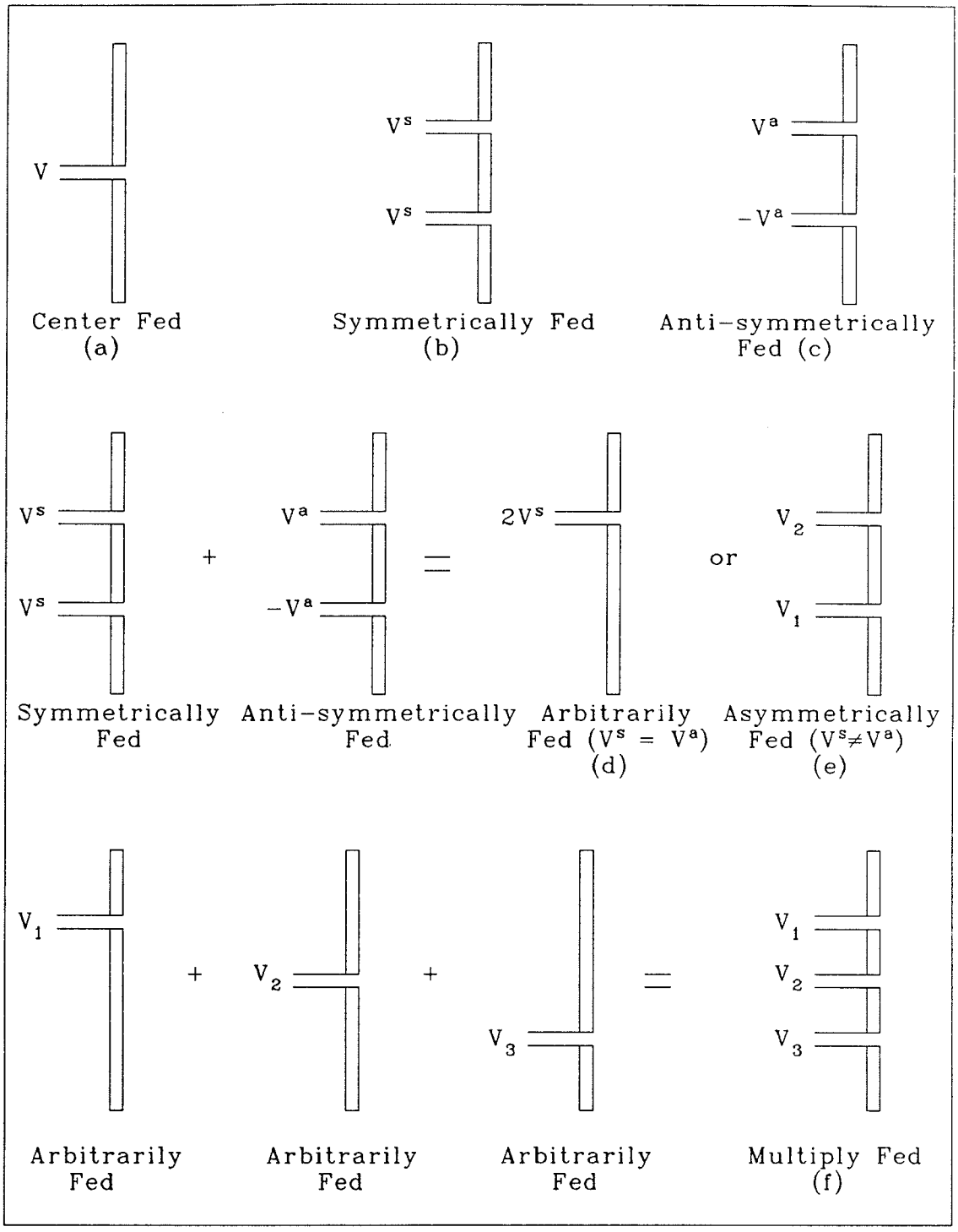

Fig. 4.1 : Schematic diagram of different dipoles

dipole antenna as shown in Fig. 4.1-d. The multiply fed dipole is also considered as a superposition of arbitrarily fed dipoles (see Fig. 4.1-f). Results for the input admittance, current distribution and radiation pattern for various dipole lengths are evaluated and compared with the published data [79]. It should however be emphasized that Hurd's work has not been extended to dipoles shorter than about $\lambda/2$ and therefore all dipole segments (feed to feed or feed to edge) must be longer than $\lambda/4$ for the analysis in this chapter to be valid.

4.2 *Current distribution on a symmetrically driven dipole*

4.2.1 **Formulation**

The geometry of the antenna under consideration is shown in Fig. 4.2-a. The antenna is assumed to be a thin walled, perfectly conducting tube occupying the region $\rho = a, -h \leq z \leq h$, of the (ρ,ϕ,z) cylindrical coordinate system. It is driven at $z=+l$ and $-l$ by two identical voltage sources each with a voltage V^s applied across an infinitesimal gap. The electric field component in either gap is given by

$$E_z = -V^s \{ \delta(z+l) + \delta(z-l) \} \tag{4.1}$$

where δ is the Dirac delta function. The space surrounding the antenna is divided into two regions, denoted by 1 for $\rho < a$ and 2 for $\rho > a$. Field components in these regions will henceforth be distinguished by appropriate superscripts. It is assumed that all field components are derivable from the z-component of the electric Hertz vector. In either region, one can write the z-component of the Hertz vector in the form

$$\Pi_z^{(i)} = \int_{-\infty}^{\infty} A_i(\xi)\, Z_i(\beta\rho)\, e^{j\xi z}\, d\xi \qquad , \quad i = 1,2 \tag{4.2}$$

where $\beta^2 = k^2 - \xi^2$, $A_i(\xi)$ are amplitude functions, and Z_i are Bessel functions

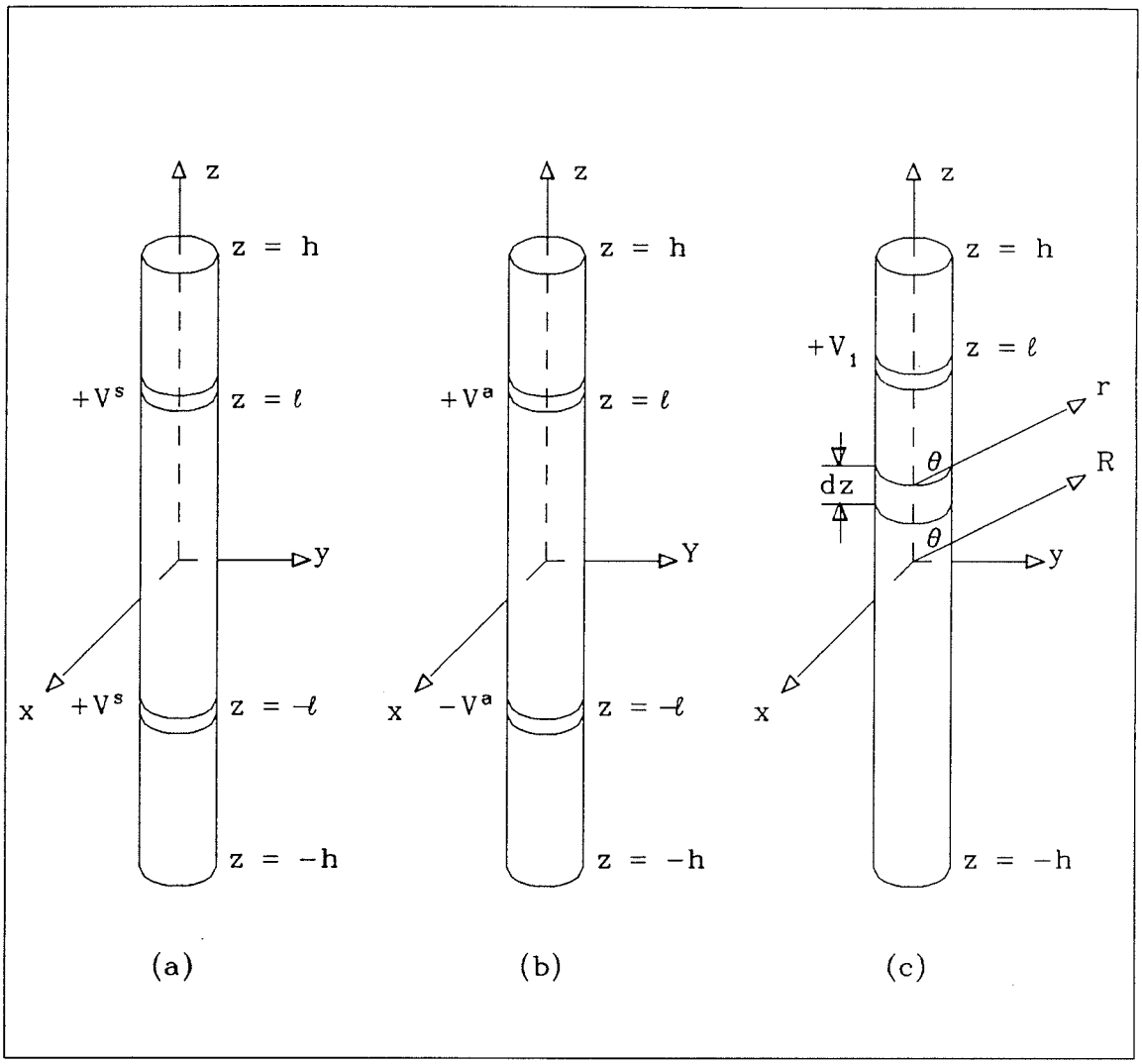

Fig. 4.2 : Geometry of the problem.

appropriate to the region. The contour of integration is assumed to be indented downward around the branch point $\xi = -k$ and upward at $\xi = k$. From (4.2), the tangential electric and magnetic field components are easily obtained as

$$E_z^i = \int_{-\infty}^{\infty} \beta^2 \, A_i(\xi) \, Z_i(\beta\rho) \, e^{j\xi z} \, d\xi \tag{4.3}$$

$$H_\phi^i = -j\omega\epsilon_o \int_{-\infty}^{\infty} \beta \, A_i(\xi) \, Z_i'(\beta\rho) \, e^{j\xi z} \, d\xi \tag{4.4}$$

The prime on the Bessel function denotes derivative with respect to the argument. At $\rho = a$, E_z must be continuous for all z, thus

$$A_1(\xi) \, Z_1(\beta a) = A_2(\xi) \, Z_2(\beta a) \tag{4.5}$$

also $E_z = 0$ for $\rho = a$, $-h \le z \le h$, with the exception of $z = \pm l$. Taking the inverse Fourier transform of (4.3), we get

$$2\pi \, \beta^2 A_i(\xi) \, Z_i(\beta a) = \int_{|z'|>h} e^{-j\xi z} \, E_z(z) \, dz - V^s\{e^{j\xi l} + e^{-j\xi l}\} \tag{4.6}$$

In the region $z > h$, $\rho = a$, H_ϕ must be continuous. Therefore, from (4.4),

$$\int_{-\infty}^{\infty} \beta \, e^{j\xi z} \left[A_1(\xi) \, Z_1'(\beta a) - A_2(\xi) \, Z_2'(\beta a) \right] d\xi = 0 \quad , \; |z| > h \tag{4.7}$$

For $|z| < h$ and $\rho = a$, the total current I_t on the antenna is given by

$$I_t(z) = -2\pi a \left[H_\phi^{(1)} - H_\phi^{(2)} \right] \tag{4.8}$$

Substituting (4.4) into (4.8), we obtain

$$I_t(z) = 2\pi j \omega \epsilon_o a \int_{-\infty}^{\infty} \beta e^{j\xi z} \left[A_1(\xi) Z_1'(\beta a) - A_2(\xi) Z_2'(\beta a) \right] d\xi \quad , \quad |z| < h \tag{4.9}$$

Use is now made of (4.5) and (4.6) to remove $A_1(\xi)$ and $A_2(\xi)$ from (4.7) and (4.9). This leads to the result

$$\int_{-\infty}^{\infty} \frac{e^{j\xi z} d\xi}{\beta^2 J_o(\beta a) H_o^{(2)}(\beta a)} \left\{ \int_{|z'|>h} e^{-j\xi z'} E_z(z') dz' - 2V^s \cos\xi l \right\} =$$

$$\begin{cases} 0 & , \ |z| > h \qquad (4.10) \\ \dfrac{-\pi I_t(z)}{2\omega\epsilon_o} & , \ |z| < h \qquad (4.11) \end{cases}$$

where Z_1 has been replaced by J_o and Z_2 by $H_o^{(2)}$ and the Wronskian relation $J_o H_o^{(2)'} - H_o^{(2)} J_o' = -2j/\pi\beta a$ has been used. Interchanging the order of integration and writing $E(z)$ for $E_z(z)$ yield the following integral equations for $E(z)$

$$\int_{|z'|>h} E(z') K(z-z') dz' = V^s \{ K(z+l) + K(z-l) \} \quad , \quad |z| > h \tag{4.12}$$

and

$$\int_{|z'|>h} E(z') K(z-z') dz' = V^s \{ K(z+l) + K(z-l) \} - \frac{\pi I_t(z)}{2\omega\epsilon_o} \quad , \quad |z| < h \tag{4.13}$$

where

$$K(z) = \int_{-\infty}^{\infty} \frac{e^{j\xi z}}{\beta^2 J_o(\beta a) H_o^{(2)}(\beta a)} d\xi \tag{4.14}$$

Assume the propagation constant k to be complex, i.e. $k = p - jq$ with $p, q > 0$.

Extending the definition of $E(z)$ and $I(z)$, equations (4.12) and (4.13) can be combined as

$$\int_{|z'|>h} E(z')\,K(z-z')\,dz' = V^s\,\{K(z+l)+K(z-l)\} - \frac{\pi I_t(z)}{2\omega\epsilon_o} \tag{4.15}$$

which now holds for all z, provided that $E(z)=0$ for $|z|<h$ and $I(z)=0$ for $|z|>h$.

It is noticed that integral equation (4.15) is of the Wiener-Hopf type. The solution of such an equation needs a definition of the following Fourier transforms :

$$e_-(\xi) = \int_h^\infty e^{-j\xi z}\;E(z)\;dz \tag{4.16}$$

$$e_+(\xi) = \int_{-\infty}^h e^{-j\xi z}\;E(z)\;dz \tag{4.17}$$

$$i(\xi) = \int_{-\infty}^\infty e^{-j\xi z}\;I(z)\;dz \tag{4.18}$$

$$k(\xi) = \int_{-\infty}^\infty e^{-j\xi z}\;K(z)\;dz \tag{4.19}$$

where $e_-(\xi)$ and $e_+(\xi)$ are regular functions in the lower and upper halves of the ξ plane, respectively. The current $i(\xi)$ is regular in the whole ξ plane, while $k(\xi)$ is regular in the strip $-q<\mathrm{Im}(\xi)<q$.

The behavior of these transforms for large $|\xi|$ is required for the Wiener-Hopf technique. This can be determined from the asymptotic relations between the functions and their Fourier transforms. Consider the function

$$F_+(\alpha) = \frac{1}{\sqrt{2\pi}} \int_0^\infty f(x)\, e^{-j\alpha x}\, dx \tag{4.20}$$

in which

$$f(x) \approx A\, x^u \qquad , \quad \begin{cases} x \to 0_+ \\ x \to \infty \end{cases} \tag{4.21}$$

and $-1 < u < 1$. Upon using (4.21) in (4.20), we have

$$F_+(\alpha) \approx \frac{A}{\sqrt{2\pi}}\, \Gamma(u+1)\, e^{3/2\pi j(u+1)}\, \alpha^{-(u+1)} \qquad , \quad \begin{cases} \alpha \to \infty \\ \alpha \to 0_+ \end{cases} \tag{4.22}$$

Now, changing the variable z to $x+h$ in the transformation of e_-, we obtain

$$e_-(\xi) = e^{-j\xi h} \int_0^\infty e^{-j\xi x}\, E(x+h)\, dx \tag{4.23}$$

The edge condition described in [80] gives

$$E(x+h) = O(x^{-1/2}) \qquad as \qquad x \to 0_+ \tag{4.24}$$

Thus, a comparison between $e_-(\xi)$ and $F_+(\alpha)$ yields

$$e_-(\xi) = O(e^{-j\xi h} |\xi|^{-1/2}) \qquad as \qquad |\xi| \to \infty \tag{4.25}$$

Similarly

$$e_+(\xi) = O(e^{j\xi h}\ |\xi|^{-1/2}) \qquad as \qquad |\xi| \to \infty \tag{4.26}$$

Since $I(x+h) = O(x^{1/2})$ as $x \to 0_-$ and $I(x-h) = O(x^{1/2})$ as $x \to 0_+$, (4.22) yields

$$i(\xi) = O(e^{-j\xi h}\ |\xi|^{-3/2}) \qquad as \qquad |\xi| \to \infty \tag{4.27}$$

in the upper half-plane, and

$$i(\xi) = O\left(e^{j\xi h}\ |\xi|^{-3/2}\right) \qquad as \qquad |\xi| \to \infty \tag{4.28}$$

in the lower half-plane. From equation (4.14) and (4.19) we find that

$$k(\xi) = \frac{2\pi}{\beta^2 J_o(\beta a)\, H_o^{(2)}(\beta a)} \tag{4.29}$$

The asymptotic behavior of $k(\xi)$ as $|\xi| \to \infty$ can be easily obtained from (4.29) as

$$k(\xi) = O\left(|\xi|^{-1}\right) \tag{4.30}$$

4.2.2 Solution of the integral equation using the Wiener-Hopf technique

The basic tools of this technique are analytic continuation, Liouville's theorem and the factorization of analytic functions. It is assumed that these tools are understood throughout the solution. Now, by taking the Fourier transform of equation (4.15), we obtain

$$\left[e_-(\xi) + e_+(\xi) - 2V^s \cos(\xi l) \right] k(\xi) = \frac{-\pi i(\xi)}{2\omega\epsilon_o} \tag{4.31}$$

which holds in the common strip of regularity (i.e $-q < \mathrm{Im}(\xi) < q$) of all the functions. Suppose that $k(\xi)$ can be factorized into functions regular in the upper and lower half-planes given by

$$k(\xi) = \frac{k_-(\xi)}{k_+(\xi)} \tag{4.32}$$

When equation (4.31) is multiplied by $e^{j\xi h}$, and $k(\xi)$ is factored as in (4.32), the result is

$$e_-(\xi)\, k_-(\xi)\, e^{j\xi h} + \frac{\pi}{2\omega\epsilon_o}\, i(\xi)\, k_+(\xi)\, e^{j\xi h}$$

$$= e^{j\xi h} \left[2V^s \cos(\xi l) - e_+(\xi) \right] k_-(\xi) \tag{4.33}$$

According to the asymptotic behaviors (4.25) and (4.27) the first term on the left hand side of equation (4.33) is regular in the lower half-plane, while the second term on the same side is regular in the upper half-plane. The right hand side of equation (4.33) is regular in the common strip. An equation similar to (4.33) can be found by multiplying (4.30) by $e^{-j\xi h}$ instead of $e^{j\xi h}$, with the result

$$\frac{e_+(\xi)\, e^{-j\xi h}}{k_+(\xi)} + \frac{\pi}{2\omega\epsilon_o}\,\frac{i(\xi)\, e^{-j\xi h}}{k_-(\xi)} = \frac{\left[\, 2V^s\, \cos(\xi l) - e_-(\xi)\,\right] e^{-j\xi h}}{k_+(\xi)} \tag{4.34}$$

Again the region of regularity for the first term on the left hand side is the upper half-plane and that for the second term is the lower half-plane, while the right hand side is regular in the common strip. The right hand side of equations (4.33) and (4.34) can be written as the sum of upper and lower functions by using Cauchy's formula, i. e.

$$F(\xi) = \frac{1}{2\pi j}\int_{C_-+C_+} \frac{F(t)\; dt}{t - \xi} \tag{4.35}$$

where $F(\xi)$ is a function which decays quickly enough at infinity and is regular in the strip containing C_- and C_+ as shown in Fig. 4.3. The integral along C_- is regular in the lower half-plane, while the integral along C_+ is regular in the upper half-plane. Making use of equation (4.35) in(4.33) and (4.34), with F equal to the right hand side, gives

$$e_-(\xi)\, k_-(\xi)\, e^{j\xi h} + \frac{\pi}{2\omega\epsilon_o}\, i(\xi)\, k_+(\xi)\, e^{j\xi h}$$

$$= \frac{1}{2\pi j}\int_{C_-+C_+} \frac{e^{j\xi h}\left[\, 2V^s\, \cos(\xi l) - e_+(\xi)\,\right] k_-(\xi)\, dt}{t - \xi} \tag{4.36}$$

and

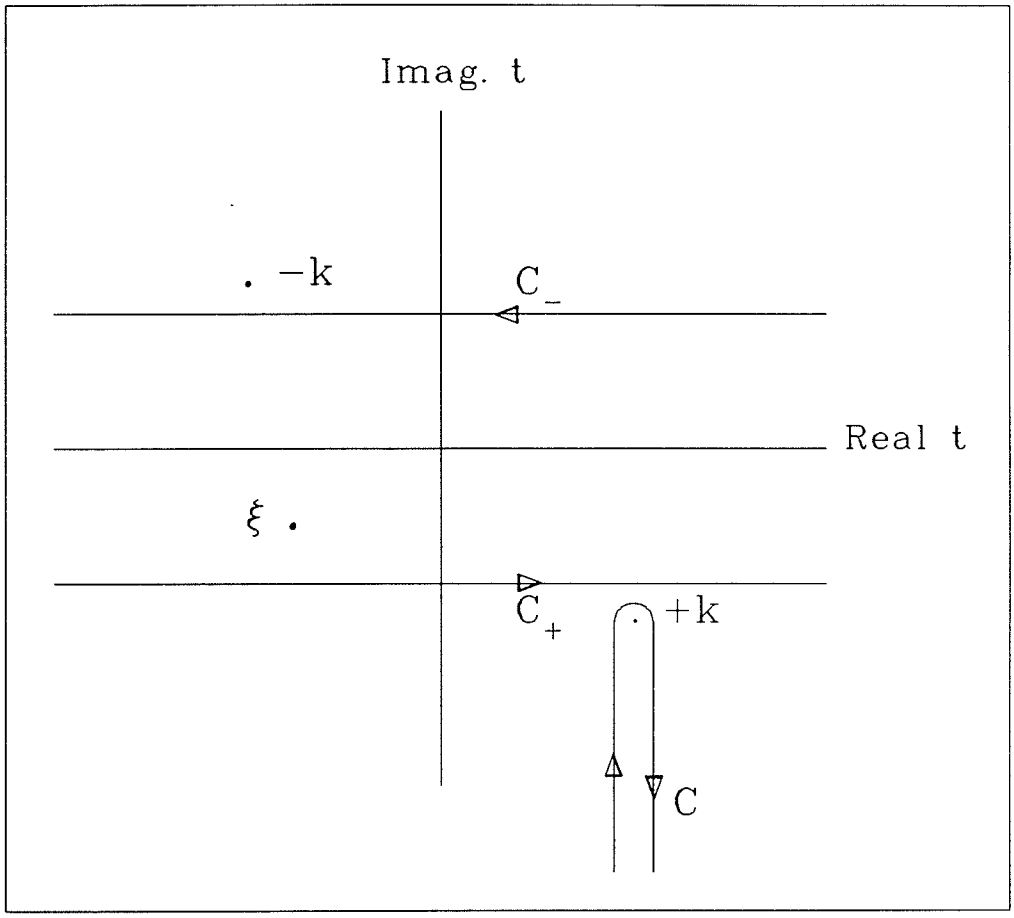

Fig. 4.3 : The integration contours in the complex t plane.

$$\frac{e_+(\xi)\, e^{-j\xi h}}{k_+(\xi)} + \frac{\pi}{2\omega\epsilon_o}\,\frac{i(\xi)\, e^{-j\xi h}}{k_-(\xi)}$$

$$= \frac{1}{2\pi j}\int_{C_-+C_+} \frac{e^{-j\xi h}\left[\, 2V^s\, \cos(\xi l) - e_-(\xi)\,\right] dt}{k_+(\xi)(t-\xi)} \tag{4.37}$$

Equations (4.36) and (4.37) can be re-written as

$$e_-(\xi)\, k_-(\xi)\, e^{j\xi h} + \frac{1}{2\pi j}\int_{C_-} \frac{e^{jht}\left[\, e_+(t) - 2V^s\, \cos(lt)\,\right] k_-(t)\, dt}{t-\xi}$$

$$= \frac{-1}{2\pi j}\int_{C_+} \frac{e^{jht}\left[\, e_+(t) - 2V^s\, \cos(lt)\,\right] k_-(t)\, dt}{t-\xi}$$

$$- \frac{\pi}{2\pi\epsilon_o}\, i(\xi)\, k_+(\xi)\, e^{jh\xi} = P_1(\xi) \tag{4.38}$$

$$\frac{e_+(\xi)\, e^{-j\xi h}}{k_+(\xi)} + \frac{1}{2\pi j}\int_{C_+} \frac{e^{-jht}\left[\, e_-(t) - 2V^s\, \cos(tl)\,\right] dt}{k_-(t)\,(t-\xi)}$$

$$= \frac{-1}{2\pi j}\int_{C_-} \frac{e^{-jht}\left[\, e_-(t) - 2V^s\, \cos(tl)\,\right] dt}{k_-(t)\,(t-\xi)}$$

$$- \frac{\pi}{2\omega\epsilon_o}\,\frac{i(\xi)\, e^{-j\xi h}}{k_-(\xi)} = P_2(\xi) \tag{4.39}$$

Since the first part of equation (4.38) is regular in the lower half-plane and the second part is regular in the upper half-plane, analytic continuation indicates that $P_1(\xi)$ is regular in the whole ξ plane. Similarly, the first part in equation (4.39) is regular in the upper half-plane and the second part is regular in the lower half-plane, so that $P_2(\xi)$ is regular in the whole ξ plane. The integrals in (4.38) and (4.39) go to zero for large $|\xi|$ while $k_-(\xi)$ and $k_+(\xi)$ are bounded, thus the first term in (4.38)

and (4.39) tend to zero at infinity and thus $P_1(\xi)$ and $P_2(\xi)$ tends to zero at infinity. Hence by Liouville's theorem they are constants, which can only be zero. Equations (4.38) and (4.39) with $P_1(\xi) = P_2(\xi) = 0$, constitute a pair of simultaneous integral equations in the two unknowns $e_-(\xi)$ and $e_+(\xi)$. Since the problem is completely symmetric with respect to z, we have $E(z) = E(-z)$ and thus from (4.16) and (4.17) it is clear that $e_-(\xi) = e_+(-\xi)$. Also it is shown in appendix B that $k_-(\xi)k_+(\xi) = 1$, so if we substitute $-\xi$ for ξ and $-t$ for t in the first term of equation (4.38), we find

$$e_-(-\xi)\, k_-(-\xi)\, e^{-j\xi h}$$

$$+ \frac{1}{2\pi j} \int_{C_-} \frac{e^{-jht}\left[e_+(-t) - 2V^s \cos(lt) \right] k_-(t)\,(-dt)}{-t + \xi} = 0 \qquad (4.40)$$

Using the above argument one obtains

$$\frac{e_+(\xi)\, e^{-j\xi h}}{k_+(\xi)} + \frac{1}{2\pi j} \int_{C_+} \frac{e^{-jht}\left[e_-(t) - 2V^s \cos(tl) \right] dt}{k_-(t)\,(t - \xi)} = 0 \qquad (4.41)$$

which is the same as the first part in equation (4.39). Because equations (4.38) and (4.39) are identical it is sufficient to proceed with one of the equations , the solution of the other being obtained by symmetry.

Introducing a new function

$$f^s(\xi) = e_-(\xi)\, k_-(\xi)\, e^{j\xi h} \qquad (4.42)$$

which is regular in the lower half-plane, integral equation (4.40) takes the form

$$f^s(-\xi) + \frac{1}{2\pi j}\int_{C_+} \frac{e^{-2jht}\ f^s(t)\ k(t)\ dt}{(t-\xi)\,k_-^2(t)}$$

$$= \frac{V^s}{2\pi j}\int_{C_+} \frac{\left[e^{-j(h-l)t} + e^{-j(h+l)t}\right] k(t)\ dt}{(t-\xi)\,k_-(t)} \qquad (4.43)$$

The asymptotic solution of an integral equation similar to (4.43) has been given by Hurd [58] which we will follow. The main difference lies in the calculation of the integral over C_+ which we will do by a different method, which allows h to take values as small as 0.15λ. The dominant contribution to the first integral in (4.43) comes at the singularities of the integrand. Because $f^s(t)(t-\xi)^{-1}[k_-(t)]^{-2}$ is regular in the lower half-plane when ξ lies above C_+, the only singularities are contributed by $k(t)$. Now $k(t)$ has branch points at $t = \pm k$ and poles at the zeros of $J_o(\beta a)$. Since for most practical antennas a is a small fraction of the wavelength, the poles occur at large negative imaginary values of t and , owing to the exponential in the integrand, give small contributions to the integral. If we deform the contour C_+ around the branch-cut as shown in Fig. 4.3, the dominant contribution comes from the point $t = k$. Moreover the higher order terms can be obtained by expanding the regular part of the integrand in a Taylor series about this point. The integral on the right hand side of equation (4.43) can be evaluated in the same way. The expansions of the integrand in a Taylor series around $t = k$ are given by

$$f^s(t) \approx \sum_{n=0}^{N-1} \frac{f_n^s(k)}{n!}\,(t-k)^n \qquad (4.44)$$

where $f_n^s(k) = \left[\frac{\partial^n f^s(t)}{\partial t^n}\right]_{t=k}$, and

$$\frac{1}{k_-^2(t)\,(t-\xi)} \approx \sum_{n=0}^{N-1} A_n(\xi)\,(t-k)^n \qquad (4.45)$$

$$\frac{1}{k_{-}(t)\,(t-\xi)} \approx \sum_{n=0}^{N-1} B_n(\xi)\,(t-k)^n \tag{4.46}$$

Substituting from (4.44), (4.45) and (4.46) into (4.43), we obtain after some algebraic manipulation and neglecting the terms of order higher than $(N-1)$, the result

$$f^s(-\xi) = V^s \sum_{n=0}^{N-1} B_n(\xi)\{ R_n(h+l) + R_n(h-l)\}$$

$$-\sum_{n=0}^{N-1} R_n(2h) \sum_{m=0}^{n} \frac{f^s_{n-m}(k)\, A_m(\xi)}{(n-m)!} \tag{4.47}$$

where

$$R_n(h) = \frac{1}{2\pi j} \int_{C_+} e^{-jht}\; k(t)\; (t-k)^n \; dt \tag{4.48}$$

Since the unknown constants $f^s_n(k)$ are produced by taking the nth derivative of $f^s(\xi)$ at $\xi = k$, one can determine these constants by taking the pth derivatives of equation (4.47) for $p = 0,1,\cdots,N-1$, and putting ξ equal to $-k$. This process will produce $N-1$ simultaneous algebraic equations in the unknowns $f^s_n(k)$, i. e.

$$(-1)^p f^s_p(k) = V^s \sum_{n=0}^{N-1} B_{n,p}(-k)\,\{ R_n(h-l) + R_n(h+l)\}$$

$$-\sum_{n=0}^{N-1} R_n(2h) \sum_{m=0}^{n} \frac{f^s_{n-m}(k)\, A_{m,p}(-k)}{(n-m)!} \tag{4.49}$$

where $A_{m,p}(-k) = \left[\partial^p A_m(\xi)/\partial\xi^p\right]_{\xi=-k}$, and similarly for $B_{n,p}(-k)$. The order of the solution is determined from the number of equation chosen in (4.49). It is found that after the lowest order (i.e $N = 1$) the addition of one equation leads to a slight modification in the solution. In this case we choose $N = 3$, which yields a good

result provided that the antenna is reasonably long.

The asymptotic solution of integrals $R_n(h)$ given by Hurd is restricted to large h, but we notice that these integrals can be evaluated recursively from the relation

$$R_{n+1}(h) = j \frac{dR_n(h)}{dh} - k\, R_n(h) \tag{4.50}$$

Since equation (4.50) gives the higher order integrals in terms of the lower order ones, one needs to evaluate

$$R_o(h) = \frac{1}{2\pi j} \int_{C_+} e^{-jht}\ k(t)\ dt \tag{4.51}$$

This integral is evaluated in Appendix A and the final result is

$$R_o(h) = \frac{\pi}{2k} e^{-jkh}\ M(h) \tag{4.52}$$

where

$$M(h) = \ln\left[1 - \frac{2\pi j}{2C_w + \ln(kh + \sqrt{(kh)^2 + e^{-2\gamma}}) + \gamma + j\frac{\pi}{2}}\right] \tag{4.53}$$

$$C_w = -ln(ka) - \gamma \tag{4.54}$$

and $\gamma = 0.57721\cdots$ is Euler's number. When (4.52) is substituted in (4.50) we obtain

$$R_n(h) = \frac{j^n \pi}{2k} e^{-jkh}\ M^{(n)}(h) \tag{4.55}$$

where $M^{(n)}(h)$ is the n*th* derivative of $M(h)$. Equation (4.55) gives a solution for the integrals $R_n(h)$ which is simple and more accurate than that given by Hurd.

The current distribution along the symmetrically fed dipole can be evaluated from equation (4.15) as follows

$$I_t^s(z) = \frac{2\omega\epsilon_o}{\pi}\left\{ V^s\left[K(z+l)+K(z-l)\right] - \int_{-\infty}^{\infty} E(z')\,K(z-z')\,dz' \right\} \tag{4.56}$$

Substituting for $K(z-z')$ from (4.14), (4.56) can be written as

$$I_t^s(z) = \frac{2\omega\epsilon_0}{\pi}\left\{ V^s\left[K(z+l)+K(z-l)\right] - \int_{-\infty}^{\infty} E(z') \int_{-\infty}^{\infty} \frac{e^{j\xi(z-z')}}{2\pi} k(\xi)\,d\xi\,dz' \right\} \tag{4.57}$$

After some mathematical manipulations and using the Fourier transform of the electric field and the definition of $f^s(\xi)$ in (4.42), the current distribution is obtained in the following algebraic form

$$I_t^s(z) = \frac{2\omega\epsilon_o}{\pi}\left\{ V^s\left[K(z+l)+K(z-l)\right] - j\left[\sum_{n=0}^{N-1}\left\{R_n(h+z)+R_n(h-z)\right\}\sum_{m=0}^{n}\frac{f^s_{n-m}\,C_m}{(n-m)!}\right]\right\} \tag{4.58}$$

where

$$K(z \pm l) = j\,R_o(|l \pm z|) \tag{4.59}$$

and C_m is given from the Taylor expansion

$$\frac{1}{k_-(\xi)} = \sum_{m=0}^{N-1} C_m(\xi - k)^m \tag{4.60}$$

The asymptotic expressions for C_m are calculated in Appendix B. Once the values of f_n^s are calculated from (4.49), the current distribution of the symmetrically-fed dipole is totally known from equation (4.58).

4.3 *Current distribution on anti-symmetrically driven dipole*

The geometry of the antisymmetrically driven dipole is shown in Fig. 4.1-b where the driving voltages at $z=+l$ and $z=-l$ are V^a and $-V^a$, respectively. The electric field component in the gaps is given by

$$E_z = -V^a \{ \delta(z-l) - \delta(z+l) \} \tag{4.61}$$

Following the same steps described in section 4.2 we get the following integral equation

$$-f^a(-\xi) + \frac{1}{2\pi j}\int_{C_+} \frac{e^{-2jht}\ f^a(t)\ k(t)\ dt}{(t-\xi)\ k_-^2(t)}$$

$$= \frac{V^a}{2\pi j}\int_{C_+} \frac{\left[e^{-j(h+l)t} - e^{-j(h-l)t}\right] k(t)\ dt}{(t-\xi)\ k_-(t)} \tag{4.62}$$

Employing the approximations and definitions used in equation (4.41), we can evaluate a set of algebraic equations in the unknown $f^a(k)$, i. e.

$$(-1)^p f_p^a(k) = -V^a \sum_{n=0}^{N-1} B_{n,p}(-k) \left\{ R_n(h+l) - R_n(h-l) \right\}$$

$$+ \sum_{n=0}^{N-1} R_n(2h) \sum_{m=0}^{n} \frac{f_{n-m}^a(k)\ A_{m,p}(-k)}{(n-m)!} \tag{4.63}$$

Once we evaluate the function $f^a(k)$, the current distribution can be calculated using the equation

$$I_t^a(z) = \frac{2\omega\epsilon_o}{\pi}\left\{ V^a\,[\,K(z-l) - K(z+l)] - \int_{-\infty}^{\infty} E(z')\,K(z-z')\,dz' \right\} \tag{4.64}$$

which is simplified to the following algebraic form

$$I_t^a(z) = \frac{2\omega\epsilon_o}{\pi}\left\{ V^a\left[K(z-l) - K(z+l)\right] + j\left[\sum_{n=0}^{N-1}\left\{R_n(h+z) - R_n(h-z)\right\}\sum_{m=0}^{n}\frac{f^a_{n-m}\,C_m}{(n-m)!}\right]\right\} \tag{4.65}$$

4.4 *Current distribution on the arbitrarily driven and asymmetrically driven dipole*

The asymmetrically driven dipole shown in Fig. 4.1 is a dipole driven by two different voltages V_1 and V_2 at $z = +l$ and $z = -l$, respectively. When V_2 equals zero it will be an arbitrarily driven dipole. The current distribution on the asymmetrically driven dipole can be evaluated by superposition of the current distribution on symmetrically and antisymmetrically driven dipoles. The driving voltage V^s and V^a can be evaluated from the relations

$$V^s = (V_1 + V_2)/2 \tag{4.66}$$

$$V^a = (V_1 - V_2)/2 \tag{4.67}$$

and the total current distribution on the asymmetrically driven dipole is given by

$$I(z) = I_t^s(z) + I_t^a(z) \tag{4.68}$$

Using equations (4.58) and (4.65) in (4.68) we obtain

$$I(z) = \frac{2\omega\epsilon_o}{\pi} \left\{ \left[V_1 K(z-l) + V_2 K(z+l) \right] \right.$$

$$- j \left[\sum_{n=0}^{N-1} \left\{ R_n(h+z) + R_n(h-z) \right\} \sum_{m=0}^{n} \frac{f^{s}_{n-m} C_m}{(n-m)!} \right]$$

$$\left. + j \left[\sum_{n=0}^{N-1} \left\{ R_n(h+z) - R_n(h-z) \right\} \sum_{m=0}^{n} \frac{f^{a}_{n-m} C_m}{(n-m)!} \right] \right\} \qquad (4.69)$$

It is found that for $N = 1$ equation (4.69) gives the same expression for the current distribution as the one given by Shen et al.[52]. For higher accuracy of the current distribution it is sufficient to use $N = 3$, which is used later throughout the calculations of the current distribution.

4.5 *Input admittance of arbitrarily driven dipole*

The current distribution on the arbitrarily fed dipole driven by a voltage V_1 at $z = +l$ is given by (4.69) when $V_2 = 0$. Thus,the current at $z = +l$ is given by

$$I(l) = \frac{2\omega\epsilon_o}{\pi} \left\{ V_1 K(0) - j \left[\sum_{n=0}^{N-1} \left\{ R_n(h+l) + R_n(h-l) \right\} \sum_{m=0}^{n} \frac{f^{s}_{n-m} C_m}{(n-m)!} \right] \right.$$

$$\left. + j \left[\sum_{n=0}^{N-1} \left\{ R_n(h+l) - R_n(h-l) \right\} \sum_{m=0}^{n} \frac{f^{a}_{n-m} C_m}{(n-m)!} \right] \right\} \qquad (4.70)$$

If (4.70) is divided by V_1, and use is made of the relation

$$\frac{2\omega\epsilon_o K(0)}{\pi} = Y_\infty \qquad (4.71)$$

we obtain

$$Y - Y_\infty = \frac{2\omega\epsilon_o}{\pi V_1}\left\{ - j \left[\sum_{n=0}^{N-1} \left\{ R_n(h+l) + R_n(h-l) \right\} \sum_{m=0}^{n} \frac{f^{s}_{n-m}\, C_m}{(n-m)!} \right] \right.$$

$$\left. + j \left[\sum_{n=0}^{N-1} \left\{ R_n(h+l) - R_n(h-l) \right\} \sum_{m=0}^{n} \frac{f^{a}_{n-m}\, C_m}{(n-m)!} \right] \right\} \qquad (4.72)$$

where Y_∞ is the admittance of the infinitely long cylindrical antenna which has been studied by many investigators. Among the several different versions of Y_∞ we choose the one given by Miller [20], namely

$$G = - \frac{\pi}{Z_0 ln(\Gamma ka/\sqrt{2})} \qquad (4.73)$$

$$B = - \frac{2ka}{Z_0}\{ 0.9 [2ka\ ln(\Gamma ka/\sqrt{2})]^{-1} + ln(k\Delta/2)\} \qquad (4.74)$$

where G is the conductance, B is the susceptance, Z_0 is the intrinsic impedance of free space and Δ is the gap thickness. In our calculation we choose Δ as small as possible (i. e. $0.1a$) in the susceptance calculations in order to satisfy the infinitesimal condition on the gap thickness assumed before. Also all the numerical results presented correspond to $N = 3$.

4.6 *Radiation pattern*

Fig. 4.2-c shows the geometry of the arbitrarily driven dipole and the spherical coordinate system used in the pattern calculation. The current distribution is calculated and given by equation (4.69). The far-field pattern at $P(R,\theta,\phi)$can be evaluated from the relation

$$P(\theta) = - \lim_{R \to \infty} E_\theta(R,\theta)\, R\, e^{jkR} \qquad (4.75)$$

where E_θ is given by

$$E_\theta = \frac{j\omega\mu_o}{4\pi} \frac{\sin\theta}{R} e^{-jkR} \int_{-h}^{h} e^{jkz\cos\theta} I(z)\, dz \tag{4.76}$$

In the following analysis we will use the first order ($N = 1$) expression for the current distribution in equation (4.76) which is given by

$$I(z) = \frac{2\omega\epsilon_o}{\pi} [\, V_1 j R_o(|l - z|) + j R_o(h+z)(f_o^a - f_o^s) C_o - j R_o(h-z)(f_o^a + f_o^s) C_o \,] \tag{4.77}$$

Substituting from (4.77) into (4.76), integrals of the type $\int_{\alpha_1}^{\alpha_2} e^{jkz\cos\theta} R_o(D \pm z)\, dz$ will appear, where D, α_1 and α_2 are constants. In order to solve this integral, R_o may be approximated as

$$R_o(x) \approx \frac{\pi^2}{jk} \frac{e^{-jkx}}{F + ln(\, kx + \sqrt{(kx)^2 + e^{-2\gamma}})} \tag{4.78}$$

where

$$F = 2C_w + \gamma - j\frac{\pi}{2} \tag{4.79}$$

Using the binomial expansion in (4.78), we obtain

$$R_o(x) \approx \frac{\pi^2}{jk} \frac{e^{-jkx}}{F} [\, 1 - \frac{\ln(\, kx + \sqrt{(kx)^2 + e^{-2\gamma}})}{F} + \cdots] \tag{4.80}$$

Since a is small, the magnitude of F is large. Thus for x not very large one can take the first two terms of the above expansion. Upon using (4.80) and (4.77) in (4.76) and carring out the integration term by term, the final result is given by

$$P(\theta) = \frac{\sin\theta}{2F} \{ V_1 [S_+(l,\theta) - S_-(l,\theta)] - S_-(-h,\theta) (f_o^a - f_o^s) C_o$$

$$- S_+(h,\theta) (f_o^a + f_o^s) C_o \} \qquad (4.81)$$

where

$$S_\pm(D,\theta) = \frac{1}{\cos\theta \pm 1} \{ [1 + \frac{\gamma - G[k(h \pm D),(1 \pm \cos\theta)]}{F}] e^{jkcos\,\theta D} -$$

$$[1 - \frac{\ln[k(h \pm D) + \sqrt{(k(h \pm D))^2 + e^{-2\gamma}}]}{F}] e^{-jk(h \pm h\cos\theta \pm D)} \} \qquad (4.82)$$

$$G(\beta,\alpha) = \int_0^\beta \frac{e^{-j\alpha x}\, dx}{\sqrt{x^2 + e^{-2\gamma}}} \qquad (4.83)$$

An analytical solution for integral (4.83) is described in Appendix C with the result

$$G(\beta,\alpha) = \sum_{n=-\infty}^{\infty} \frac{\{ e^{n \sinh^{-1}\beta\Gamma} - 1 \}}{n} J_n(\frac{\alpha}{j\Gamma}) \qquad (4.84)$$

Unfortunately this series converges very slowly. In the numerical examples presented in the next section, integral (4.83) is evaluated numerically. The accuracy of this calculation is checked with large number of terms of (4.84).

4.7 *Results and discussion*

For purpose of comparison we will use our solution to recalculate the examples of the arbitrarily fed dipole given in Harrington [79]. Fig. 4.4 shows the variation of the input admittance of an arbitrarily fed dipole as a function of the half length h. The ratio of h to the radius a is taken as 74.2. Four cases are shown in Fig. 4.4 corresponding to variable feed positions at $z = 0, -h/4, -h/2$ and $-3h/4$. In Fig. 4.5 the input impedances of the same examples are shown. Comparison with the numerical results published by Harrington shows very close agreement. The main discrepancy lies at the first resonance point where our solution gives higher values .

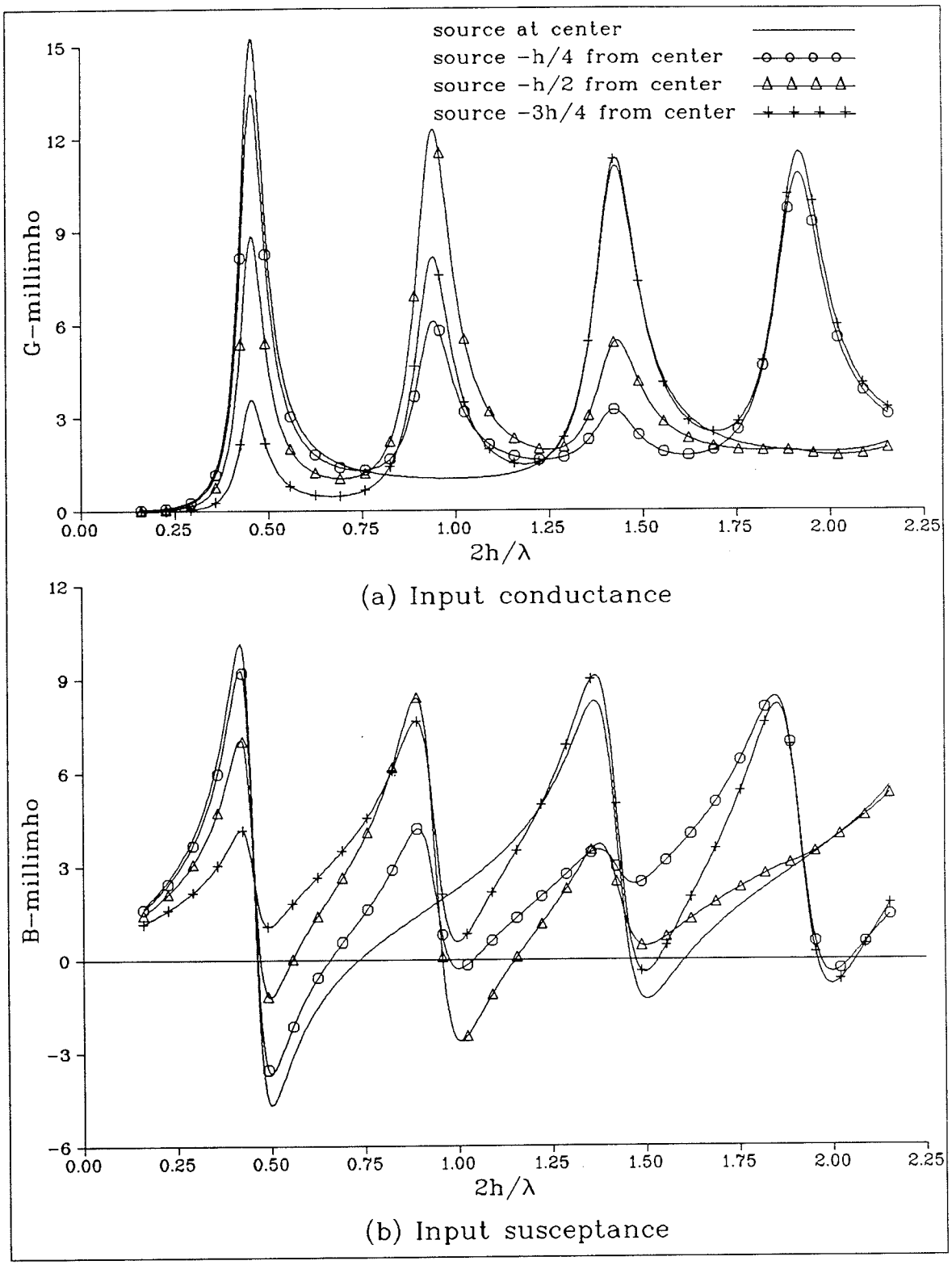

Fig. 4.4 : Input admittance Y = G + jB for a dipole antenna (h/a = 74.2)

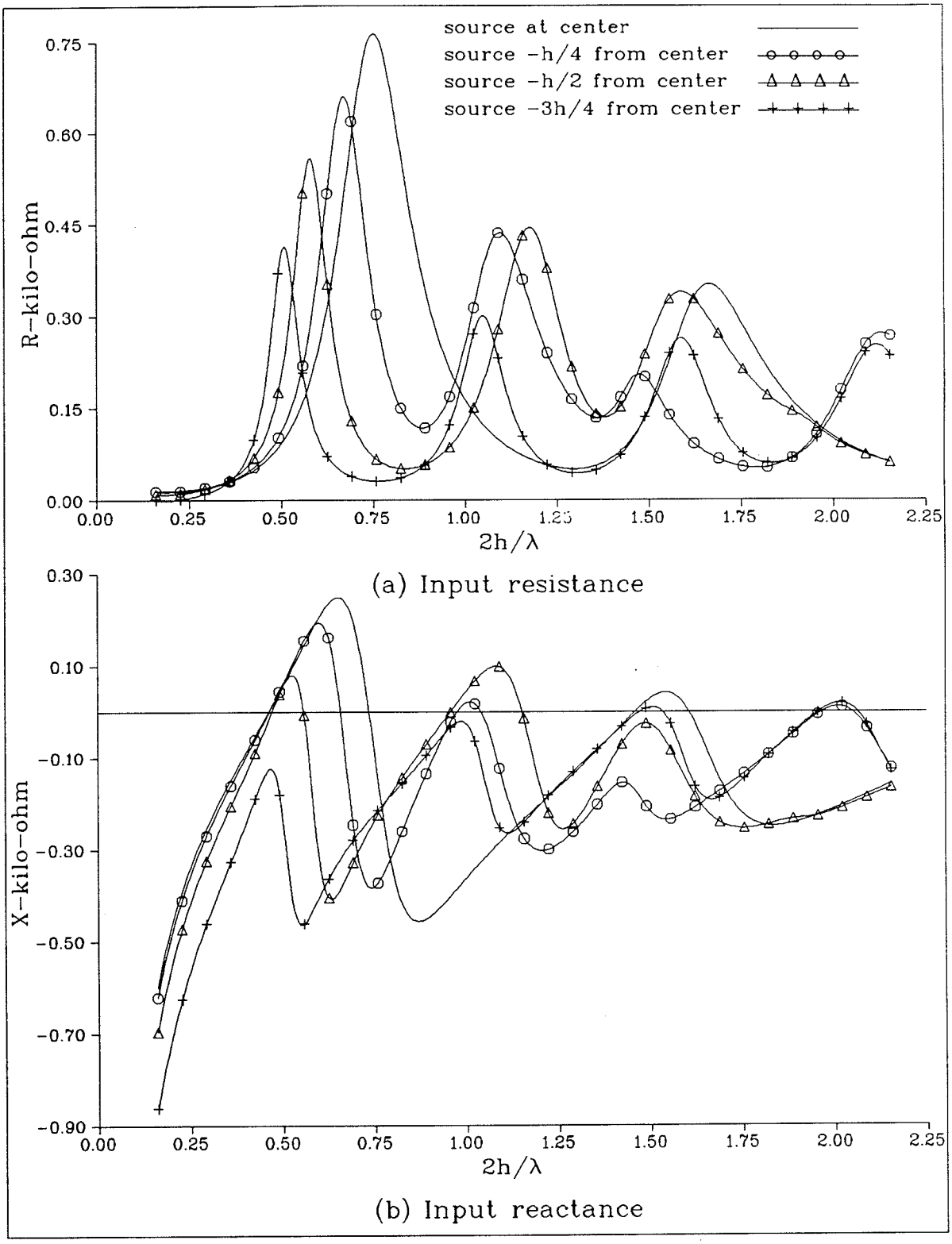

Fig. 4.5 : Input impedance Z = R + jX for a dipole antenna (h/a = 74.2)

This discrepancy is due to the approximations in the calculation of $R_n(h)$, which is less accurate for $h < 0.15\lambda$. Even so, the expressions of $R_n(h)$ are more accurate than those given by Hurd . In the numerical evaluation of the admittance of the infinite dipole involved in the solution, (δ/a) was taken as 0.1.

The current distribution on a dipole antenna of half length 0.5 λ is given in Fig. 4.6. Four cases are shown corresponding to various feed positions at $z = 0$, $-h/4, -h/2$ and $-3h/4$. Comparison with Harrington's results show a good agreement except at the open ends of the antenna where our solution gives higher values. Again this discrepancy is due to the approximations in $R_n(h)$ made to overcome the singularity at $h = 0$. Figure 4.7 presents the current distribution on a dipole antenna of half length 0.75λ. Four cases are shown corresponding to the same four variable feed positions. In both Figs. 4.6 and 4.7 the phase of the current distribution given is very close to that given by Harrington while the discrepancy appears in the magnitudes. For a more fair comparison, one can compare our results with those given by Shen el al. [52]. It is found that the current distribution given in Fig. 4.6-a is very close to the same example given by Shen even at the open ends.

The radiation patterns of the same two examples given before are shown in Figs. 4.8 and 4.9. Comparison of the normalized power patterns with those given by Harrington shows very close agreement. This agreement indicates that our expression for the radiation pattern is highly accurate. One can see from Fig. 4.8 a slight effect on the radiation pattern due to the variation of the feed positions in cases b, c and d , while in Fig. 4.9 this variation in the feed position has a large effect on the radiation pattern. It shows that varying the feed position along a long dipole has a larger effect on the radiation pattern than for a short dipole. Moreover, the long dipole antenna could be fed at different points such that a broadside narrow beam could be produced, which is the case of a multi-fed dipole antenna.

There are many variables affecting the radiation patterns and gain of the multi-fed dipole antenna. For example the number of feeds, feed positions, feed voltages

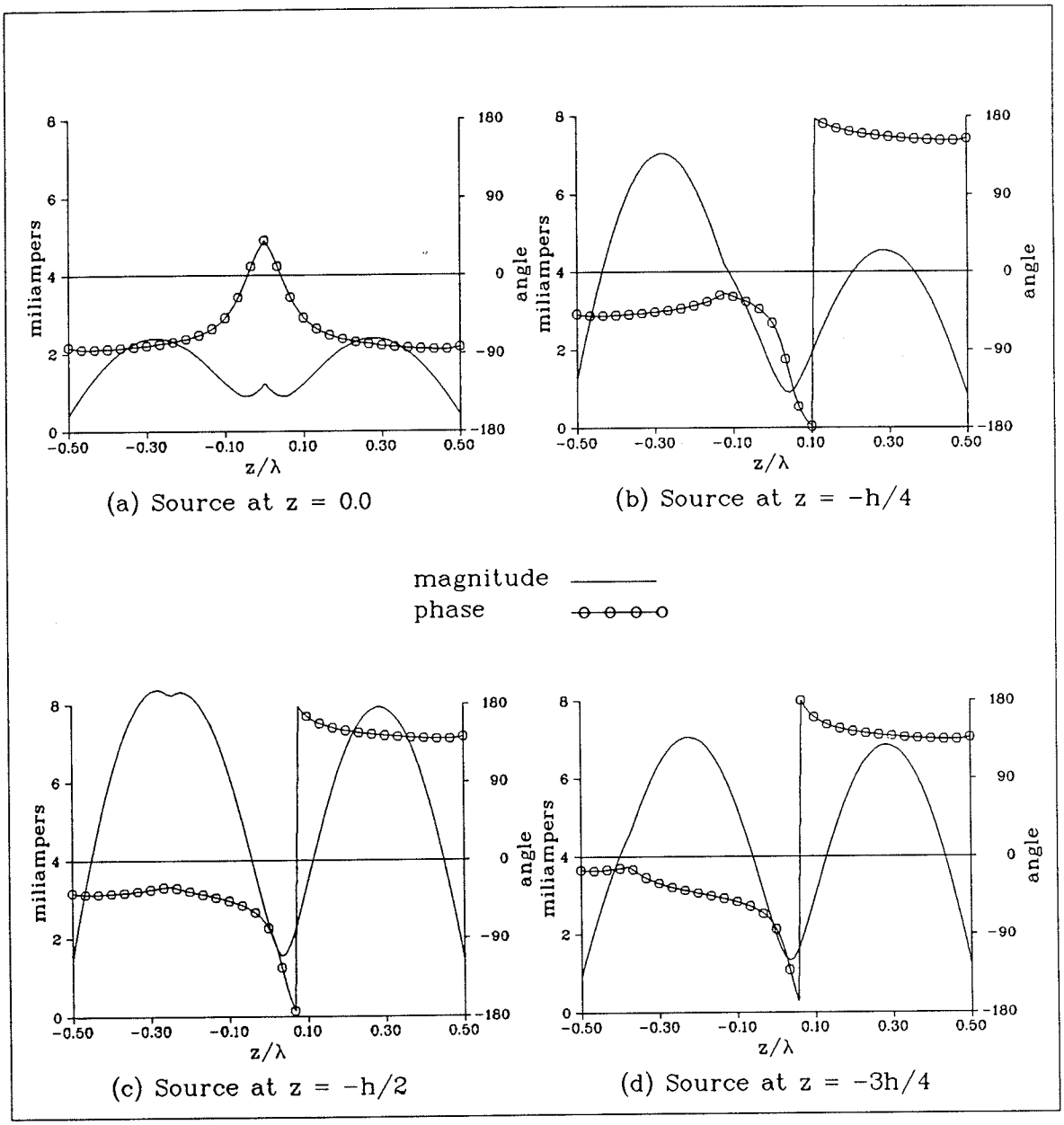

Fig. 4.6 : Current distribution on a dipole antenna (h/a = 74.2, h = 0.5λ)

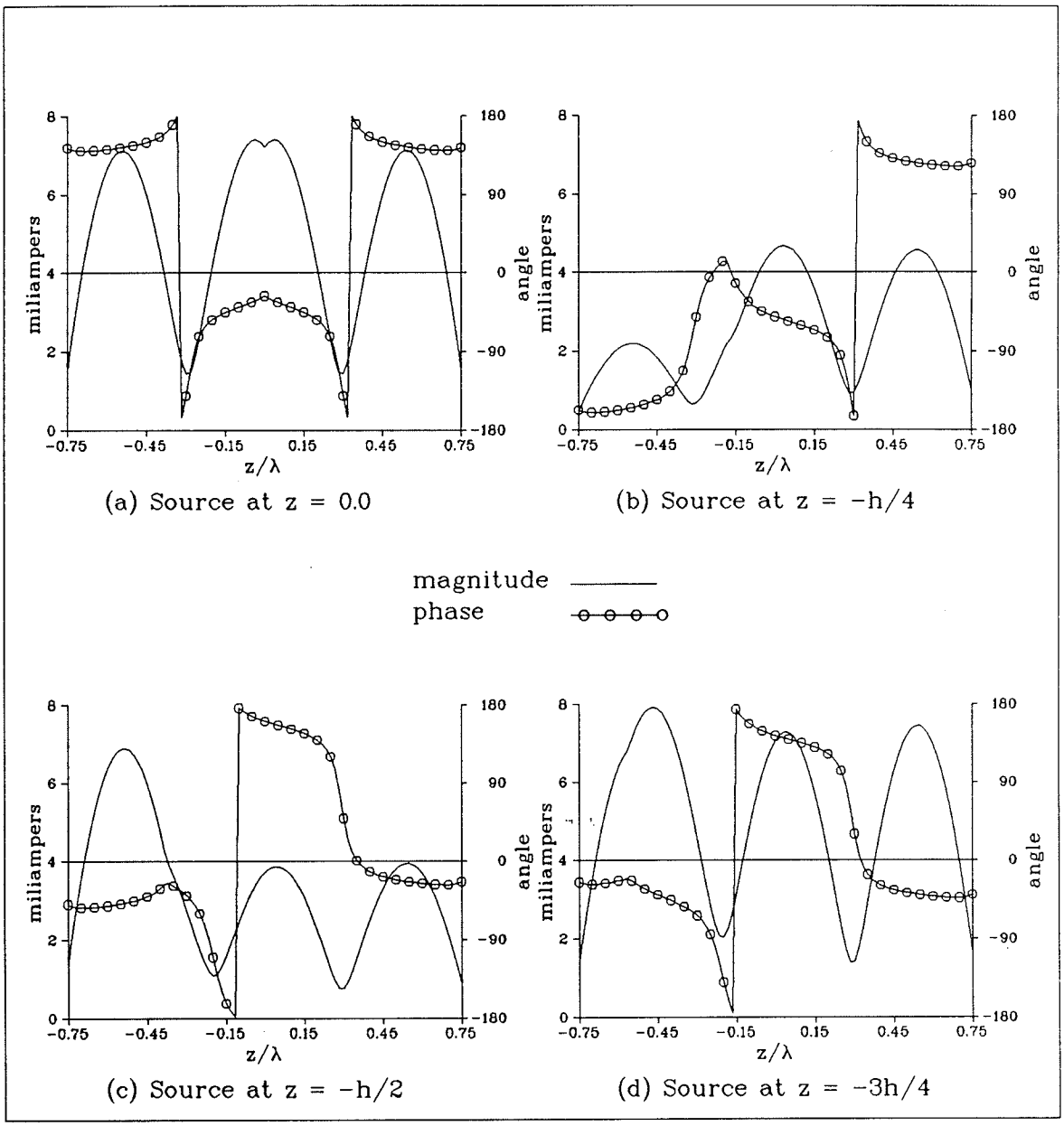

Fig. 4.7 : Current distribution on a dipole antenna (h/a = 74.2, h = 0.75λ)

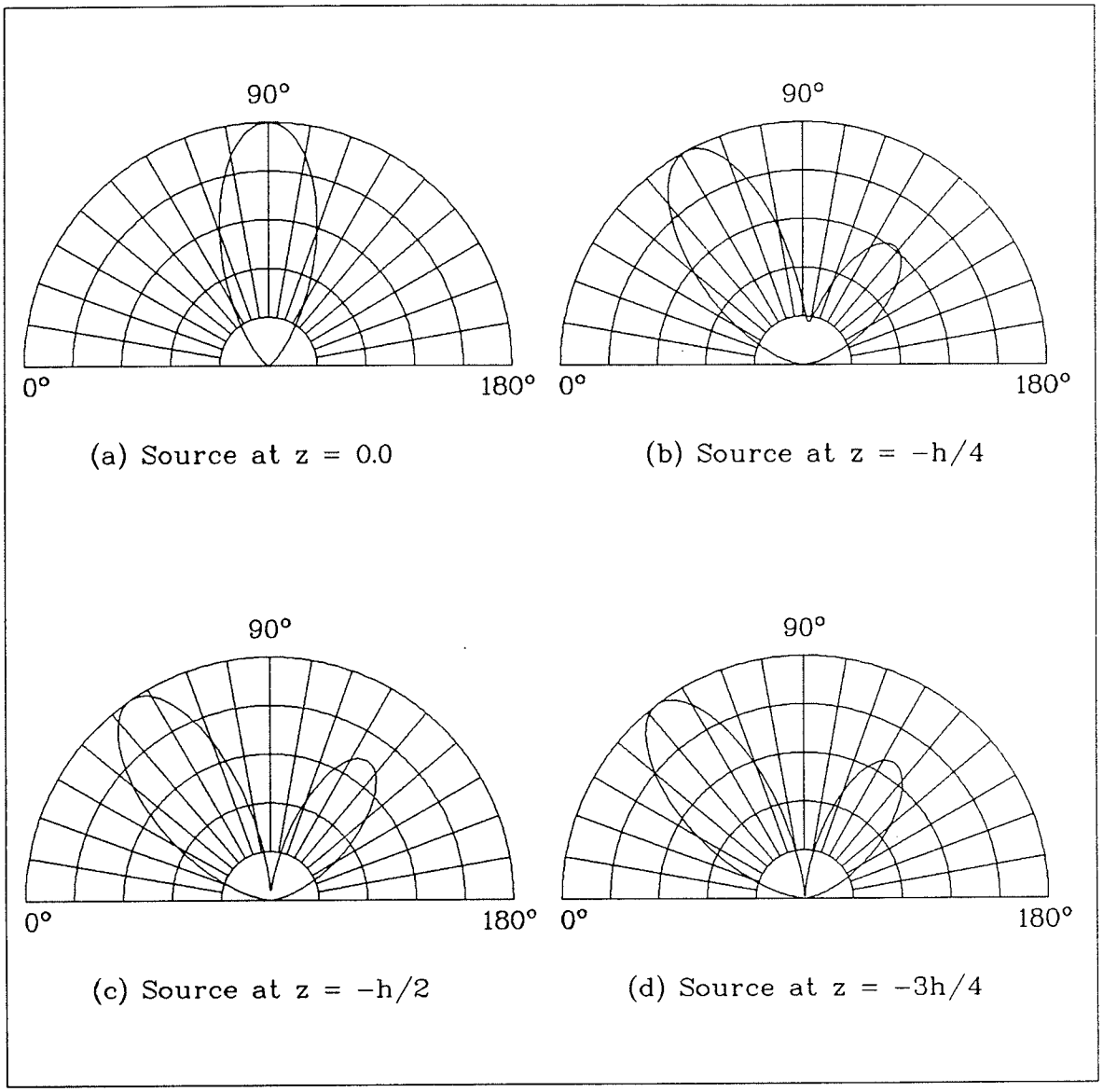

Fig. 4.8 : Normalized power pattern of dipole antenna
(h/a = 74.2 , h = 0.5 λ)

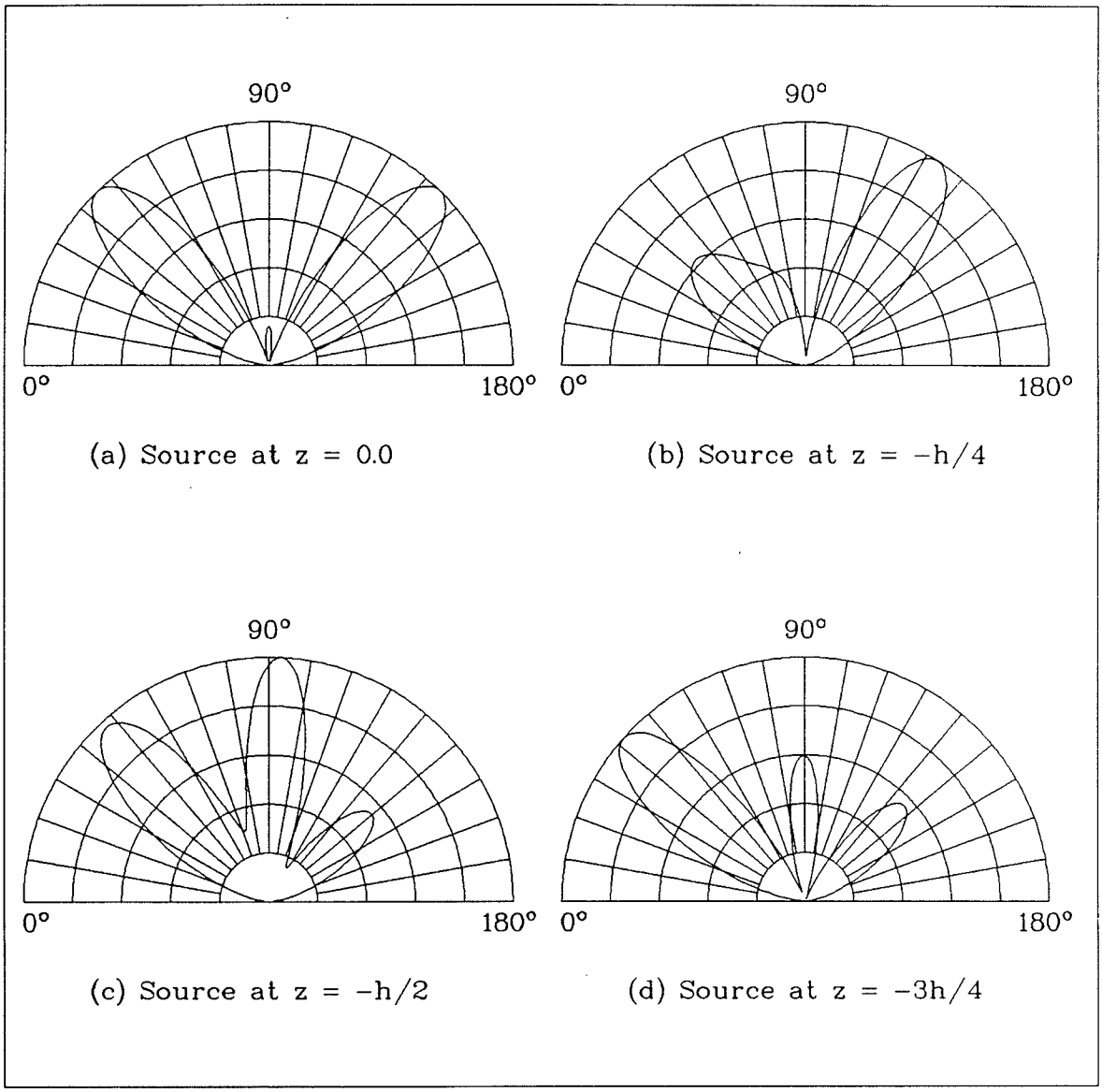

Fig. 4.9 : Normalized power pattern of dipole antenna
(h/a = 74.2 , h = 0.75 λ)

and the overall length of the dipole. The proper choice of these variables for a maximum gain at a certain dipole length was investigated numerically by Saoudy and Hamid [81] and Strait and Hirasawa [82]. The normalized power patterns for typical examples is presented in Fig. 4.10-a which shows an example due to Saoudy and Hamid while Fig. 4.10-b shows one due to Strait and Hirasawa. The half length of the dipole in both examples is 0.75 λ and the radii are 0.005 λ and 0.01 λ , respectively. Although the first example has different feed positions and voltages than the second, they nevertheless give almost the same patterns except for a 2^o reduction in the beam width of the first example. The input admittances of the two examples are given in Table 4.1.

The current distribution on a dipole of half length 1 λ and radius 0.01 λ is shown in Fig. 4.11-a. The dipole fed at $z = 0.5\lambda, 0$ and -0.5λ with voltage sources having the values 1.0, 1.1 and 1.0 volts, respectively. The input admittance for this example is also given in Table 4.1 while the normalized power pattern is shown in Fig. 4.11-b. It should be mentioned here that the multi-fed dipole antenna is treated as a superposition of the arbitrarily fed one. The agreement with the example by Strait and Hirasawa is satisfactory and gives confidence in our expression for the radiation pattern.

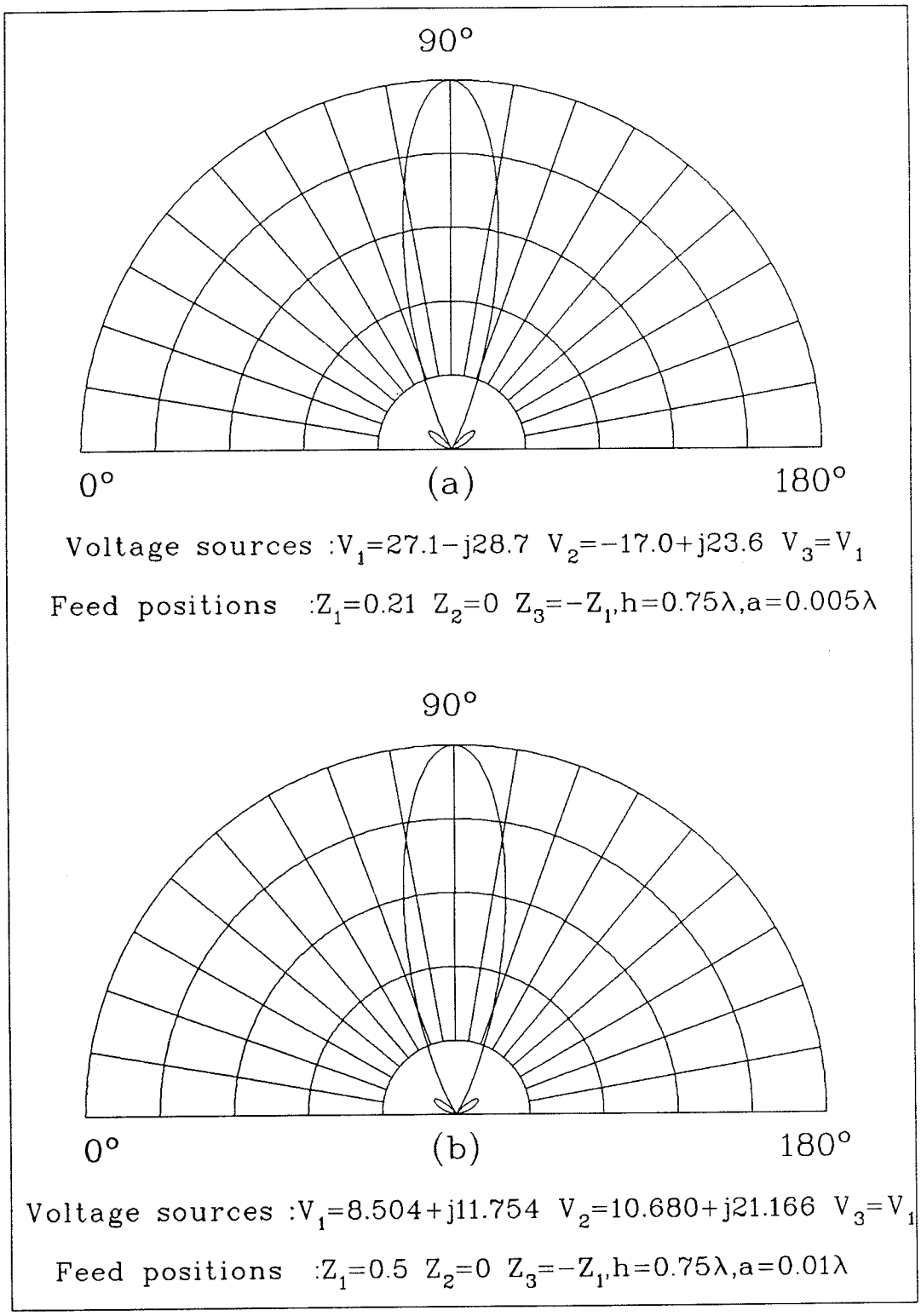

Fig. 4.10 : Normalized power patterns of multiply fed dipole antenna.

$Y_3 = Y_1$ since $z_1 = z_3$

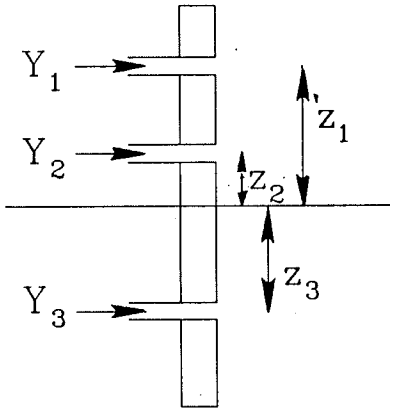

h/λ	a/λ	V_1	V_2	V_3	z_1/λ	z_2/λ	z_3/λ	$Y_1 \times 10^{-3}$	$Y_2 \times 10^{-3}$
1.0	0.01	1.0	1.1	1.0	0.5	0.0	−0.5	3.66−j2.50	10.65−j7.57
0.75	0.005	27.1−j28.7	−17.+j23.6	27.1−j28.7	0.21	0.0	−0.21	7.00−j 1.79	−4.81+j6.39
0.75	0.01	8.5+j11.75	10.68+j21.17	8.5+j11.75	0.5	0.0	−0.5	.27+j 3.0	0.67+j1.76

Table 4.1 : Input admittance of a multiply fed dipole.

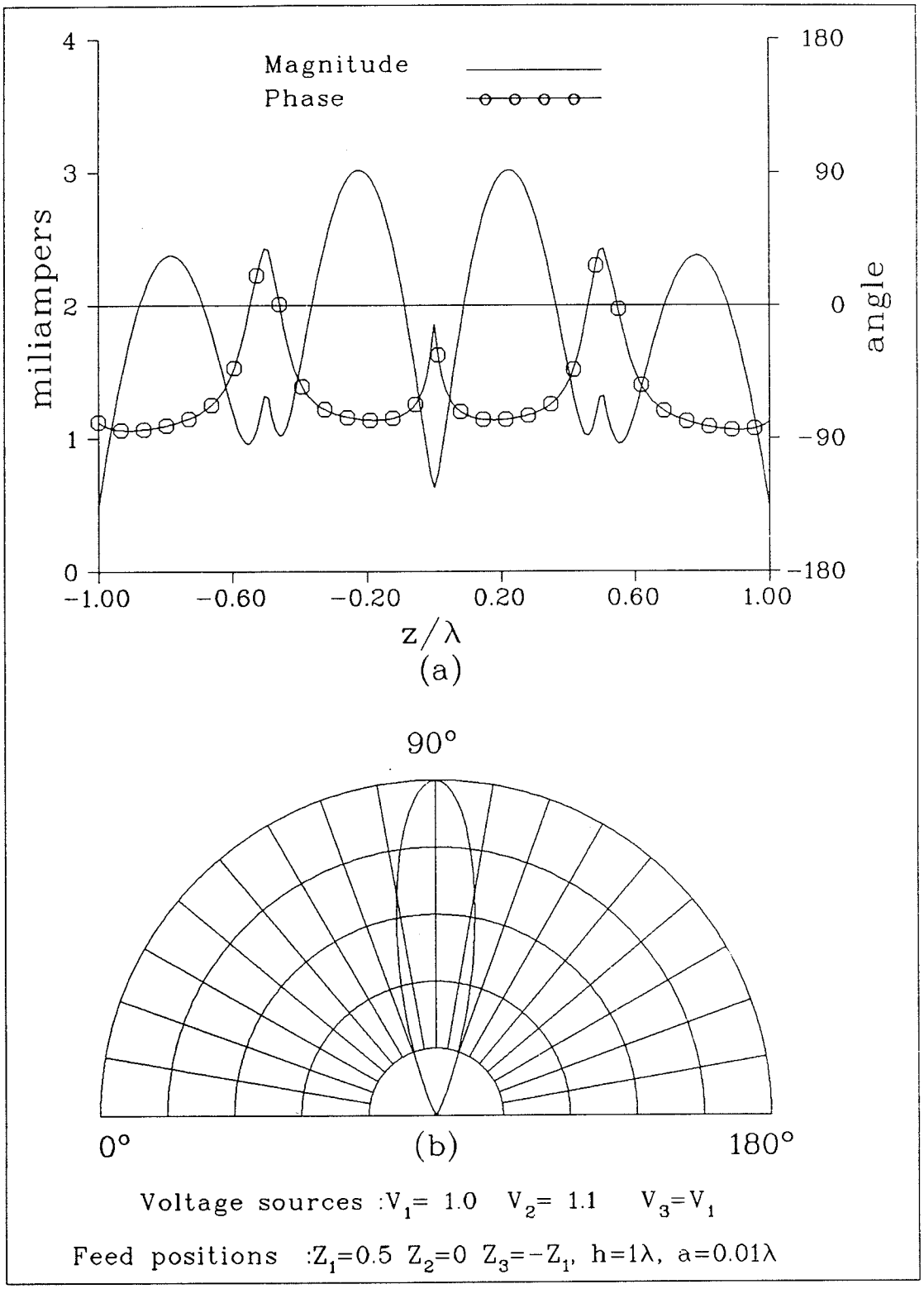

Fig. 4.11 : (a) Current distribution.
(b) Normalized power pattern.

CHAPTER 5

SIMULATION BY CIRCULAR CYLINDERS WITH A LONG DIPOLE EXCITATION

5.1 *Introduction*

The simulation of a cylindrical reflector antenna by circular cylinders in which the feed is a long dipole is considered in this Chapter. The cylinders are again parallel to each other and to the dipole axis while the dipole field is considered as the incident field on the cylinders. Multiply scattered fields are then introduced among the cylinders as well as between each cylinder and the dipole. The method employed for solving the multiple scattering problem is a combination of self consistent and iterative procedures which can be summarized as follows :

1- the multiply scattered fields from the cylinders due to the dipole radiation field are calculated.

2- the multiply scattered fields evaluated in step 1 are considered as incident on the dipole and the first order scattered field from the dipole is calculated using an approximate method.

3- step 1 is repeated with an incident field given by the scattered field from the dipole.

4- steps 2 and 3 are repeated for calculating the higher order scattered fields.

5- the total far zone scattered field is finally calculated by imposing the far field conditions on the resulting integrals which can only be solved asymptotically.

Examples illustrating the radiation pattern of simulated parabolic and circular cylindrical and corner reflector antennas are shown. The field of a long

dipole antenna perturbed by one or more cylinders is given. It is also shown how one can improve the simulated reflector pattern over the solid reflector by proper choice of the radii and positions of the simulating cylinders along the reflector trajectory. The excitation of a cylindrical reflector by a long dipole will give rise to interaction (multiple scattering) terms which were not present in the case of line source excitation.

5.2 *Radiation field of the dipole*

The dipole antenna is assumed to be an infinitely thin-walled, perfectly conducting, circular tube of radius a and length $2h$. At $z = l$ the dipole is driven by a voltage V applied across an infinitesimal gap δ. The electric field in the gap is given by

$$E_z = -V\ \delta(z-l)\ e^{j\omega t} \tag{5.1}$$

As stated in Chapter 4 the arbitrarily fed dipole is splited into symmetrical and anti-symmetrical dipoles. In this case one can write the z-component of the electric field for the arbitrarily driven dipole as

$$E_z^{(d\,0)}(\rho,z) = E_z^{(s)}(\rho,z) + E_z^{(a)}(\rho,z) \tag{5.2}$$

where $E_z^{(s)}(\rho,z)$ and $E_z^{(a)}(\rho,z)$ are the z-components of the electric field for the symmetrical and anti-symmetrical driven dipoles, respectively. From equation (4.3) we can write

$$E_z^{(s)}(\rho,z) = \int_{-\infty}^{\infty} \beta^2 A_2^s(\xi)\, H_0^{(2)}(\beta\rho)\, e^{j\xi z}\, dz \tag{5.3}$$

where

$$A_2^s(\xi) = \frac{1}{2\pi\beta^2 H_0^{(2)}(\beta a)} \int_{|z'|>h} e^{-j\xi z'} E_z(z')\, dz' - 2V^s \cos(\xi l) \tag{5.4}$$

Substituting for $A_2^s(\xi)$ from (5.4) in (5.3) and using the Fourier transforms (4.16) and (4.17), we obtain

$$E_z^{(s)}(\rho,z) = \frac{1}{2\pi}\int_{-\infty}^{\infty} \frac{H_0^{(2)}(\beta\rho)}{H_0^{(2)}(\beta a)}\Big[e_-(\xi) + e_+(\xi) - 2V^s \cos(\xi l)\Big] e^{j\xi z}\, d\xi \tag{5.5}$$

Now,(4.31) can be used to simplify (5.5), with the result

$$E_z^{(s)}(\rho,z) = \frac{-1}{4\omega\epsilon_0}\int_{-\infty}^{\infty} \frac{H_0^{(2)}(\beta\rho)}{H_0^{(2)}(\beta a)} \frac{i_s(\xi)}{k(\xi)} e^{j\xi z}\, d\xi \tag{5.6}$$

Using (4.28) to eliminate $k(\xi)$ from (5.6), we get

$$E_z^{(s)}(\rho,z) = \frac{-1}{8\pi\omega\epsilon_0}\int_{-\infty}^{\infty} \beta^2 J_0(\beta a)\, i_s(\xi)\, H_0^{(2)}(\beta\rho)\, e^{j\xi z}\, d\xi \tag{5.7}$$

Similarly for the anti-symmetrically driven dipole one can write

$$E_z^{(a)}(\rho,z) = \frac{-1}{8\pi\omega\epsilon_0}\int_{-\infty}^{\infty} \beta^2 J_0(\beta a)\, i_a(\xi)\, H_0^{(2)}(\beta\rho)\, e^{j\xi z}\, d\xi \tag{5.8}$$

Thus the total z-component of the electric field due to the arbitrarily fed dipole is given by

$$E_z^{(d\,0)}(\rho,z) = \frac{-1}{8\pi\omega\epsilon_0}\int_{-\infty}^{\infty} \beta^2 J_0(\beta a)\, i_0(\xi)\, H_0^{(2)}(\beta\rho)\, e^{j\xi z}\, d\xi \tag{5.9}$$

where $i_0(\xi) = i_s(\xi) + i_a(\xi)$ is the Fourier transform of the current distribution along the arbitrarily fed dipole. In the following analysis we will use the first

order expression $(i.e\ N = 1)$ for the current distribution given in (4.76) as

$$I(z) = \frac{2\omega\epsilon_0}{\pi}\Big[VjR_0(|l-z|) + jR_0(h+z)\,(f_0^a - f_0^s)C_0 - jR_0(h-z)\,(f_0^a + f_0^s)\,C_0\Big] \tag{5.10}$$

This current distribution can be rearranged and written in the following form

$$I(z) = I_\infty(|l - z|) + g_1 I_\infty(h + z) + g_2 I_\infty(h - z) \tag{5.11}$$

where I_∞ is the current distribution along the infinitely long dipole antenna which is given by

$$I_\infty(x) = \frac{jV}{Z_0} e^{-jkx} \ln\left[1 - \frac{2\pi j}{2C_w + \ln(kx + \sqrt{(kx)^2 + e^{-2\gamma}}) + \gamma + j\frac{\pi}{2}}\right] \tag{5.12}$$

The constants g_1 and g_2 are given by

$$g_1 = -\rho_\Gamma\left[\frac{I_\infty(h + l) - I_\infty(h - l)\,I_\infty(2h)\,\rho_\Gamma}{1 - I_\infty^2(2h)\,\rho_\Gamma^2}\right] \tag{5.13}$$

$$g_2 = -\rho_\Gamma\left[\frac{I_\infty(h - l) - I_\infty(h + l)\,I_\infty(2h)\,\rho_\Gamma}{1 - I_\infty^2(2h)\,\rho_\Gamma^2}\right] \tag{5.14}$$

where

$$\rho_\Gamma = -j\pi Z_0\left[\frac{C_0}{2k}\right]^2 \tag{5.15}$$

is the reflection coefficient at either dipole end. The first term in the current distribution (5.11) is due to the source at $z = l$ of an infinite dipole. The other two terms are due to the reflected current at the dipole ends. The reflection

coefficient given by Shen et al. [52] for a semi-infinite dipole is equal to ρ_Γ. Also, in the case of plane wave incident on a dipole, discussed by Shen [83], the reflection coefficient of the current wave at the open ends is equivalent to ρ_Γ when the plane wave is normally incident.

Now, the Fourier transform of the current distribution $I(z)$ is given by

$$i_0(\xi) = \int_{-\infty}^{\infty} I(z)\, e^{-j\xi z}\, dz \tag{5.16}$$

Substituting for $I(z)$ from (5.11) and using the same steps described in section 4.6, the final result is given by

$$i_0(\xi) = \frac{2j\pi V}{Z_0 F}\Big[S_-(l,\xi) - S_+(l,\xi) - g_1 S_+(-h,\xi) + g_2 S_-(h,\xi)\Big] \tag{5.17}$$

where

$$S_\pm(D,\xi) = \frac{e^{\pm jkD}}{\xi \mp k}\left\{\left[1 + \frac{\gamma - G[k(h \mp D),(1\pm \xi/k)]}{F}\right] e^{-j(\xi \pm k)D}\right.$$

$$\left. - \left[1 - \frac{\ln[k(h \mp D) + \sqrt{[k(h \mp D)]^2 + e^{-2\gamma}}}{F}\right] e^{\mp j(\xi \pm k)h}\right\} \tag{5.18}$$

The functions F and G are given by (4.79) and (4.83), respectively. Now, the z-component of the radiated field from the dipole can be evaluated from (5.9). We will proceed to calculate the scattered field from the cylinders due to an incident field $E_z^{(d\,0)}(\rho,z)$ given by (5.9).

5.3 *First order fields scattered by cylinders*

A schematic diagram of the problem in hand is shown in Fig. 5.1. The center of the ith cylinder is located at (s_i, ψ_i) with respect to the origin of the local cylindrical coordinate system, while the dipole center is located at (s_0, ψ_0). The radius of the ith cylinder is denoted by b_i. In order to facilitate the transformation process of the scattering fields among cylinders and the dipole, another $(N+1)$ cylindrical coordinate systems are defined at the centers of the N cylinders and dipole. The radiation field (5.9) is considered as an incident field on the cylinders and multiple scattering process among the cylinders and dipole will take place. The first step, as stated before, is to evaluate the scattered field from cylinders due to the dipole radiated field (5.9) including all multiple scattering fields among cylinders. In this case one can write the electric Hertz potential for the scattered field from the lth cylinder as a combination of Fourier integral in z_l with Fourier series in ϕ_l, namely

$$\Pi_l^c = \int_{-\infty}^{\infty} \sum_{n=-\infty}^{\infty} A_n^{(l1)}(\xi)\ H_n^{(2)}(\beta\rho_l)\, e^{j\xi z_l}\, e^{jn\phi_l}\, d\xi \tag{5.19}$$

where $A_n^{(l1)}(\xi)$ are the scattering coefficients to be calculated. It should be mentioned that the scattering Hertz potential (5.19) from the lth cylinder includes all the multiply scattered fields among the cylinders. Using (5.19) and Maxwell's equations one can calculate the z-component of the scattered electric field from the lth cylinder, i. e.

$$E_{zl}^{(c1)}(\rho_l, \phi_l, z_l) = \int_{-\infty}^{\infty} \beta^2 \sum_{n=-\infty}^{\infty} A_n^{(l1)}(\xi)\, H_n^{(2)}(\beta\rho_l)\, e^{j\xi z_l} e^{jn\phi_l}\, d\xi \tag{5.20}$$

where the superscript (c1) denotes the first order scattered field from the lth cylinder in the multiple scattering process between the cylinders and dipole.

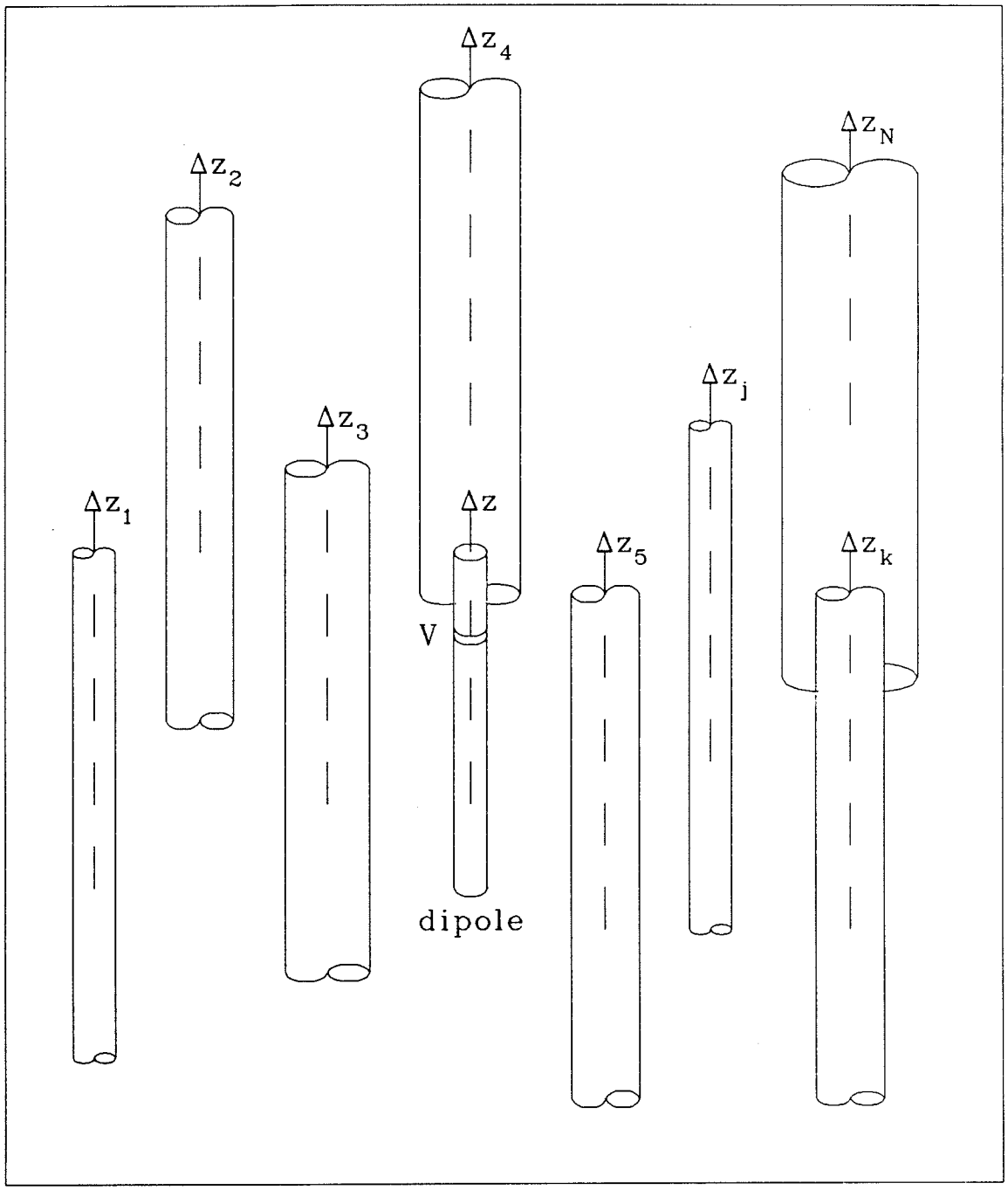

Fig. 5.1 : Schematic diagram of a long dipole in the presence of cylinders.

In order to apply the boundary conditions on the cylindrical surfaces, the expressions for the scattered fields from all cylinders other than the l th cylinder must be transformed in terms of the l th coordinate system. This process could be done using the addition theorem of the Hankel function (3.8).

The total z-component of the first order electric field is given by

$$E_z^{(t\,1)} = E_z^{(d\,0)} + \sum_{q=1}^{N} E_{zq}^{(c\,1)} \tag{5.21}$$

Since the cylinders are perfectly conducting, the total tangential component of the first order electric field on their surfaces should vanish. Now assume the application of this boundary condition on the the surface of the l th cylinder. In this case one has to transfer all the scattered fields from the coordinates of the other cylinders and the radiated field from the dipole coordinate in terms of the l th cylinder coordinate system, i.e

$$E_z^{(d\,0)}(\rho_l,\phi_l,z_l) = \int_{-\infty}^{\infty} \beta^2\, Q_0(\xi) \sum_{m=-\infty}^{\infty} e^{-jm\psi_{l0}}\, J_m(\beta\rho_l)$$

$$H_m^{(2)}(\beta s_{l0})\, e^{jm\phi_l}\, e^{j\xi z_l}\, d\xi \tag{5.22}$$

and

$$E_{zq}^{(c\,1)}(\rho_l,\phi_l,z_l) = \int_{-\infty}^{\infty} \beta^2 \sum_{n=-\infty}^{\infty} A_n^{(q\,1)}(\xi) \sum_{m=-\infty}^{\infty} e^{-j(m-n)\psi_{lq}} J_m(\beta\rho_l)$$

$$H_{m-n}^{(2)}(\beta s_{lq})\, e^{jm\phi_l}\, e^{j\xi z_l}\, d\xi \tag{5.23}$$

$$Q_0(\xi) = \frac{-1}{8\pi\omega\epsilon_0}\, J_0(\beta a)\, i_0(\xi) \tag{5.24}$$

The boundary condition on the l th cylinder surface yields

$$E_z^{(d\,0)}(b_l,\phi_l,z_l) + \sum_{q=1}^{N} E_{zq}^{(c\,1)}(b_l,\phi_l,z_l) = 0 \tag{5.25}$$

Substituting from (5.22) and (5.23) in (5.25) we obtain after some mathematical manipulations

$$A_n^{(l\,1)}(\xi) = -e^{-jn\psi_{l0}} \frac{J_n(\beta b_l)}{H_n^{(2)}(\beta b_l)} H_n^{(2)}(\beta s_{0l}) Q_0(\xi) - \sum_{q=1}^{N} \frac{J_n(\beta b_l)}{H_n^{(2)}(\beta b_l)}$$

$$\sum_{m=-\infty}^{\infty} e^{-j(n-m)\psi_{lq}} H_{n-m}^{(2)}(\beta s_{lq})\, A_m^{(q\,1)}(\xi) \quad , \quad l \neq q \tag{5.26}$$

Similarly one can apply the boundary condition (5.25) on the surfaces of the other cylinders. Upon doing this the following N matrix equations are obtained

$$A^{(l\,1)} = L^{(l\,1)} + \sum_{q=1}^{N} B^{(lq)}\, A^{(q\,1)} \quad , \quad q \neq l \tag{5.27}$$

where l takes the values 1 to N, while $A^{(l\,1)}$ and $A^{(q\,1)}$ are infinite vectors containing the first order scattering coefficients corresponding to the lth and qth cylinders, respectively. The matrices $B^{(lq)}$ are infinitely dimensional and their elements are given by

$$B_{nm}^{(lq)} = -\frac{J_n(\beta b_l)}{H_n^{(2)}(\beta b_l)} H_{n-m}^{(2)}(\beta s_{lq})\, e^{-j(n-m)\psi_{lq}} \quad , \quad l \neq q \tag{5.28}$$

while the elements of $L^{(l\,1)}$ are given by

$$L_n^{(l\,1)} = -e^{-jn\psi_{l0}} Q_0(\xi) \frac{J_n(\beta b_l)}{H_n^{(2)}(\beta b_l)} H_n^{(2)}(\beta s_{0l}) \tag{5.29}$$

The matrices and vectors in (5.27) are infinitely dimensional, therefore some truncation must be performed in order to generate numerical results. The basis of truncating these matrices and vectors has been discussed in Chapter 3, and a

similar approach is taken here. Therefore one can write the matrix equations (5.27) in a single matrix equation, i.e

$$(I - B)\, A^{(1)} = L^{(1)} \tag{5.30}$$

where B is a square matrix of dimension $[N(2M+1)]$, $A^{(1)}$ and $L^{(1)}$ are vectors of the same dimensions. The matrix equation (5.30) can be solved for the first order scattering coefficients $A^{(1)}$ which contain N vectors each of length $(2M+1)$ corresponding to N cylinders.

Once the scattering coefficients are evaluated, one can write the first order z-component of the scattered field from the cylinders as

$$E_{zi}^{(c\,1)}(\rho,\phi,z) = \sum_{l=1}^{N} \int_{-\infty}^{\infty} \beta^2 \sum_{m=-\infty}^{\infty} A_m^{(l\,1)}(\xi)\, H_m^{(2)}(\beta\rho_l)\, e^{jm\phi_l}\, e^{j\xi z_l}\, d\xi \tag{5.31}$$

The infinite series over m will be truncated to $2M+1$ terms in the numerical calculations. This field is considered as an incident field on the dipole and an iterative procedure for calculating the multiple scattering fields between the dipole and the cylinders is described next.

5.4 *First order field scattered by the dipole*

The scattered field (5.31) can be expressed in terms of the dipole coordinate system (*i.e* ρ_0,ϕ_0,z_0) by using the transformation (3.8), i.e

$$E_{zi}^{(c\,1)}(\rho_0,\phi_0,z_0) = \sum_{l=1}^{N} \int_{-\infty}^{\infty} \beta^2 \sum_{n=-\infty}^{\infty} J_n(\beta\rho_0)\, e^{jn\phi_0}$$

$$\sum_{m=-\infty}^{\infty} e^{j(m-n)\psi_{0l}}\, H_{n-m}^{(2)}(\beta s_{0l})\, A_m^{(l\,1)}(\xi)\, e^{j\xi z_0}\, d\xi \tag{5.31}$$

The scattered field from the dipole may be calculated from the current induced

on the dipole surface due to the incident field (5.31). The exact treatment of this part of the solution appears to be a difficult task. However, a reasonable approximate treatment leads to an accurate solution. An approximate method has been introduced by Kuehl [62] for calculating the current distribution on a finite cylinder in the presence of an infinitesimal dipole. Upon using his approximation, one may consider that the dipole is an infinitely long cylinder of radius a with no gap at the center. Then the current induced on the cylinder surface (I_s) due to the incident wave (5.31) can be evaluated and considered as an approximate estimate of the first order induced current on the dipole.

Now consider the dipole as an infinitely long cylinder of radius a. In this case the electric Hertz potential of the scattered field has only a z-component, namely

$$\Pi = \int_{-\infty}^{\infty} \sum_{n=-\infty}^{\infty} W_n(\xi)\, H_n^{(2)}(\beta\rho_0)\, e^{jn\phi_0}\, e^{j\xi z_0}\, d\xi \quad , \quad \rho_0 > a \tag{5.32}$$

where $W_n(\xi)$ are unknown scattering coefficients to be calculated. The z-component of the scattered field can be calculated using (5.32) and Maxwell's equations,i.e

$$E_z(\rho_0,\phi_0,z_0) = \int_{-\infty}^{\infty} \beta^2 \sum_{n=-\infty}^{\infty} W_n(\xi)\, H_n^{(2)}(\beta\rho_0)\, e^{jn\phi_0}\, e^{j\xi z_0}\, d\xi \quad , \rho_0 > a \tag{5.33}$$

The total z-component of the electric field on the cylinder surface should be equal to zero since it is perfectly conducting. Hence

$$E_z(a,\phi_0,z_0) + E_{zi}^{(c\,1)}(a,\phi_0,z_0) = 0 \tag{5.34}$$

Substituting from (5.31) and (5.33) into (5.34), one obtains

$$W_n(\xi) = -\frac{J_n(\beta a)}{H_n^{(2)}(\beta a)} \sum_{l=1}^{N} \sum_{m=-\infty}^{\infty} e^{j(m-n)\psi_{0l}}\, H_{n-m}^{(2)}(\beta s_{0l})\, A_m^{(l\,1)}(\xi) \tag{5.35}$$

In order to calculate the current induced on the cylinder surface the ϕ-component of the scattered magnetic field should be evaluated. In this case one can use the Hertz vector potential (5.32) with Maxwell's equations to obtain H_ϕ, i. e.

$$H_\phi(\rho_0,\phi_0,z_0) = -j\omega\epsilon_0 \sum_{n=-\infty}^{\infty} \int_{-\infty}^{\infty} \beta\, W_n(\xi) H_n^{(2)'}(\beta\rho_0)\, e^{jn\phi_0}\, e^{j\xi z_0}\, d\xi \tag{5.36}$$

where the prime superscript denotes the derivative of the Hankel function with respect to the argument. Using (5.36) and the magnetic incident field, the current induced on the cylinder surface is given by

$$I_s^{(1)}(z) = -2\pi a j\omega\epsilon_0 \left\{ \int_{-\infty}^{\infty} \beta\, W_0(\xi)\, H_0^{(2)'}(\beta a)\, e^{j\xi z_0}\, d\xi \right.$$

$$\left. + \int_{-\infty}^{\infty} \beta\, J_0'(\beta a) \sum_{l=1}^{N} \sum_{m=-\infty}^{\infty} (-1)^m\, e^{jm\psi_{0l}}\, H_m^{(2)}(\beta s_{0l})\, A_m^{(l1)}\, e^{j\xi z_0}\, d\xi \right\} \tag{5.37}$$

where the superscript (1) denotes the first order induced current. In order to simplify the analysis we define

$$T_n^{(l)}(\xi) = \frac{A_n^{(l1)}(\xi)}{Q_0(\xi)} \tag{5.38}$$

Substituting for $W_0(\xi)$ from (5.35) into (5.37) and using the definition (5.38), we obtain

$$I_s^{(1)}(z) = \frac{1}{2\pi} \int_{-\infty}^{\infty} i_1(\xi)\, e^{j\xi z_0}\, d\xi \tag{5.39}$$

where

$$i_1(\xi) = Y(\xi)\, i_0(\xi) \tag{5.40}$$

and

$$Y(\xi) = -\frac{J_0(\beta a)}{H_0^{(2)}(\beta a)} \sum_{l=1}^{N} \sum_{m=-\infty}^{\infty} (-1)^m\, e^{jm\psi_{0l}}\, H_m^{(2)}(\beta s_{0l})\, T_m^{(l)}(\xi) \tag{5.41}$$

Here $i_1(\xi)$ is the inverse Fourier transform of the first order induced current distribution along the dipole.

Since the z-component of the radiated field from the dipole due to the original current distribution $I(z)$ is given by (5.11), a similar field expression can be used for calculating the scattered field from the dipole due to the current $I_s^{(1)}(z)$. In this case one can write the z-component of the first order scattered field from the dipole in the form

$$E_z^{(d\,1)}(\rho_0, z_0) = \int_{-\infty}^{\infty} \beta^2\, Q_1(\xi)\, H_0^{(2)}(\beta\rho_0)\, e^{j\xi z_0}\, d\xi \tag{5.43}$$

where

$$Q_1(\xi) = \frac{-1}{8\pi\epsilon_0\omega}\, J_0(\beta a)\, i_1(\xi) \tag{5.44}$$

The radiation and first order scattered fields from the dipole are calculated in integral form. For the higher order scattered fields from the dipole and cylinders the same procedure can be used as shown next.

5.5 *Higher order fields scattered by the dipole and cylinders*

The higher order fields scattered by the dipole and group of cylinders may be evaluated in terms of the lower order scattered fields. For evaluating the z-component of the second order scattered electric field from the cylinders, we

consider the first order scattered field from the dipole (5.44) to be incident again on the cylinders. In this case the same steps described in section 5.3 are employed leading to

$$E_{zl}^{(c\,2)}(\rho_l,\phi_l,z_l) = \sum_{l=1}^{N} \int_{-\infty}^{\infty} \beta^2 \sum_{m=-\infty}^{\infty} A_m^{(l\,2)}(\xi)\, H_m^{(2)}(\beta\rho_l)\, e^{jm\phi_l}\, e^{j\xi z_l}\, d\xi \qquad (5.45)$$

where

$$A^{(2)} = [I - B]^{-1} L^{(2)} \qquad (5.46)$$

and

$$L_n^{(l\,2)}(\xi) = -e^{-jn\psi_{l0}}\, Q_1(\xi)\, \frac{J_n(\beta b_l)}{H_n^{(2)}(\beta b_l)}\, H_n^{(2)}(\beta s_{0l}) \qquad (5.47)$$

Also the second order scattered field from the dipole can be calculated using the same steps described in section 5.4. Using the expression for the second order scattered field from the cylinders (5.45), one can derive the z-component of the second order field scattered by the dipole. The final result is given by

$$E_z^{(d\,2)}(\rho_0,z_0) = \int_{-\infty}^{\infty} \beta^2\, Q_2(\xi)\, H_0^{(2)}(\beta\rho_0)\, e^{j\xi z_0}\, d\xi \qquad (5.48)$$

where

$$Q_2(\xi) = \frac{-1}{8\pi\epsilon_0\omega}\, J_0(\beta a)\, i_2(\xi) \qquad (5.49)$$

$$i_2(\xi) = Y(\xi)\, i_1(\xi) \qquad (5.50)$$

Similarly one can proceed to calculate the third, fourth, ... and nth orders of the scattered fields from the cylinders and dipole using the same technique. Thus the total z-component of the scattered and radiated electric field from the dipole is

given by

$$E_z^{(dt)}(\rho_0,z_0) = \int_{-\infty}^{\infty} \beta^2 Q(\xi) H_0^{(2)}(\beta\rho_0) e^{j\xi z_0} d\xi \tag{5.51}$$

where

$$Q(\xi) = \frac{-1}{8\pi\epsilon_0\omega} J_0(\beta a) \sum_{j=0}^{\infty} i_j(\xi) \tag{5.52}$$

The zero order current $i_0(\xi)$ is given by (5.15), while the higher order currents can be calculated from the recurrence relation

$$i_n(\xi) = Y(\xi)\, i_{n-1}(\xi) \tag{5.53}$$

Equations (5.52) and (5.53) can be combined together leading to the result

$$Q(\xi) = \frac{-1}{8\pi\epsilon_0\omega} \frac{J_0(\beta a)\, i_0(\xi)}{1 - Y(\xi)} \tag{5.54}$$

Similarly the total z-component of scattered electric field from the cylinders is given by

$$E_z^{(ct)}(\rho_l,\phi_l,z_l) = \sum_{l=1}^{N} \int_{-\infty}^{\infty} \beta^2 Q(\xi) \sum_{m=-\infty}^{\infty} T_m^{(l)}(\xi) H_m^{(2)}(\beta\rho_l) e^{j\xi z_l} e^{jm\phi_l} d\xi \tag{5.55}$$

where

$$T = [I - B]^{-1} L \tag{5.56}$$

and

$$L_n^{(l)} = -e^{-jn\psi_{l0}} \frac{J_n(\beta b_l)}{H_n^{(2)}(\beta b_l)} H_n^{(2)}(\beta s_{0l}) \tag{5.75}$$

where l takes the values from 1 to N. The total z-component of the scattered field for the dipole exciting the group of cylinders is given by (5.51) and (5.55). This field is derived in an integral form. In the next section the z-component of the far electric field will be evaluated by solving the integrals asymptotically.

5.6 *Radiation field*

The total far field will be calculated in terms of the spherical coordinate system (r,θ,ϕ) and subject to the far field assumption $k\rho >> 1$. From (5.51) and (5.55), one can write the z-component of the total field in the form

$$E_z^{tot} = \int_{-\infty}^{\infty} \beta^2 Q(\xi) H_0^{(2)}(\beta\rho_0) e^{j\xi z_0} d\xi$$

$$+ \sum_{l=1}^{N} \sum_{n=-\infty}^{\infty} \int_{-\infty}^{\infty} \beta^2 Q(\xi) T_n^{(l)}(\xi) H_n^{(2)}(\beta\rho_l) e^{jn\phi_l} e^{j\xi z_l} d\xi \quad (5.58)$$

Now, the integral to be evaluated is of the form

$$J = \int_{-\infty}^{\infty} M(\xi) H_n^{(2)}(\beta\rho) e^{j\xi z} d\xi \quad (5.59)$$

The integration is along the real axis of ξ from $-\infty$ to $+\infty$ with an indentation above the branch point $\xi = k$ and below the branch point at $\xi = -k$. No indentations are required if k is allowed to have a small negative part. It should also be remembered that the square root in $(k^2 - \xi^2)^{1/2}$ is chosen such that the real part is positive in accordance with the usual convention. In the present instance, it is assumed that $k\rho >> 1$. This corresponds to the radiation field when the distance from the dipole center is very large compared to the wavelength. It is then permissible to replace the Hankel function by the first term of its asymptotic expansion. The resulting integral for J is now in a form which may be evaluated

by the saddle point method if the integration is transformed to the complex α plane via the substitution $\xi = -k\cos\alpha$. This leads to the form

$$J = j^n \sqrt{2} \int_{\pi - j\infty}^{j\infty} \left[\frac{k\sin\alpha}{\pi\rho}\right]^{1/2} M(-k\cos\alpha)\, e^{-jkr\cos(\theta-\alpha)}\, d\alpha \tag{5.60}$$

with r and θ defined by

$$\rho = r\sin\theta \qquad \text{and} \qquad z = r\cos\theta \tag{5.61}$$

The contour is along a line parallel to the negative imaginary axis, from π to 0 on the real axis, and then along the positive imaginary axis. Following a procedure by Wait [13] for an integral similar to (5.60) we obtain the result

$$J = 2j^{n+1} \frac{e^{-jkr}}{r} M(-k\cos\theta) \tag{5.62}$$

Applying (5.60) to the expression for E_z^{tot}, the far electric field is then given by

$$E_\theta(r,\theta,\phi) = \frac{e^{-jkr}}{r} P(\theta,\phi) \tag{5.63}$$

where

$$P(\theta,\phi) = -2jk^2\sin\theta\, Q(-k\cos\theta) \left\{ e^{jks_0\sin\theta\cos(\phi-\psi_0)} + \sum_{l=1}^{N} e^{jks_l\sin\theta\cos(\phi-\psi_l)} \sum_{m=-M}^{M} j^m T_m^{(l)}(-k\cos\theta)\, e^{jm\phi} \right\} \tag{5.64}$$

Equation (5.64) gives the far field pattern for the dipole in the presence of conducting cylinders. This equation includes infinite interactions between the dipole and the cylinders which will be truncated to a finite number in the numerical calculation.

5.7 *Simulation of cylindrical scattering surface by cylinders*

The cylinders are placed on the trajectory of the specified geometry forming the cylindrical reflector while the long dipole is considered to be the feed of the antenna which is placed parallel to the cylinders. The most important property of the simulated reflector surface is to have the same scattering characteristics as the solid surface. In order to verify this criterion a numerical technique is employed to obtain the far field pattern of a solid surface cylindrical reflector antenna. A pattern comparison between the solid surface and simulated cylindrical reflector antennas is presented. The numerical method is based on the electric field integral equation (EFIE) and magnetic field integral equation (MFIE) which are solved using the moment method. For this purpose a numerical electromagnetic code (NEC) program designed by Poggio et al. [84] and based on the EFIE, MFIE and hybrid EFIE-MFIE for modeling the electromagnetic response of general structures is used. The EFIE is used for thin wire structures, the MFIE for surface structures while for structures consisting of both wires and surfaces the hybrid EFIE-MFIE is used.

The geometry of our problem is modeled as wire segments for the dipole and surface patches for the reflector. The NEC program has the capability of specifying the excitation to a certain geometry in different forms, such as plane wave, voltage sources and current sources, etc. In our problem the feed voltage of the dipole is given in magnitude, phase and position at a specific wire segment.

5.8 *Numerical results and discussion*

A general solution of any geometrical arrangement of N parallel conducting circular cylinders in the vicinity of a long dipole antenna is introduced. Many variables are involved in this problem such as the number N, positions and radii of the cylinders and the dipole geometrical parameters. The latter parameters are fixed at $h = 0.5\lambda$, $a = 0.016\lambda$ and $l = 0$ (center feed dipole) throughout our

numerical examples.

The simplest case considered is a single cylinder in the vicinity of the dipole. Figure 5.2 shows the radiation pattern in the horizontal plane along with the values of the geometrical parameters for the dipole-cylinder configuration. Two different techniques are employed for the pattern calculation, the first is our analytical technique while the second is the numerical NEC program. Good agreement between the results corresponding to both techniques is found. The optimum distance between the dipole and cylinder is found to be 0.3λ. This can be realized from Fig. 5. 3 where patterns of dipole-cylinder configuration are calculated using our analytical technique at different separations. As can be seen in Fig. 5. 3 the peak of the far field pattern intensity increases with increasing separation, then it decreases again followed by the appearance of two main lobes. On the other hand, the presence of a cylinder in the dipole vicinity leads to a directive pattern. However a more directive pattern can be achieved using two cylinders in the dipole vicinity. Figure 5.4 shows the effect of two cylinders on the dipole far field pattern. The pattern has a higher directivity at $\phi = 0$ than the single cylinder with dipole. The positions and radii of the cylinders are also given in Fig. 5. 4. Again the numerical technique is employed for the pattern calculation in this case and comparison shows good agreement with our analytical technique pattern. The maximum deviation between patterns using analytical and numerical techniques is 3%, and this is largely due to truncation errors and modeling the cylinder surface in the NEC program.

Four cases of simulating cylindrical reflector antenna surfaces using parallel conducting circular cylinders are presented. Throughout these cases, cylinders of 0.016λ radius each and equal spacing along the surface trajectories are used. Also the numerical technique is employed for calculating the far field patterns of the corresponding solid surface cylindrical reflector antennas. The antenna feed is a long dipole for both simulated and solid reflectors.

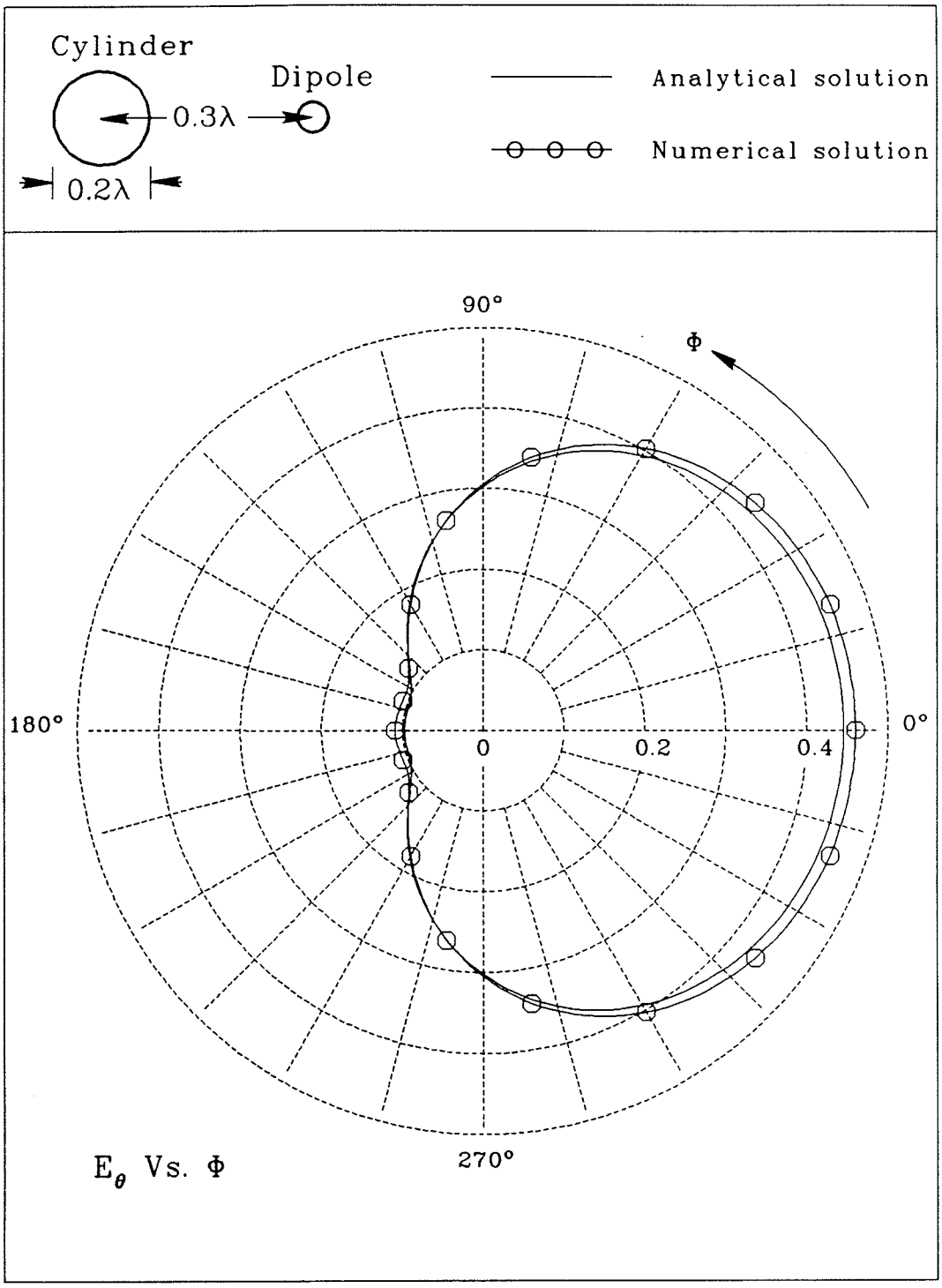

Fig. 5.2 : Far field pattern of a long dipole antenna in the presence of a cylinder.

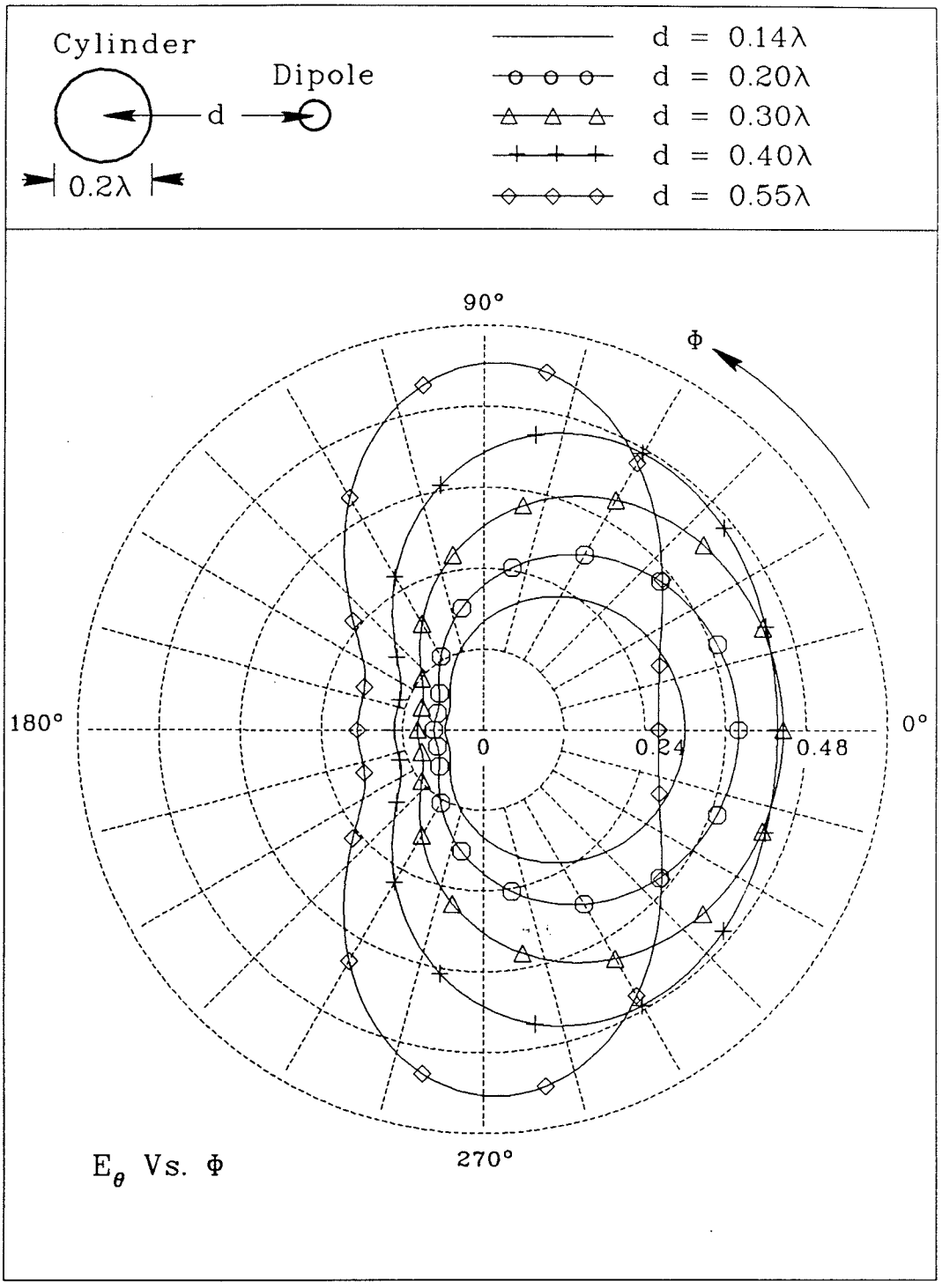

Fig. 5.3 : Effect of the dipole–cylinder separation on the far field pattern.

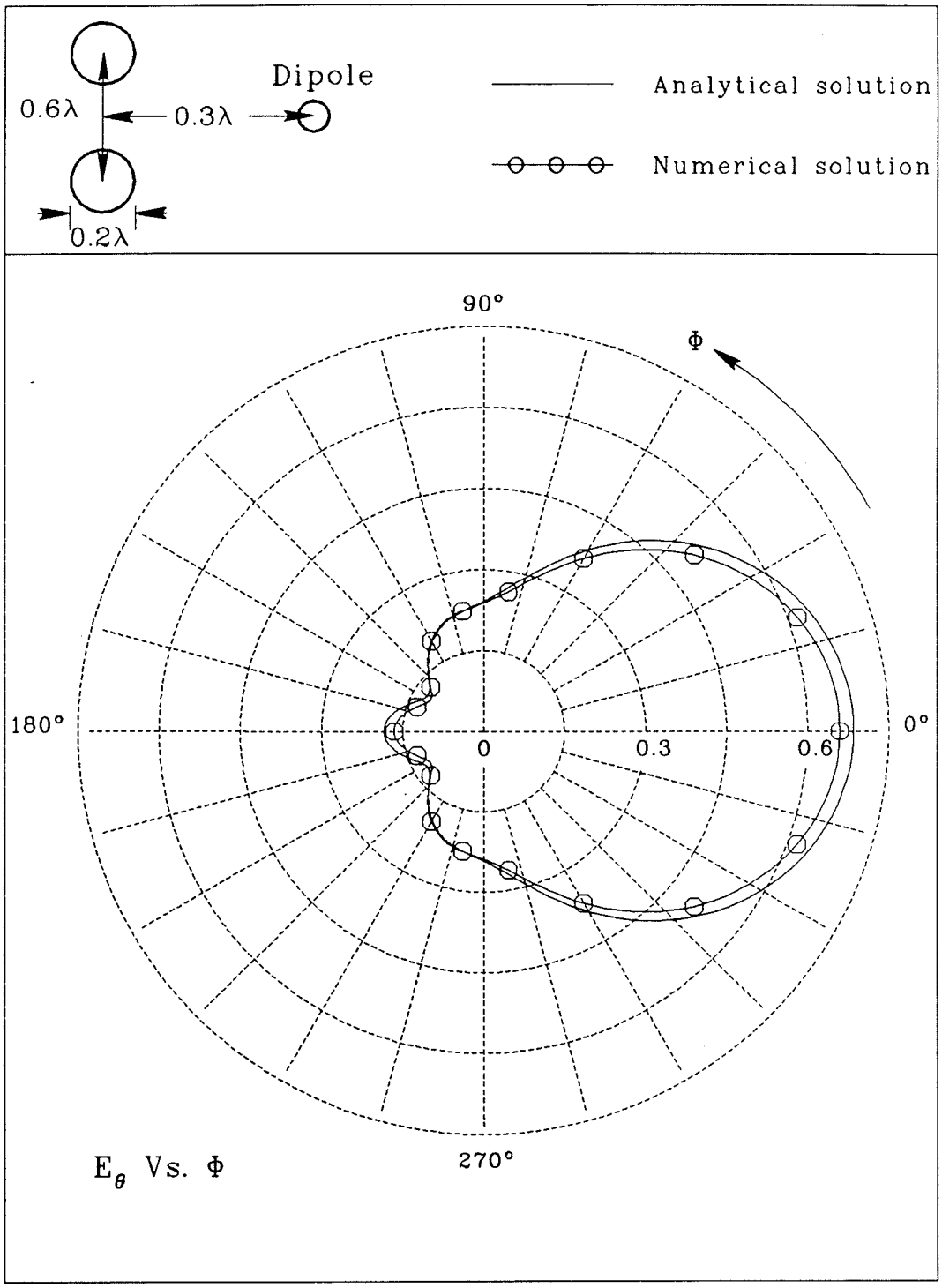

Fig. 5.4 : Far field pattern of a long dipole antenna in the presence of two cylinders.

In the first example a strip of 1λ width excited by a long dipole placed at 0.75λ from the ribbon center is simulated by 11 cylinders. The resulting far field patterns corresponding to solid surface and simulated strips are compared in Fig. 5.5 which shows a very close agreement with a maximum deviation of 5%.

The second case is a parabolic cylindrical reflector antenna of 2λ width and 0.8λ focal length simulated by 17 cylinders. The dipole is placed along the focal line of the antenna. As can be seen from Fig. 5.6 the far field patterns corresponding to the solid and simulated reflectors are in good agreement with each other.

In the third case a circular cylindrical reflector antenna of 1.4λ radius and 2λ width is considered. The reflector is simulated by 19 cylinders while the dipole is placed along the center line of the circular reflector. The far field patterns of both simulated and solid reflectors are in good agreement as shown in Fig. 5. 7.

In the last case, a corner reflector antenna of 60^o corner angle and 1.2λ reflector length is considered. The corner reflector surface is simulated by 17 cylinders while the dipole is placed on the reflector axis parallel to and at 0.5λ from the apex. Figure 5.8 shows good agreement between the far field patterns of both the simulated and solid reflectors.

In the previous cases the solid reflector lengths are truncated in the numerical solution to the finite value of 3λ which may cause the small deviations between patterns of solid and simulated reflector antennas. On the other hand the scattering characteristics of the simulated reflectors are affected by the number, radius of and spacing between the cylinders. Therefore a study of the effect of some variables on the far field pattern is undertaken.

The effect of the radius on the far field pattern of a simulated parabolic cylindrical reflector antenna of 2λ width and 0.8λ focal length is shown in Fig. 5. 9. The reflector is simulated by 17 cylinders of equal radii and spacing along the

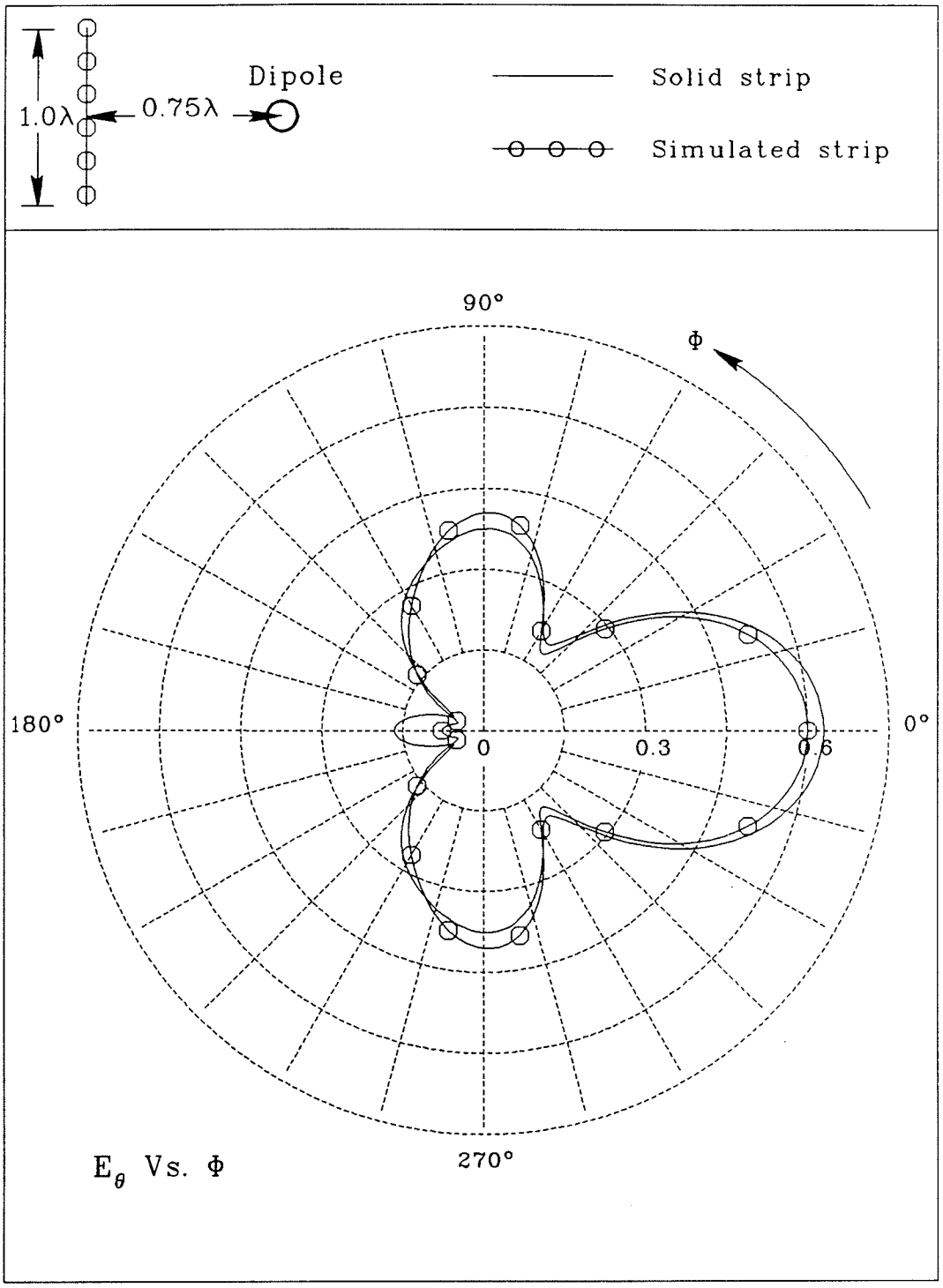

Fig. 5.5 : Far field pattern of a simulated strip nearby a long dipole

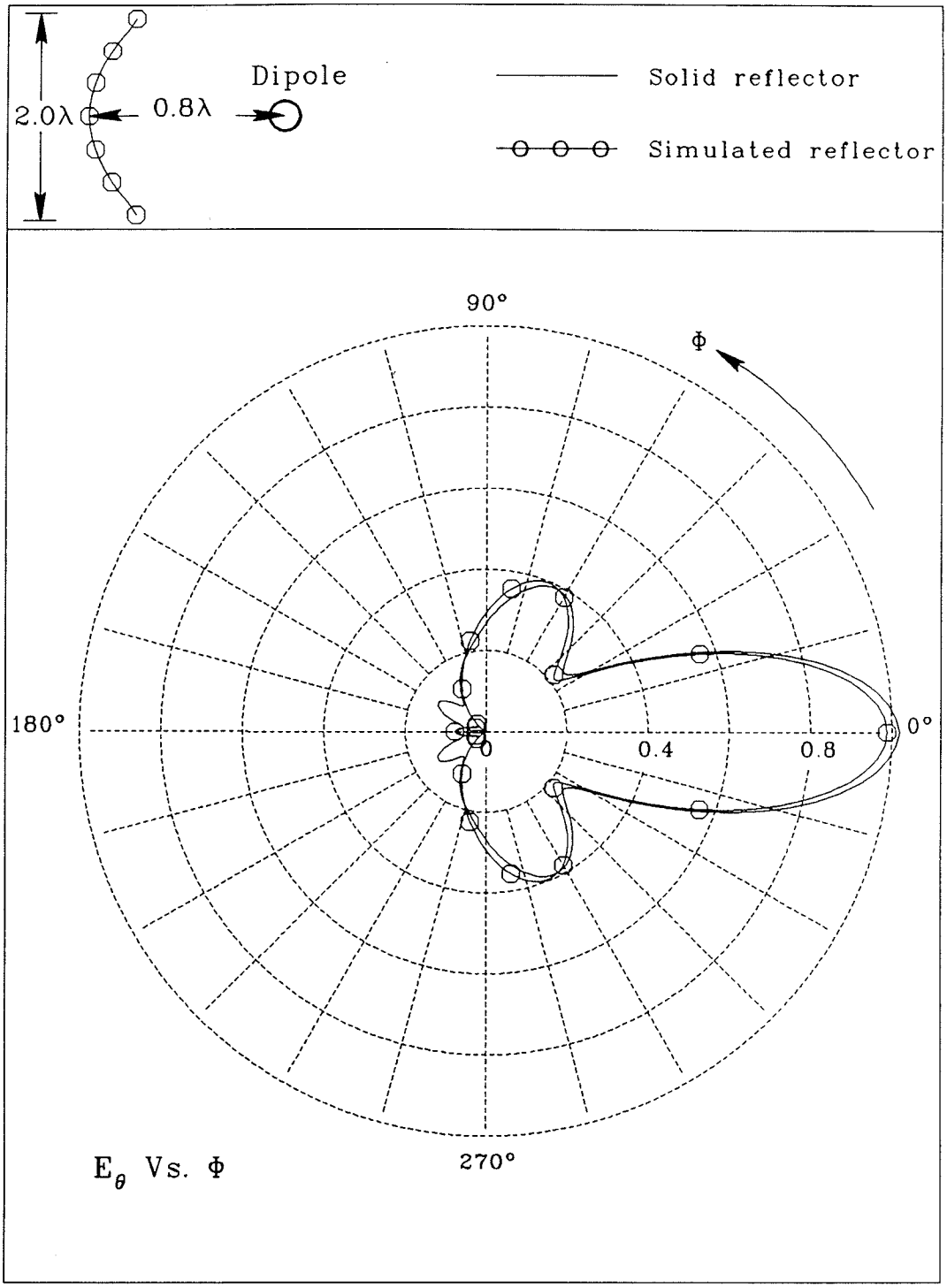

Fig. 5.6 : Far field pattern of a cylindreical parabolic reflector antenna.

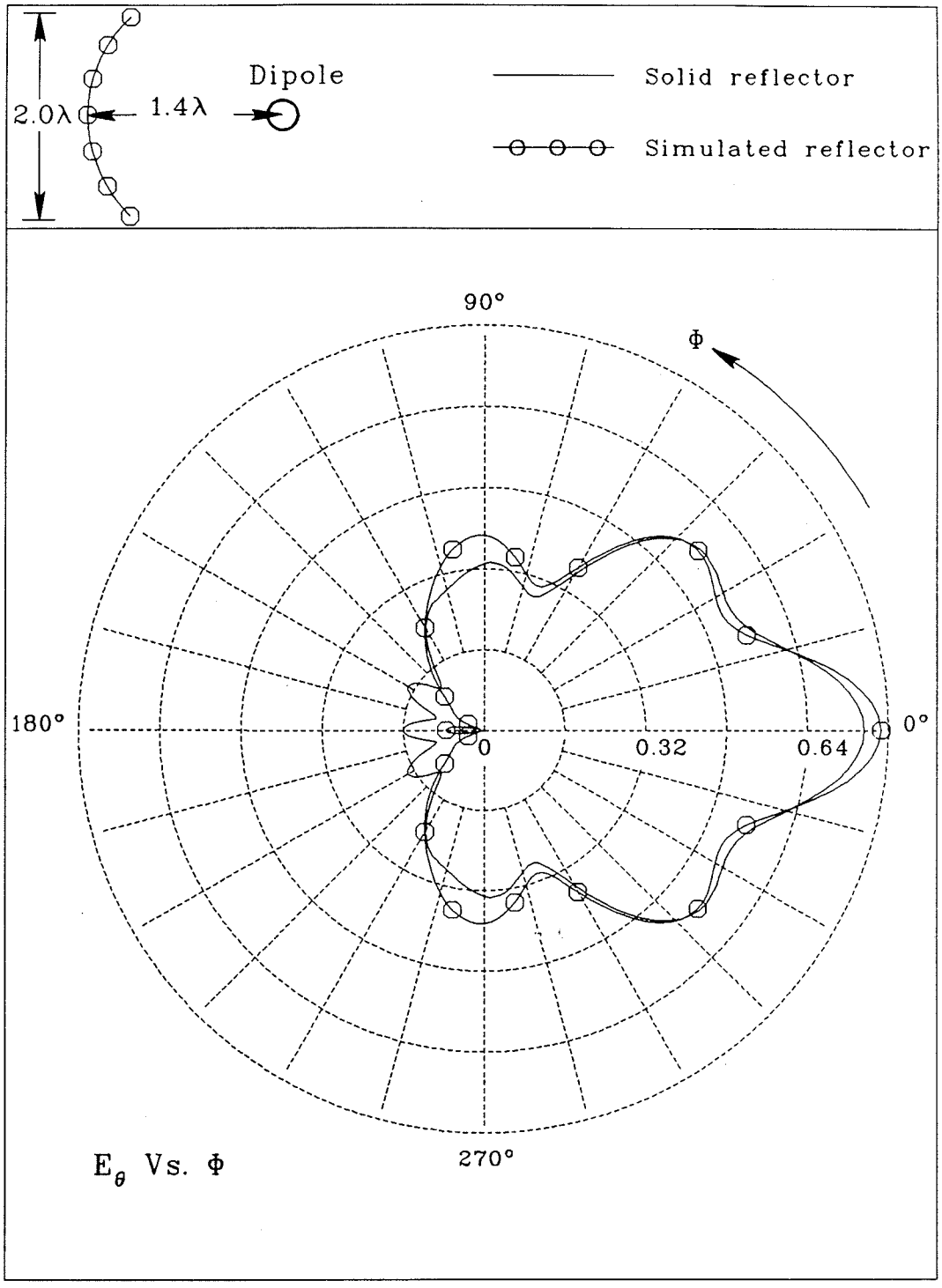

Fig. 5.7 : Far field pattern of a cylindrical circular reflector antenna.

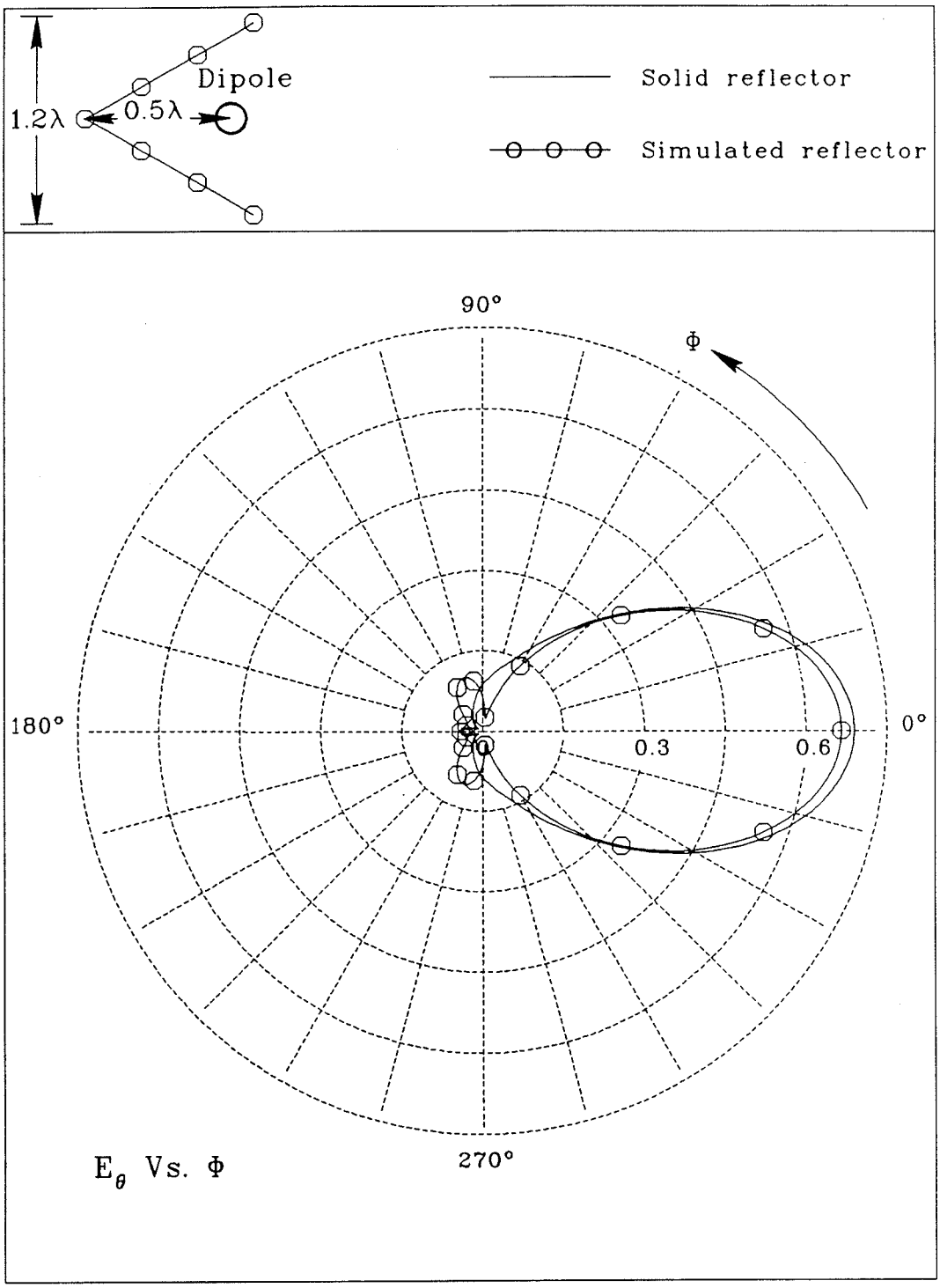

Fig. 5.8 : Far field pattern of a corner reflector antenna.

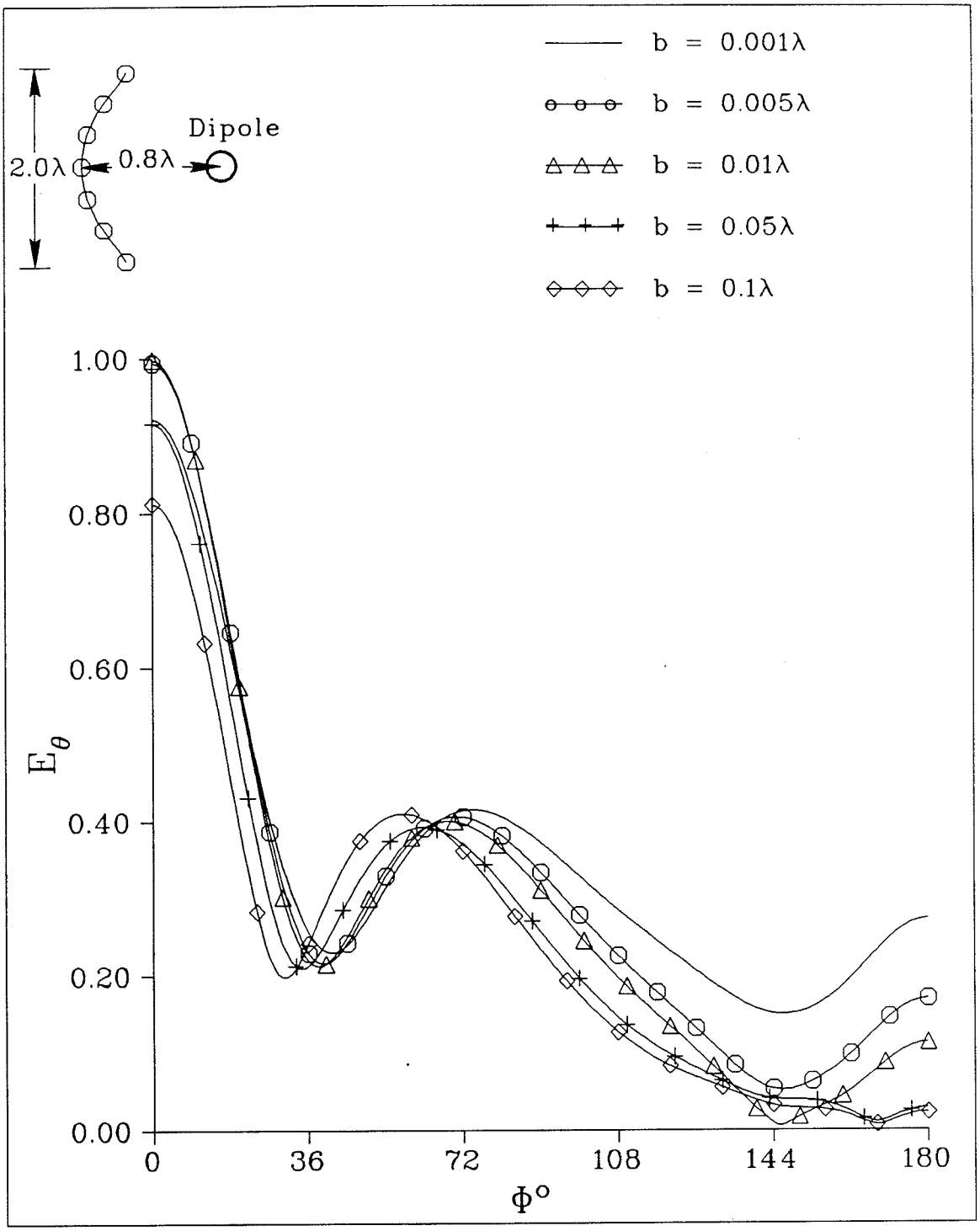

Fig. 5.9 : Far field pattern of simulated parabolic reflector antenna.

reflector trajectory. Five cases are shown in Fig. 5. 9 corresponding to the radii 0.001λ, 0.005λ, 0.01λ, 0.05λ and 0.1λ. It is found that for the first case the peak value of the far field is lower than that of the solid reflector while the back lobe is higher. In cases 2 and 3 the far field pattern is very close to that of the solid reflector. With an increase in radius as in the 4th and 5th cases the value of the peak starts to decrease again.

In order to improve the far field pattern of the simulated reflector, different radii and spacings of the simulating cylinders are used. Figure 5.10 indicates the far field patterns of a simulated parabolic cylindrical reflector antenna of 5.0λ width and 1.0λ focal length. The first pattern corresponds to a simulation by 35 cylinders of equal radius (0.03λ each) and spacing along the reflector trajectory, while the second pattern is due to simulation using 25 cylinders of unequal radii and spacings. The radius of the cylinder at the center of the reflector is 0.01λ and the radii of the other cylinders are increased by an increment of 0.004λ while the spacing is increased by 0.008λ towards the edges. As can be seen from Fig. 5. 10, improvement in the far field peak value and the first side lobe level for the second case over the first is found. Therefore, a better far field pattern can be obtained by choosing proper radii and positioning of the simulating cylinders.

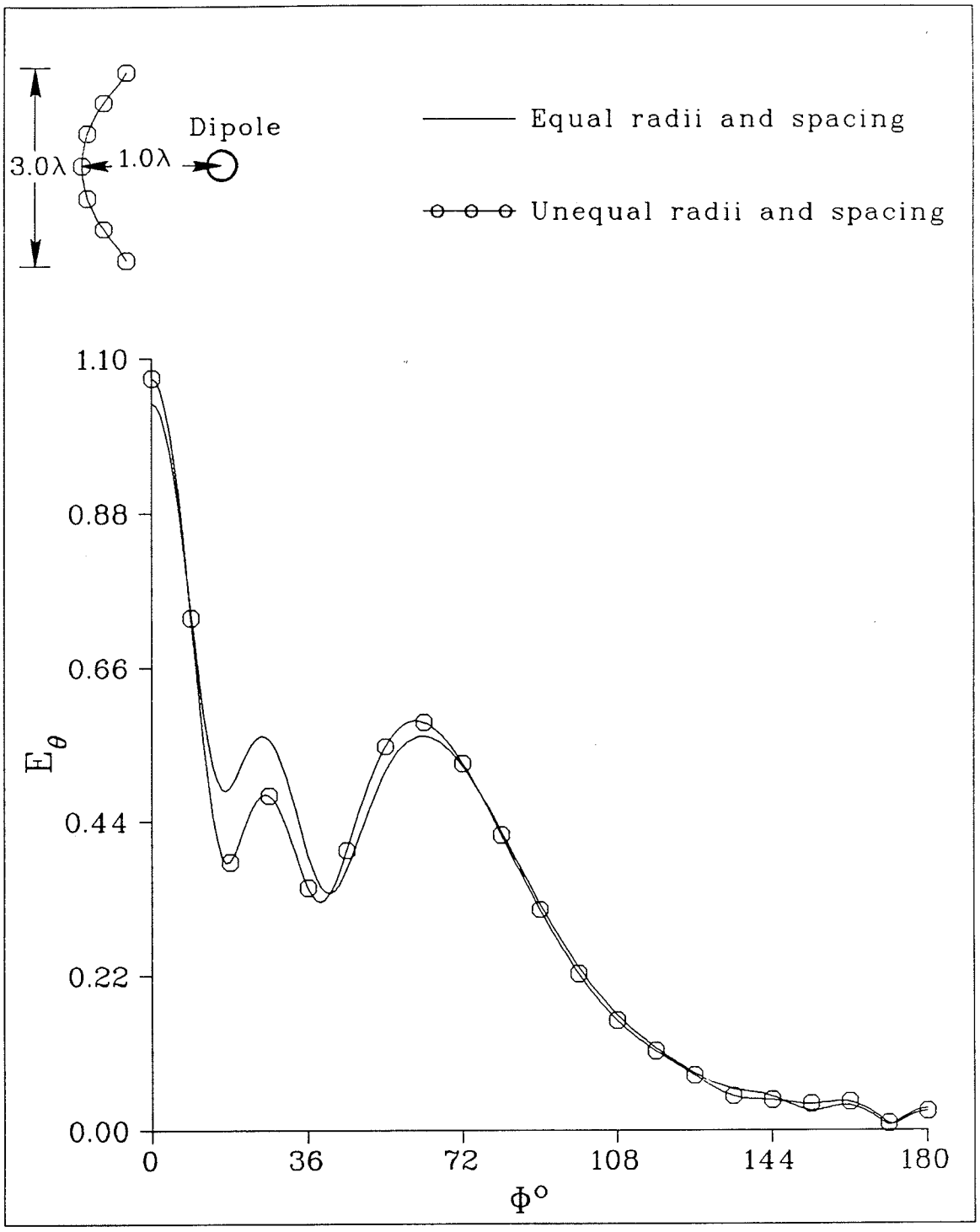

Fig. 5.10 : Far field pattern of simulated parabolic reflector antenna.

CHAPTER 6

GENERAL DISCUSSION AND CONCLUSIONS

The entire objective of simulating a reflector antenna surface is to start with a solid surface and to eliminate parts of it without significantly sacrificing the electrical properties or performance of the antenna. Removing part of the surface may be in terms of planar array of trapezoids, triangles, circles, strips or any combination thereof. Unfortunately the analysis of the scattering of an electromagnetic wave by a conducting sheet after such arbitrary shapes are removed is extremely difficult and the problem does not have an exact solution except for a single circular disc or strip. Also the scattering by a circular conducting disc or circular hole in an infinite conducting sheet involves very complicated mathematics which can not be easily extended to the many object scattering problem. Therefore the simulation of a cylindrical reflector surface was initially limited in this thesis to conducting strips as presented in Chapter 2. The strip widths are arbitrary and in one extreme may be considered as wires. Hence the idea of using circular cylinders instead of wires for simulation is an attempt to generalize previous work by Richmond and others. Whether simulation is done by strips or circular cylinders, a further limitation is introduced in this thesis whereby no material was removed near the outermost edge of the reflector, thus preserving the outer dimensions of the frame of the reflector to be simulated. For example at the outer boundaries of the simulated reflector two strips are placed as the framing elements in case of simulation by strips or two cylinders in the case of simulation by cylinders, while the remaining strips or cylinders are contained within the frame.

When an arbitrary polarized electromagnetic wave is incident on a circular cylinder or a strip it can be analyzed in terms of a component along the cylinder or strip axis and another perpendicular to it and these are usually denoted by the E-polarization and H-polarization cases, respectively. In terms of analysis, either

polarization may be handled by the same technique with appropriate boundary conditions, but it is important to chose the proper orientation of the simulated cylinders and strips relative to the incident wave polarization in order to maximize the backscattering echo width and in turn the simulation efficiency. For this we have employed the result of Mullin et al. [94] who reported that the backscattering cross section of a conducting circular or elliptic cylinder is higher for an E-polarized wave than for an H-polarized wave. Moreover the oscillatory behaviour and frequency sensitivity of the H-polarization backscattering cross section Vs. kb or kd is highly undesirable for simulation. A similar response obtained for the strip when the minor axis of the elliptic cylinder goes to zero, thus implying that E-polarized cylinders and strips are clearly more efficient for simulation of a flat plate. This becomes even more mandatory when simulating curved reflector surfaces since the H-polarization option requires the solution of scattering by bent cylinders and strips which is not available and represents an escalation in complexity of the problem. Since such a solution is also needed for simulating a three dimensional reflector, our proposed simulation technique had to be limited to two-dimensional cylindrical type reflectors.

The truncation in the axial direction of the cylinders and strips employed for simulation of cylindrical reflectors slightly affects the scattering pattern or the radiation pattern if the reflector is converted to an antenna by adding a feed element. If a dipole feed is used, as is commonly done in practice, then the dipole should be E-polarized for the same reasons mentioned earlier. The analysis of radiation and reradiation by a finite but long feed dipole in the presence of parallel cylinder and strip elements simulating the reflector is necessary and applies even when the length of these elements becomes finite to truly simulate an actual cylindrical reflector.

There are many obvious advantages of using arrays of parallel conducting cylinders or strips (which are special cases of elliptic cylinders) for simulating a cylindrical reflector surface such as reducing the weight, wind load and physical material and possibly increasing the rigidity of the reflector. Moreover the radiation

pattern of the simulated reflector antenna could be improved over that of the solid reflector due to change in the reflection mechanism. The reflection from the simulated reflector is based on single and multiple scattering and diffraction by individual cylinders or strips rather than the radiation from induced surface currents on the solid reflector surface. The improvement in the pattern appears as a reduction in the side lobe levels and an increase in the main beam level. In fact, the reduction in the back lobe level seems to be impossible at the present time but it is feasible to increase that level which is beneficial in some spacecraft applications. The design parameters mentioned in Chapter 1 were not completely included in the present study; some were left for future research such as the conductivity of the cylinders or strips and the dielectric coated conducting cylinders and strips.

The analysis given throughout this thesis led to accurate expressions for the scattered field by a collection of cylinders or strips which can be used to optimize the design of the simulated reflector antennas. In this analysis the scattering of a plane or cylindrical wave by N parallel infinitely long arbitrarily distributed planar conducting strips was presented. An expression which included the multiple scattered fields among the strips was derived by two methods based on the boundary value approach and the Karp-Russek technique, respectively. The solution of this problem applies to other electromagnetic problems such as scattering of a plane wave by strip grating or a finite number of slits in a plane screen which can be achieved using Babinet's principle. Also it can be used to obtain the scattered field of an incident electromagnetic wave on a cylindrical scatterer of arbitrary cross section using the proposed simulation technique. The major difficulty lies in evaluating the Mathieu functions of order higher than 6 which limited our solution to strip width less than 1.5λ. However since the simulation of any cylindrical surface can be done more efficiently using thin strips, this difficulty no longer applies. The asymptotic solution is restricted to the cases where the separation between any two strips is much greater than the maximum width of either. The usefulness of such a solution may be

relevant in problems requiring a very large number of strips for which the boundary value solution needs large size matrices.

Satisfactory simulation of a corner reflector antenna and circular and parabolic cylindrical reflector antennas was illustrated. It was also found that about 50% of the original surface metal in any of these types of cylindrical surfaces is sufficient for simulation using equally spaced strips of about 0.1λ width each.

The infinitely long circular conducting cylinder was used as the basic building block for simulating cylindrical scattering surfaces [85,86]. The boundary value and asymptotic solutions were applied again for solving the multiple scattering of a plane or cylindrical wave by N circular conducting parallel cylinders [87,88]. Expressions for the echo width pattern due to plane wave incidence and far field pattern due to line source excitation were derived by both methods. It was shown that the simulated reflector by equi-spaced and equally radii cylinders with a line source excitation gave the same radiation characteristics as the solid reflector antenna when suitable radii and number of cylinders were used. Moreover the simulated reflector by unequi-spaced and unequal radii cylinders may produce an improved radiation pattern over that of the solid reflector. The solution given in Chapter 3 can be applied to wire simulation (cylinders of very small radii) which was already established by other investigators. Also it can be used for solving the problem of electromagnetic scattering by a cylindrical scatterer of arbitrary cross section which does not have an exact solution. It was found that increasing the number of slits (separating strips or cylinders) is more effective for simulation as long as the slit size is kept small rather than increasing the width of the strip or the radius of cylinder.

Besides the many advantages of the simulated reflector antenna mentioned earlier the unwanted cross polarization may be reduced while there is no reason to suspect any suffering in the bandwidth. Perhaps the only disadvantage at the present time is the restriction on polarization, but this may be overcome by extending our

solution to combine the above with the solution for the case where the magnetic field is parallel to the axes of the simulating objects.

An ideal line source was used for exciting the simulated reflectors , by both strips and circular cylinders. In order to complete the design of practical reflector antennas, the long dipole antenna was selected to excite the simulated reflector. Therefore the arbitrarily fed long dipole antenna was considered. An extension of Hurd's formulation for the input admittance of a center fed long dipole to the general case of a long arbitrarily fed dipole was presented. Satisfactory expressions for the radiation pattern, current distribution and input admittance were derived by using the Wiener-Hopf technique. Moreover, the symmetrically and antisymmetrically fed dipoles were examined. It was found that the long dipole antenna can be fed at different points for producing a narrow broadside beam [89,90]. The results indicated good agreement with Harrington's numerical results for the arbitrarily fed dipole. For a multiply-fed dipole, a comparison with Strait and Hirasawa [82] indicated that our expression for the radiation pattern was highly accurate, even if it only corresponds to the first order expression for the current distribution.

The long dipole antenna was employed to excite N parallel infinitely long conducting cylinders [91]. An expression for the far electric field including the multiple scattering terms of the radiated and scattered fields from the long dipole and cylinders using a combined self consistent-iterative method was derived. The multiply scattered field among the cylinders was calculated using the boundary value solution described in Chapters 2 and 3 while that between the dipole and each cylinder was calculated iteratively. Even for the simple case of one cylinder in the dipole vicinity the contribution from the present work [92,93] lies in calculating the multiple interaction which was neglected by former investigators [60-65]. It is worthwhile to emphasize that two extensions are made in Chapter 5, the first for dealing with N cylinders instead of one, while the second for including the interaction effects between the dipole and each cylinder. Again the far field patterns of different

configurations of simulated reflectors fed by a long dipole were presented and compared with the corresponding solid reflectors. In spite of the finite length of the solid reflectors used in the numerical evaluations, the resulting patterns are in good agreement with those of the simulated reflectors which shows that the solution of the infinitely long simulated reflector is also applicable to the finite simulated reflectors without appreciable error.

6.1 *Recommendations for future research*

It is found throughout the present study that new problems should be investigated because of their importance in simulation. As an example, extending the solution for the scattering of a plane wave by two dielectric coated conducting cylinders [24] to the multiple scattering of plane or cylindrical waves by N dielectric coated conducting cylinders is important. Also an extension to multiple scattering of a plane or cylindrical wave by two strips with touching edges needs to be examined due to its usefulness in problems involving corners.

The long dipole antenna in the presence of N strips is also one of the useful problems which can be investigated. The only difficulty at the present time is that the strip geometry coincides with elliptical cylindrical coordinates while the dipole geometry coincides with the circular cylindrical coordinates and this makes the transformation of the field from the dipole coordinates to the strip coordinates very difficult. However once this difficulty is overcome the solution of the problem will follow the same steps mentioned in Chapter 5.

The Karp-Russek technique on which we based our asymptotic solution can also be extended to deal with the long dipole in the presence of N circular cylinders or conducting strips.

The simulation of cylindrical scattering surfaces could be performed using bent cylinders or strips. In this case the cylinders or strips would follow the reflector

curvature and would be arranged parallel to each other along the reflector trajectory. The polarization of the incident wave on the bent cylinders or strips would no longer be along their axes but would be perpendicular to them. This problem may be helpful in studying various polarizations of simulated reflector antennas. Also it could be extended in order to use bent dipoles for simulating a reflector surface which would lead to a mixture of reflecting and radiating reflector at the same time.

Another problem of practical interest would to use a sectoral horn instead of the long dipole to excite the simulated reflector. This problem needs knowledge of the plane wave spectrum in order to analyze the sectoral horn field in terms of a spectrum of plane waves, then by using the boundary value or the asymptotic solutions described in Chapter 2, one could obtain the scattered field from the simulated reflector.

REFERENCES

[1] R. I. Primich,"Some Electromagnetic Transmission and Reflection Properties of a Strip Grating", IRE Trans. on Antennas and Prop. AP-5, pp. 176-182, 1957.

[2] J. H. Richmond,"A Wire-Grid Model for Scattering by Conducting Bodies", IEEE Trans. on Antennas and Prop., Vol. AP-14, pp. 782-786, 1966.

[3] G. A. Otteni,"Plane Wave Reflection From a Rectangular-Mesh Ground Screen", IEEE Trans. on Antennas and Prop., AP-21, pp. 843-851, 1973.

[4] D. A. Hill and J. R. Wait,"Electromagnetic Scattering of an Arbitrary Plane Wave by a Wire With Bonded Junctions", Can. J. of Phys., Vol. 54, pp. 353-361, 1976.

[5] T. Larsen," A Survey of the Theory of Wire Grids", IRE Trans on Microwave Theory and Tech. MTT-10, 191-201 1962.

[6] J. H. Richmond," Scattering by an Arbitrary Array of Parallel Wires", IEEE Trans. on Microwave Theory and Tech. MTT-13, pp. 408-412, 1965.

[7] V. Twersky,"On Multiple Scattering of Waves", J. Research Natl. Bur. Stds., Vol. 64D, pp. 715-739, 1960.

[8] L. Rayleigh,"On the Dynamical Theory of Gratings", Proc. Roy. Soc. (London), Vol. [A]79, pp. 399-416, 1907.

[9] S. Karp,"Diffraction by a Combination of Cylinders", Proc. McGill Symposium, on Microwave optics, McGill University, Montereal, Canada, pp. 146-201, 1953.

[10] N. Okamoto,"Electromagnetic Scattering by Many Gyrotropic Cylinders of Different Kinds', IEEE Trans. on Antennas and Prop., Vol. AP-22, pp. 701-706, 1974.

[11] J. W. Young and J. C. Bertrand,"Multiple Scattering by two Cylinders", J. Acoust. Soc. Am., Vol. 58, pp. 1190-1195, 1975.

[12] R. Millar,"The Scattering of a Plane Wave by a Row of Small Cylinders", Can J. Phys., Vol. 38, pp. 272-289, 1960.

[13] N. Zitron and S. Karp,"Higher-Order Approximation in Multiple Scattering. I. Two-Dimensional scalar case", J. Math. Phys., Vol. 2, pp. 394-402, 1961.

[14] N. Zitron and S. Karp,"Higher-Order Approximation in Multiple Scattering. II. Three-Dimensional scalar case", J. Math. Phys., Vol. 2, pp. 402-406, 1961.

[15] S. N. Karp and A. Russek,"Diffraction by a Wide Slit", J. Appl. Phys., Vol. 27, pp. 886-894, 1956.

[16] A. Elsherbeni and M. Hamid,"Diffraction by a Wide Double Wedge", IEEE Trans. on Antennas and Prop., Vol. AP-32, 1262-1264, 1984.

[17] E. B. Hansen,"The Diffraction of a Plane Wave Through Two or More Slits in a Plane Screen", Appl. Sci. Research B8, pp. 73-83 1959.

[18] K. Saermark," Scattering of a Plane Monochromatic Wave by a System of Strips", Appl. Sci. Research B7, 417-440 1959.

[19] K. Saermark," Transmission Coefficient For a System of Parallel Slits in a Thin Plane Screen", Appl. Sci. Research B8, 29-34 1959.

[20] V. Twersky,"Multiple Scattering of Radiation by an Arbitrary Configuration of Parallel Cylinders", J. Acous. Soc. Am., Vol. 24, pp. 42-46, 1952.

[21] V. Twersky,"Multiple Scattering of Radiation by an Arbitrary Planar Configuration of Parallel Cylinders", J. Acous. Soc. Am., Vol. 23, pp. 407-414, 1952.

[22] V. K. Germey,"Die Beugung einer Ebenen Elektromagnetischen welle an Zwei Parallelen Unendlich Langen Idealleitenden Zylindern von Elliptischem Querschnill", Ann. Phys., Vol. 13, pp. 237-251, 1964.

[23] N. Okamoto, Y. Yoshimara, Y. Nakanishi and N. Kumagai,"Scattering of Plane Electromagnetic Wave by Two Parallel Infinitely Long Ferrimagnetic Cylinders", J. Inst. Elec. Commun. Eng. Japan, Vol. 49, pp. 2431-2438, 1966.

[24] H. A. Ragheb and M. Hamid,"Scattering by Two Parallel Multi-layered Dielectric Cylinders", International Journal of Electronics, vol. 61, pp. 323-342, 1986.

[25] A. El-Sherbeni, H. A. Ragheb and M. Hamid,"Rigorous Solution of The Scattering by Two Multi-layered Dielectric Cylinders", Proc. of URSI/IEEE AP-Meeting, Philadelphia, U.S.A., 1986.

[26] H. A. Ragheb and M. Hamid,"Scattering by Two Conducting Strips with Parallel Edges", Submitted for Publication in the Can. J. of Phys.

[27] H. A. Ragheb and M. Hamid,"Multiple Scattering by Two Conducting Strips", Proc. of URSI/IEEE AP-Meeting, Blacksburg, Virginia, U.S.A., June 15-19, 1987.

[28] K. K. Mei,"Unimoment Method Of Solving Antenna and Scattering Problems", IEEE Trans. on Antennas and Prop., Vol. Ap-22. PP. 760-766, 1974.

[29] S. Chang and K. K. Mei,"Application of the Unimoment Method to Electromagnetic Scattering of Dielectric Cylinders", IEEE Trans. on Antennas and Prop., Vol. AP-24, pp. 35-42, 1976.

[30] J. H. Richmond,"Scattering by A Dielectric Cylinder of Arbitrary Cross Section Shape', IEEE Tans. on Antennas and Prop., Vol. AP-13, pp. 334-341, 1965.

[31] J. H. Richmond,"TE-Wave Scattering by A Dielectric Cylinder of Arbitrary Cross Section Shape', IEEE Tans. on Antennas and Prop., Vol. AP-14, pp. 460-464, 1966.

[32] R. F. Harrington,"Field Computation by Moment Methods", New York; Mac-Millan, 1968.

[33] M. G. Andreasen,"Scattering from Parallel Metallic Cylinders with Arbitrary Cross-Sections", IEEE Trans. on Antennas and Prop., Vol. AP-12, pp. 746-754, 1964.

[34] J. A. Kinzel,"Large Reflector Antenna Pattern Computation Using Moment Methods", IEEE Trans. on Antennas and Prop., Vol. AP-22, pp. 116-118, 1974.

[35] B. Azarbar and L. Shafai,"Application of Moment Method to Large Cylindrical Reflector Antennas", IEEE Trans. on Antennas and Prop., Vol. AP-26, pp. 500-502, 1978.

[36] L. Shafai," Currents Induced on a Conducting Strip", Canadian J. of Phys., Vol. 49, pp. 495-498, 1971.

[37] L. Shafai and Y. S. El-Moazzen,"Radiation Patterns of an Antenna Near a Conducting Strip", IEEE Trans. Antennas and Prop., Vol. AP-20, pp. 642-644, 1972.

[38] D. R. Wilton and S. Govind," Incorparation of Edge Condition in Moment Method Solutions", IEEE Trans. on Antennas and Prop., Vol. AP-25, pp. 845-850, 1977.

[39] L. L. Tsai, D. R. Wilton, M. G. Harrion and E. H. Wright," A Comparison of Geometrical Theory of Diffraction and Integral Equation Formulation for Analysis of Reflector Antennas", IEEE Trans. on Antennas and Prop., Vol. AP-20, pp. 705-712, 1972.

[40] J. H. Richmond," On the Edge Mode in The Theory of TM Scattering by a Strip or Strip Grating", IEEE Trans. on Antennas and Prop., Vol. AP-28, pp. 883-887, 1980.

[41] D. L. Knepp and J. Goldhirsh,"Numerical analysis of electromagnetic Radiation Properties of Smooth Conducting Bodies of Arbitaray Shape", IEEE Trans. on Antennas and Prop., Vol. AP-20, pp. 383-388, 1972.

[42] N. C. Albertsen, J. E. Hansen and N. E. Jensen,"Computation of Radiation from Wire Antennas on Conducting Bodies", IEEE Trans. on Antennas and Prop., Vol. AP-22, pp. 200-206, 1974.

[43] A. Sankar and T. C. Tong," Current Compution on Complex Structures by Finite Element Method", Electronics Letters, Vol. 11, pp. 481-482, 1975.

[44] E. Hallen,"Properties of a long Antenna", J. Appl. Phys., Vol. 19, pp. 1140-1147, 1948.

[45] E. Hallen,"Exact Treatment of Antenna Current Wave Reflection at the End of a Tube-Shaped Cylindrical Antenna", IRE Trans. on Antennas and Prop., Vol. AP-4, pp.479-491, 1956.

[46] R. King,"Asymmetrically Driven Antennas and the Sleeve Dipole", Proc. IRE, Vol. 38, pp. 1154-1164, 1950.

[47] E Hallen,"Exact Solution of the Antenna Equation", Pure and Appl. Math. and Phys., Vol. 20, pp. 1-22, 1961.

[48] T. T. Wu,"Theory of the Dipole Antenna and the Two-Wire Transmission Line", J. Math. Phys., Vol. 2, pp. 550-574, 1961.

[49] Y. M. Chen and J. B. Keller," Current on and Input Impedance of a cylindrical Antenna", J. Res. Nat. Bur. Stds., Vol. 66D, pp. 15-21, 1962.

[50] R. King and T. T. Wu,"The cylindrical Antenna With Arbitrary Driving Point", IEEE Trans. on Antennas and Prop., Vol. AP-13, pp. 710-718, 1965.

[51] L. C. Shen,"Current Distribution on a Long Dipole Antenna", IEEE Trans. on Antennas and Prop., Vol. AP-16, pp. 353-354, 1968.

[52] L. C. Shen, T. T. Wu and R. King," A Simple Formula of Current in Dipole Antennas", IEEE Trans. on Antennas and Prop., Vol. AP-16, pp. 542-547, 1968.

[53] R. H. Duncan,"Theory of Infinite Cylindrical Antenna Including the Feed Point Singularity in Antenna Current," J. Res. Natl. Bur. Stds., Vol. 66D, pp. 181-188, 1962.

[54] K. S. Kunz,"Asymptotic Behavior of the Current on an Infinite Cylindrical Antenna", J. Res. Natl. Bur. Stds., Vol. 67D, pp. 417-431, 1963.

[55] R. L. Fante,"On the Admittance of the Infinite Cylindrical Antenna", Radio Sci., 1(new series), Vol. 9, pp. 1041-1044, 1966.

[56] E. K. Miller," Admittance Dependence of the Infinite Cylindrical Antenna Upon Exciting Gap Thickness", Radio Sci., 2(new series), Vol. 12, pp. 1431-1435, 1967.

[57] R. A. Hurd,"Variational Solution for the Admittance of a Long Cylindrical Antenna", J. Res. Natl. Bur. Stds., Vol. 68D, pp. 311-316, 1964.

[58] R. A. Hurd,"Admittance of a Long Linear Antenna", Can. J. of Phys., Vol. 44, pp. 1723-1743, 1966.

[59] J. R. Wait,"Electromagnetic Radiation from Cylindrical Structures", New York : Pergamon Press, 1959.

[60] P. S. Carter,"Antenna Arrays Around Cylinders", Proc. IRE, Vol. 31, pp. 671-693, 1943.

[61] W. S. Luck,"Electric Dipole in the Presence of Elliptic and Circular Cylinders", J. Appl. Phys., Vol. 22, pp. 14-19, 1951.

[62] H. H. Kuehl,"Radiation from a Radial Electric Dipole near a Long Finite Circular Cylinder", IRE Trans. on Antennas and Prop., Vol. AP-9, pp. 346-353,1961.

[63] J. Goldhirsh, D. L. Knepp and R. J. Doviak,"Radiation from a Dipole Near a Conducting Cylinder of Finite Length", IEEE Trans. on Electromagnetic Compat., Vol. EMC-12, pp. 96-105, 1970.

[64] Z. Mao and D. K. Cheng,"Scattering and Pattern Perturbation by a Conducting Tubular Cylinder of Finite Length", IEEE Trans. on Electromagnetic Compat., Vol. EMC-25, pp. 441-447, 1983.

[65] G. N. Tsandoulas,"Scattering of a Dipole Field by Finitely Conducting and Dielectric Circular Cylinders", IEEE Trans. on Antennas and Prop., Vol. AP-16, pp. 324-328, 1968.

[66] P. M. Morse and P. J. Rubenstein," The Diffraction of Waves by Ribbons and by Slits", Phys. Rev. 54, pp. 895-898, 1938.

[67] E. B. Moullin and F. M. Phillips," On the Current Induced in a Conducting Ribbon by the Incidence of a Plane Electromagnetic Wave", Proc. IEE 99, pp. 137-150, 1952.

[68] J. M. Myers," Wave Scattering and the Geometry of a Strip", J. Math. Phys. 6, pp. 1839-1846, 1965.

[69] R. F. Millar," Diffraction by a Wide Slit and Complementary Strip. I.", Proc. Camb. Phil. Soc. 54, pp. 479-496, 1958.

[70] R. F. Millar," Diffraction by a Wide Slit and Complementary Strip. II.", Proc. Camb. Phil. Soc. 54, pp. 497-511, 1958.

[71] J. A. Stratton,"Electromagnetic Theory", McGraw-Hill Book, 1941.

[72] K. Saermark," A Note on Addition Theorems for Mathieu Functions", Z. Math. Phys. 10, pp. 426-428, 1959.

[73] F. W. Schafke," Das Additionstheorem der Mathieuschen Funktionen", Math. Z. 58, pp. 436-447, 1953.

[74] J. Meixner," Reihenentwicklungen von Produkten zeweier Mathieuschen Funktionen nach Produkten von Zylinder- and Exponentialfunktionen", Math Nachr. 3, pp. 14-19, 1949.

[75] J. Meixner and F. W. Schafke, " Mathieusche Funktionen und Spharoid-Funktionen " , 1 st ed. (Springer Verlag, Berlin 1954), p. 171-187.

[76] M. Toyama and K. Shogen,' Computation of the Value of the Even and Odd Mathieu Functions of Order N for Given Parameter S and an Argument X', IEEE Trans. on Antennas and Prop., Vol. AP-32, pp. 537-539, 1984.

[77] J. J. Bowman, T. B. A. Senior and P. L. E. Uslenghi,"Electromagnetic and Acoustic Scattering by Simple Shapes", North-Holland Publishing Company - Amsterdam, 1969.

[78] Chin-Lin Chen and R. W. P. King," Theoretical and Experimental Studies on the Long Dipole Antenna", IEEE Trans. on Antennas and Prop., Vol. AP-16, pp. 664-673, 1968.

[79] R. F. Harrington and J. R. Mautz,"Straight Wires with Arbitrary Excitation and Loading", IEEE Trans. on Antennas and Prop., Vol. AP-15, pp. 502-515, 1967.

[80] C. J. Bouwkamp,"A Note on Singularities Occuring at Sharp Edge in Electromagnetic Diffraction Theory", Physica, Vol. 12, pp. 467-474, 1946.

[81] S. Saoudy and M. Hamid,"Optimum Multiple Feed of a Dipole Antenna", Proc. of URSI/IEEE-AP Meeting, Vancouver, Canada, P. 60, 1985.

[82] K. H. Strait and K. Hirasawa,"On Long Wire Antennas with Multiple Excitation and Loading", IEEE Trans. on Antennas and Prop., Vol. AP-18, pp. 699-700, 1970.

[83] L. C. Shen,"A Simple Theory of Receiving and Scattering Antennas", IEEE Trans. on Antennas and Prop., Vol. AP-18, pp. 112-114, 1970.

[84] G. J. Burke and A. J. Poggio," Numerical Electromagnetic Code (NEC)- Method of Moments", Parts I and II, Technical Document 116, Naval Ocean System Center, San Diego, California, Revised January 1980.

[85] H. A. Ragheb and M. Hamid,"Simulation of a Cylindrical Reflector by Conducting Circular Cylinders", IEEE Trans. on Antennas and Prop., Vol. AP-35, pp. ,1987.

[86] H. A. Ragheb and M. Hamid,"Radiation Characteristics of N Circular Conducting Cylinders Simulating Cylindrical Reflectors", Proc. of URSI/IEEE-AP Meeting, Vancouver, Canada, P. 243, 1985.

[87] H. A. Ragheb and M. Hamid,"Scattering by N parallel Conducting Circular Cylinders", International J. of Electronics, Vol. 59, pp. 407-421, 1985.

[88] H. A. Ragheb and M. Hamid,"Backscattering Cross-Section of N parallel Conducting Circular Cylinders", Proc. of URSI/IEEE-AP Meeting, Vancouver, Canada, P. 279, 1985.

[89] H. A. Ragheb and M. Hamid," Rigorous Solution of Multiply-fed Dipole Antenna", Can J. of Phys, Vol. 64 , pp. 303-310, 1986.

[90] H. A. Ragheb and M. Hamid,"Radiation Characteristics of Multiply-fed Dipole Antenna", Proc. National Radio Science Meeting, U. of Colorado, Boulder, Colorado,U.S.A, P. 228, 1986.

[91] H. A. Ragheb and M. Hamid,"Radiation from a Long Dipole Antenna in the Presence of Cylindrical Scatterers", International MONTECH'86 IEEE Meeting, Montreal, Canada, 1986.

[92] H. A. Ragheb and M. Hamid,"Multiple interaction between radiating dipole and parallel conducting cylinder", Accepted for Publication in the Can. J. of Phys.

[93] H. A. Ragheb and M. Hamid,"Radiation From a Long Dipole Antenna in the Presence of Infinitely Long Circular Cylinder", Symposium on Antenna Technology and Applied Electromagnetics, University of Manitoba, Winnipeg, Canada, Aug. 13-14, 1986.

[94] C. R. Mullin, R. Sandburg and C. O. Vellinem,"A Numerical Technique for the Determination of Scattering Cross Section of Infinite Cylinders of Arbitrary Geometrical Cross Section", IEE Trans. on Antennas and Prop., Vol. AP-13, pp. 141-149, 1965.

APPENDIX A

EVALUATION OF THE INTEGRAL $R_o(h)$

The integral is given by

$$R_o(h) = \frac{1}{2\pi j} \int_{C_+} e^{-jht}\, k(t)\, dt \tag{A.1}$$

where

$$k(t) = \frac{2\pi}{\beta^2 J_o(\beta a)\, H_o^{(2)}(\beta a)} \tag{A.2}$$

$$\beta^2 = k^2 - t^2 \tag{A.3}$$

The solution of a similar integral has been reported by Shen et al. [52] which we will follow.

The contour C_+ is deformed to C as shown in Fig. 4.3, so that it is wrapped around the right branch point. Suppose that kh is not too small so that the contribution to the integral comes from near $t = k$. In this case we can write $R_o(h)$ as

$$R_o(h) = \int_{-j\infty + k}^{k} \frac{\pi e^{-jht}\, dt}{j\pi\, \beta^2 J_o(\beta a)\, H_o^{(2)}(\beta a)} + \int_{k}^{-j\infty + k} \frac{\pi e^{-jht}\, dt}{j\pi\, \beta^2 J_o(\beta a\, e^{-j\pi})\, H_o^{(2)}(\beta a\, e^{-j\pi})} \tag{A.4}$$

Since a is small, one can replace the Bessel and Hankel functions by their small argument approximations. This results in

$$R_o(h) = \int_{k}^{-j\infty+k} \frac{-\pi\, e^{-jht}}{\beta^2} \left\{ \frac{1}{j\pi + 2\ln(\frac{\beta a}{2}) + 2\gamma} + \frac{1}{j\pi - 2\ln(\frac{\beta a}{2}) - 2\gamma} \right\} dt \qquad \text{(A.5)}$$

The change of variable $t = \zeta + k$ is next introduced

$$R_o(h) = \pi\, e^{-jkh} \int_{0}^{-j\infty} \frac{e^{-j\zeta h}}{\beta^2} \left\{ \frac{1}{2C_w - 2\ln(\frac{\beta}{2k}) - j\,\pi} - \frac{1}{2C_w - 2\ln(\frac{\beta}{2k}) + j\,\pi} \right\} d\zeta \qquad \text{(A.6)}$$

where

$$C_w = -\ln(ka) - \gamma \qquad \text{(A.7)}$$

Now substituting $\zeta = -j2k\eta$, obtaining

$$R_o(h) = \frac{\pi\, e^{-jkh}}{2jk} \int_{0}^{\infty} \frac{e^{-2k\eta h}}{\eta(\eta + j)} \left\{ \frac{1}{2C_w - \log\eta(\eta + j) - j\,\pi} - \frac{1}{2C_w - \ln\eta(\eta + j) + j\,\pi} \right\} d\zeta \qquad \text{(A.8)}$$

When h is not too small, it will be a reasonably good approximation to replace $ln(\eta + j)$ in the integrand by $\ln j$. Thus

$$R_o(h) \approx \frac{\pi\, e^{-jkh}}{2k} \int_0^{\infty} \frac{e^{-2k\eta h}}{\eta} \left\{ \frac{1}{2C_w - \log \eta - j\,\pi} - \frac{1}{2C_w - \ln \eta + j\,\pi} \right\} d\zeta \qquad \text{(A.9)}$$

Due to the exponential factor, the limit of the integration can be cut off at some number D'. Substituting the value of $e^{-\gamma}$ for D' which has been evaluated by Shen,

$$R_o(h) \approx \frac{\pi\, e^{-jkh}}{2k} \int_0^{D'/2kh} \frac{1}{\eta} \left\{ \frac{1}{2C_w - \ln \eta - j\,\pi} - \frac{1}{2C_w - \ln \eta + j\,\pi} \right\} d\zeta \qquad \text{(A.10)}$$

The integral of (A.10) can be evaluated,

$$R_o(h) = \frac{\pi e^{-jkh}}{2k} \ln\left[1 - \frac{2\pi j}{2C_w + ln(2kh) + \gamma + j\frac{\pi}{2}} \right] \qquad \text{(A.11)}$$

The result (A.11) is good for large kh. In order to obtain a formula for $R_o(h)$ which is good even for small kh, the term $\ln 2kh$ in (A.11) is changed to $\ln(kh + \sqrt{(kh)^2 + D})$. The constant D is determined by calculating the real part of the quantity $\frac{2kj}{\eta_o \pi} R_o(h)$ at $kh = 0$. This quantity is equivalent to the input admittance of the infinitely long antenna. The real part of $\frac{2kj}{\eta_o \pi} R_o(h)$ at $kh = 0$ is equated to the value of the conductance given by (2.72) to produce the value of D as $e^{-2\gamma}$. Thus for small kh, $R_o(h)$ can be expressed as

$$R_o(h) = \frac{\pi e^{-jkh}}{2k} \ln\left[1 - \frac{2\pi j}{2C_w + ln(kh + \sqrt{(kh)^2 + e^{-2\gamma}}) + \gamma + j\frac{\pi}{2}} \right] \qquad \text{(A.12)}$$

APPENDIX B

EVALUATION OF THE CONSTANTS C_m

Since the constants C_m are necessary in our solution, we present the procedure of evaluating them which has been given by Hurd [58]

Because $k(\zeta)$ is regular in the strip $|Im(\zeta)| < q$, we can write

$$\ln k(\zeta) = \ln k_-(\zeta) - \ln k_+(\zeta) = \frac{1}{2\pi j} \int_{c_- + c_+} \frac{\ln k(t)\, dt}{t - \zeta} \tag{B.1}$$

where the contours are those of Fig. 4.3. The first integral is regular in the lower half of the ζ plane, while the second is regular in the upper half. Thus

$$k_-(\zeta) = \exp\left[\frac{1}{2\pi j} \int_{c_-} \frac{\ln k(t)\, dt}{t - \zeta}\right] \tag{B.2}$$

$$k_+(\zeta) = \exp\left[\frac{-1}{2\pi j} \int_{c_+} \frac{\ln k(t)\, dt}{t - \zeta}\right] \tag{B.3}$$

The relation $k_-(\zeta)k_+(-\zeta) = 1$ is verified from (B.2) and (B.3) by making the changes of variable from t to $-t$ and from ζ to $-\zeta$ in the second integral.

Referring to (4.60), we see that the factor $k_-(\zeta)$ appears in the calculation only through the quantities C_m. These are easily found to be

$$C_o = \frac{1}{k_-(k)} \tag{B.4}$$

$$C_1 = \frac{-k_-'(k)}{[k_-(k)]^2} \tag{B.5}$$

$$C_2 = \frac{[k_-'(k)]^2}{[k_-(k)]^3} - \frac{k_-''(k)}{2[k_-(k)]^2} \tag{B.6}$$

Let us put

$$T_n = \frac{1}{2\pi j}\int_{c_-} \frac{\ln k(t)\, dt}{(t-k)^n} \tag{B.7}$$

then a short calculation shows that

$$C_o = exp(-T_1) \tag{B.8}$$

$$C_1 = -C_o\, T_2 \tag{B.9}$$

$$C_2 = C_o\left(\frac{T_2^2}{2} - T_2\right) \tag{B.10}$$

so that it is sufficient to calculate the integrals T_n. First it is easy to show that

$$T_n = -\frac{1}{2\pi j}\int_0^\infty \ln k(t)\left[\frac{1}{(t-k)^n} + \frac{(-1)^n}{(t+k)^n}\right] dt. \tag{B.11}$$

Then moving the integration contour to the positive imaginary axis and changing variables, we find that

$$T_n = \frac{(-1)^{n+1}}{2\pi k^{n-1}}\int_0^\infty [(1+jv)^n + (1-jv)^n]\frac{\ln k(jkv)}{(1+v^2)^n}\, dv \tag{B.12}$$

An examination of T_n shows that $k(t)$ can be replaced by its small-argument approximation with maximum error of $O(a)$. Thus

$$T_n = \frac{(-1)^{n+1}}{2\pi k^{n-1}}\int_0^\infty \frac{[(1+jv)^n + (1-jv)^n]}{(1+v^2)^n}\left\{\ln\frac{2j\pi^2}{k^2}\right.$$

$$\left. - \ln(1+v^2) - \ln\ln[\frac{1}{4}e^{j\pi}\Gamma^2 k^2 a^2(1+v^2)]\right\} dv \tag{B.13}$$

Setting $A = \frac{1}{4} e^{j\pi} \Gamma^2 k^2 a^2$, which is a small quantity, we note that $|\ln A|$ becomes large. Over the initial part of the integration range $|\ln A| >> \ln(1 + v^2)$, while on the rest of the integration range the integral value is $O(a)$ at most; hence it is permitted to use the following approximation

$$\ln \ln A(1 + v^2) = \ln \ln A + \sum_1^\infty \frac{(-1)^{n+1}}{n} \left[\frac{\ln(1 + v^2)}{\ln A} \right]^n \tag{B.14}$$

which indicates that (B.12) can be reduced to integrations of the form

$$\Phi(p,q) = \int_0^\infty \frac{\ln^p(1 + v^2)\, dv}{(1 + v^2)^q} \tag{B.15}$$

To compute the $\Phi(p,q)$, we notice that

$$\Phi(p,q) = \frac{-\partial \Phi(p - 1,q)}{\partial q} \tag{B.16}$$

and

$$\Phi(0,q) = \frac{\Gamma(\frac{1}{2})\Gamma(q - \frac{1}{2})}{2\Gamma(q)} \tag{B.17}$$

Thus $\Phi(p,q)$ of all integral orders can be evaluated. Derivatives of the gamma function are expressible in terms of the polygamma function, which, for the arguments used here, are in turn expressible as combinations of elementary functions. Omitting the details, we find that

$$C_o = k \left(\frac{2 \ln A}{j\pi^2}\right)^{\frac{1}{2}} \{ 1 + \frac{\ln 2}{\ln A} - \frac{1}{2 \ln^2 A} (\ln^2 2 + \frac{1}{6}\pi^2) + \frac{1}{2 \ln^3 A} (\ln^3 2 + \frac{1}{2}\pi^2 \ln 2 + 4 S_3)\} \tag{B.18}$$

$$T_2 = -\frac{1}{2k}\left\{1 + \frac{1}{\ln A} - \frac{1+2\,ln2}{\ln^2 A} + \frac{2 + \frac{\pi^2}{3} + 4\ln2 + 4\ln^2 2}{\ln^3 A}\right\} \tag{B.19}$$

$$T_3 = \frac{1}{8k^2}\left\{1 + \frac{1}{lnA} + \frac{\frac{1}{2} - 2\,ln2}{\ln^2 A} - \frac{\frac{5}{2} - \frac{\pi^2}{3} + 2\ln2 - 4\ln^3 2}{\ln^3 A}\right\} \tag{B.20}$$

where

$$S_3 = \sum_1^\infty \frac{1}{n^3} = 1.202\cdots \tag{B.21}$$

APPENDIX C

EXACT SOLUTION OF THE INTEGRAL $G(\beta,\alpha)$

The integral is given by

$$G(\beta,\alpha) = \int_0^{\beta} \frac{e^{-j\alpha x}}{\sqrt{x^2 + e^{-2\gamma}}}\, dx \tag{C.1}$$

Let $x = \frac{j\sin\theta}{\Gamma}$, where $\Gamma = e^{\gamma}$, thus

$$dx = \frac{j\cos\theta}{\Gamma}\, d\theta \tag{C.2}$$

The upper limit of the integral is changed to $-j\ \sinh^{-1}(\beta\Gamma)$ instead of β according to the new variable. Then, substituting for x and dx in (C.1), we obtain

$$G(\beta,\alpha) = \int_0^{-j\ \sinh^{-1}(\beta\Gamma)} e^{j\frac{\alpha}{j\Gamma}\sin\theta}\, d\theta \tag{C.3}$$

The exponential factor in the integrand can be expressed in terms of an infinite series of Bessel and exponential functions as follows

$$G(\beta,\alpha) = \int_0^{-j\ \sinh^{-1}(\beta\Gamma)} \sum_{n=-\infty}^{\infty} J_n\left(\frac{\alpha}{j\Gamma}\right) e^{jn\theta}\, d\theta \tag{C.4}$$

Now, it easy to perform the integral (C.4) and the final result is given by

$$G(\beta,\alpha) = \sum_{n=-\infty}^{\infty} \frac{e^{n\ \sinh^{-1}(\beta\Gamma)} - 1}{n}\, J_n\left(\frac{\alpha}{j\Gamma}\right) \tag{C.5}$$